

University of Virginia
Department of Engineering Systems and Environment

PHD DISSERTATION
***Mechanisms Controlling Hydraulic Conductivity and Service Life of
Bentonite-Polymer Composite Geosynthetic Clay Liners Permeated
with Aggressive Solutions***

December, 2020

Author:

SARAH ANNE GUSTITUS-GRAHAM

Committee:

DR. CRAIG H. BENSON¹ (advisor), Engineering Systems and Environment
DR. LISA COLOSI PETERSON¹ (committee chair), Engineering Systems and Environment
DR. JAMES SMITH¹, Engineering Systems and Environment
DR. ANDRES CLARENS¹, Engineering Systems and Environment
DR. STEVEN CALIARI¹, Chemical Engineering
DR. KUO TIAN², Civil, Environmental and Infrastructure Engineering

1. University of Virginia, Charlottesville, Virginia
2. George Mason University, Fairfax, Virginia

Abstract

Bentonite-polymer composite geosynthetic clay liners (BPC-GCLs) are used to line containment systems such as landfills, leach pads, and impoundments with aggressive leachates that adversely affect conventional sodium bentonite GCLs. BPC-GCLs were permeated with aggressive leachates to understand the mechanisms controlling hydraulic conductivity in BPC-GCLs under various conditions. Empirical results were compared to computational models to develop methods for predicting hydraulic conductivity and service life.

Polymer elution in BPC-GCLs resulted in preferential flow paths and dramatic increases in hydraulic conductivity for several BPC-GCLs. Low hydraulic conductivity in BPC-GCLs is maintained as long as narrow, tortuous pore paths result from the swelling of bentonite granules and/or the retention of hydrated polymer gels between bentonite granules. The product of the swell index of the bentonite component and the flow stress of the hydrated polymer component, herein referred to as flow-swell index, represents both of these mechanisms and shows promise as an index of hydraulic conductivity for BPC-GCLs to aggressive solutions. BPC-GCLs permeated or batch aged at 60 °C maintained comparable or lower hydraulic conductivity to those permeated at 20 °C, regardless of changes to swell index and flow stress, provided sufficient polymer is retained in the pore spaces. Hydraulic models developed using COMSOL are consistent with the mechanisms identified through experimental observations, whereby flow is directed at lower velocities through narrow pores when larger pores are filled with polymer gel. Computational models demonstrate that decreases in viscosity of polymer gels resulted in increased elution rates.

Acknowledgments

I would first like to express my sincere gratitude to my advisor, Dr. Craig Benson, for his support, guidance, and mentorship over the past three years. I would also like to thank my committee for their advice and insights throughout the research process. My fellow group members, especially Nick Chen, Julie Bridstrup, and Dorian Nguyen have been invaluable in helping me achieve my research goals and maintain my sanity. This research was made possible through funding from EREF, CETCO, the US Department of Energy's Consortium for Risk Evaluation with Stakeholder Participation (CRESP) III, and the Jefferson Scholars Foundation.

I could never express enough gratitude to the fantastic people who quietly keep this whole operation running: Scott, Rick, and Ricky for making just about anything happen; Lisa for helping coordinate our group; Sebring for helping a poor clueless grad student build the equipment that made this research possible; Derek for improving the safety and efficiency of our lab spaces; David for answering a steady stream of computer questions; Paul for keeping OMERF running, and Donna for keeping OMERF clean; and last, but certainly not least, the late Jesse Johnson, who improved Thornton Hall in countless ways beyond keeping our space clean. Beyond their material contributions to my work, each of the people listed here have brightened my days here.

Above all else, the support from my family has made this entire endeavor possible. My parents, Rachel and Gregory "Gus" Gustitus, laid the foundation that this degree is built upon. My husband, Stephen, keeps the world outside of the lab turning, and keeps the baby from turning into a flaming monster. How do you do it? By rolling with the punches! Because you're Mr. Incredible - not "Mr. So-So" or "Mr. Mediocre Guy!" - Mr. Incredible!

This dissertation is dedicated to my son, Samson James, who has been the best possible distraction and motivation in my final semester.

Table of Contents

Chapter 1: Introduction	1
Chapter 2: Performance of Bentonite-Polymer Composite Geosynthetic Clay Liners.....	4
2.1 INTRODUCTION.....	4
2.2 BPC-GCL COMPONENTS	5
2.2.1 Polymer Chemistry and Structure	5
2.2.2 Polymer Loading.....	8
2.2.3 Bentonite Type.....	8
2.2.4 Geotextile Type.....	9
2.3 BPC-GCL APPLICATIONS.....	10
2.3.1 Solution Chemistry	10
2.3.2 Landfill Liner Temperature.....	12
2.4 CONCLUSIONS	14
Chapter 3: Polymer Elution and Hydraulic Conductivity of Bentonite-Polymer Composite Geosynthetic Clay Liners Permeated with Aggressive Solutions.....	15
3.1 INTRODUCTION.....	15
3.2 MATERIALS AND METHODS	17
3.3 RESULTS AND DISCUSSION	18
3.4 SUMMARY AND CONCLUSIONS.....	24
Chapter 4: Flow-Swell Index for Predicting Long-Term Hydraulic Conductivity of Bentonite-Polymer Composite Geosynthetic Clay Liners.....	26
4.1 INTRODUCTION.....	26
4.2 MATERIALS	28
4.3 METHODS.....	30
4.3.1 Hydraulic Conductivity.....	30
4.3.2 In-Situ Gel Moisture Content.....	30
4.3.3 Viscoelastic Properties of Polymer Gels.....	32
4.3.4 Polymer Loading.....	32
4.4 RESULTS.....	33
4.4.1 Hydraulic Conductivity.....	33

4.4.2	Moisture Content	35
4.4.3	Flow Stress of Hydrated Polymer Gels.....	38
4.4.4	Swell Index	40
4.4.5	Polymer Elution	41
4.5	DISCUSSION	42
4.6	SUMMARY AND CONCLUSIONS.....	46
4.7	ACKNOWLEDGEMENTS	47
Chapter 5: Hydraulic Conductivity of Bentonite-Polymer Composite Geosynthetic Clay Liners to Aggressive Solutions Under Elevated Temperature		48
5.1	INTRODUCTION.....	48
5.2	MATERIALS	49
5.3	METHODS.....	50
5.3.1	Continuous Permeation at Elevated Temperature.....	50
5.3.2	Batch Aging of BPC-GCLs	52
5.3.3	Batch Aging of Polymer Gels	53
5.3.4	Flow Stress.....	53
5.3.5	Swell Index	53
5.4	RESULTS.....	54
5.4.1	Hydraulic Conductivity.....	54
5.4.2	Flow Stress of Polymer Gels.....	57
5.4.3	Swell Index	60
5.4.4	Polymer Loading.....	61
5.5	DISCUSSION	63
5.6	SUMMARY AND CONCLUSIONS.....	67
5.7	ACKNOWLEDGMENTS.....	69
Chapter 6: Pore Scale Modeling of Polymer Elution in Bentonite-Polymer Composite Geosynthetic Clay Liners.....		70
6.1	INTRODUCTION.....	70
6.2	MATERIALS AND METHODS	71
6.2.1	Materials	71
6.2.2	Methods.....	71

6.3	RESULTS AND DISCUSSION	73
6.3.1	Experimental results.....	73
6.3.2	Model results.....	74
6.4	DISCUSSION	78
6.5	RECOMMENDATIONS	80
6.6	SUMMARY AND CONCLUSIONS.....	81
Chapter 7:	Conclusions, Limitations, and Recommendations	83
7.1	SUMMARY AND CONCLUSIONS.....	83
7.2	DEVELOPED OR IMPROVED METHODOLOGIES	84
7.3	LIMITATIONS	85
7.4	RECOMMENDATIONS	85
References.....		87
Appendix A.....		98

List of Tables

Table 4.1. Characteristics of the polymers contained in the BPC-GCLs used in this study.....	29
Table 4.2. Hydraulic conductivities of GCLs. Early equilibrium refers to the first time a GCL met the termination criteria prescribed in ASTM D6766, and late equilibrium or current status refers to the final equilibrium of the GCL or the status at the time of writing. PVF is pore volumes of flow (estimated for samples currently running)	34
Table 4.3. Moisture content and flow stress of in-situ polymer gel from bentonite-polymer moisture affinity test; swell indices of NaB and BPC for each GCL; flow-swell index defined as product of polymer flow stress and NaB swell index.....	36
Table 5.1. pH and electrical conductivity (EC) of permeating solutions.....	50
Table 5.2. Hydraulic conductivities of each test at the time that this paper was prepared. “Active permeation” refers to the time that flow was being conducted through the permeameter, which was not necessarily constant when samples had hydraulic conductivity above 10^{-8} m/s.....	55
Table 6.1. Shear rate, approximate viscosity (based on Fig. 6.3), and approximate shear stress near the NaB granule, and in the center of the pore for the model with $\eta = 1 \times 10^6$ Pa·s. Approximate viscosity is based on the 500% moisture content P1 gel.....	78

List of Figures

Figure 1.1. Schematic illustration of a geosynthetic clay liner.	1
Figure 2.1. Cross-linked polymer, P1 (left) and linear polymer, P2 (right) are two proprietary polymers investigated in subsequent chapters.....	7
Figure 3.1. (A) NaB granules swell in leachate with low to modest ionic strength, closing inter-granular pores and resulting in low hydraulic conductivity; (B) NaB granules permeated with aggressive leachate do not swell, resulting in larger inter-granular pores and higher hydraulic conductivity; (C) polymer component of BPC fills inter-granular pores, creating a low hydraulic conductivity barrier; (D) elution of polymer results in BPC with higher hydraulic conductivity.....	17
Figure 3.2. Hydraulic conductivity of BPC-GCL-S and BPC-GCL-N permeated with (A) 20 mM CaCl₂ and (B) 100 mM CaCl₂. Numbers in parentheses indicate replicates.....	19
Figure 3.3. Dissolved polymer content of effluent as a function of hydraulic conductivity when the effluent was collected.....	20
Figure 3.4. Conceptual model showing how properties of the polymer hydrogel and effluent change during polymer elution from a BPC-GCL. (A) High polymer to solution ratio in the pore space at low hydraulic conductivity leads to increased contact between the pore water and the polymer gel, and higher polymer content of the effluent; (B) Lower polymer to solution ratio when the hydraulic conductivity is higher leads to less contact between the pore water and the polymer gel, and lower polymer content of the effluent.....	21
Figure 3.5. (A) Hydraulic conductivity and (B) intrinsic permeability of BPC-GCL-S permeated with 20 mM CaCl₂. Called out data represent (A) dissolved polymer content and (B) viscosity of effluent.....	22
Fig. 3.6. Example of preferential flow path dyed pink in BPC-GCL-N.....	23
Figure 3.7. (A) Sheet, (B) honeycomb, and (C) stringy polymer structures found in BPC-GCLs.....	24
Figure 4.1. (A) Bentonite with swollen granules and narrow and tortuous flow paths that yield low hydraulic conductivity; (B) bentonite with suppressed granule swelling and are larger and less tortuous flow paths that yield high hydraulic conductivity; (C) bentonite-polymer composite with polymer gel filling intergranular pores, yielding low hydraulic conductivity; and (D) bentonite-polymer composite after elution of polymer gel, with larger and less tortuous flow paths and high hydraulic conductivity.....	27
Figure 4.2. Schematic illustration of bentonite-polymer moisture affinity test (left), hydrated polymer and bentonite components at end of test (top right), and top view of filled test compartment (bottom right).....	31

Figure 4.3. Hydrated bentonite after termination of a bentonite-polymer moisture affinity test. Red box outlines portion of bentonite removed to determine moisture content.....	32
Figure 4.4. Hydraulic conductivity vs. pore volumes of flow for (A) BPC-GCL-P1 permeated with 50 mM CaCl₂ illustrating a sudden jump in hydraulic conductivity; (B) BPC-GCL-P2 permeated with CEN acidic standard solution illustrating gradual increase in hydraulic conductivity and (C) BPC-GCL-P3H permeated with synthetic bauxite solution that retained relatively consistent hydraulic conductivity.....	35
Figure 4.5. Polymer gel moisture content from bentonite-polymer moisture affinity test as a function polymer loading for each BPC hydrated in varying solutions at the same polymer loading as the BPC-GCL.....	37
Figure 4.6. Polymer gel moisture content from bentonite-polymer moisture affinity test as a function polymer loading for each BPC hydrated in 50 mM CaCl₂ at various polymer loadings at and below the loading in the BPC-GCL.....	38
Figure 4.7. Flow stress (τ_f) of hydrated polymer gels as a function of moisture content (w) for each of the polymers hydrated with 50 mM CaCl₂ (A) and polymer P1 hydrated with various permeant solutions (B).....	39
Figure 4.8. Polymer concentration of effluent (A) and polymer flux (B) versus average hydraulic conductivity of the BPC-GCL during the time that the effluent was collected... 	41
Figure 4.9. Longer term hydraulic conductivity versus the (A) flow stress of the initial condition in-situ hydrated polymer gel and (B) swell index of the BPC.....	43
Figure 4.10. Longer term hydraulic conductivity vs. flow-swell index, defined as product of polymer flow stress and NaB swell index with permeant solution.....	44
Figure 5.1. Elevated temperature permeameters used for measuring hydraulic conductivity at 60°C.....	51
Figure 5.2. Schematic illustration of hydration cell used for batch aging.....	52
Figure 5.3. Hydraulic conductivity of (A) BPC-GCL-P1 with an alkaline solution, (B) BPC-GCL-P1 with 50 mM CaCl₂ and (C) BPC-GCL-P2 with an acidic solution continuously permeated at 20 and 60 °C. BPC-GCLs had no external aging.....	56
Figure 5.4. Hydraulic conductivity of A) BPC-GCL-P1 with an alkaline solution, and B) BPC-GCL-P2 with an acidic solution.....	57
Figure 5.5. Flow stress of unaged polymer gels as a function of temperature. Polymer gels were hydrated to a moisture content of 500%.....	58
Figure 5.6. Flow stress of polymer gels aged at various temperatures for P1 with alkaline solution (A), P1 with 50 mM CaCl₂ (B) and P2 with acidic solution (C).....	59
Figure 5.7. Hydrated polymer gels batch aged at 60 °C.....	60

Figure 5.8. Swell index of base bentonite, BPC-P1, and BPC-P2 as a function of temperature.....	61
Figure 5.9. Polymer loading remaining in continuously permeated and batch aged BPC-GCLs.....	62
Figure 5.10. The moisture content of in-situ polymer gels decreases as polymer loading increases.....	62
Figure 5.11. Hydraulic conductivity of batch aged BPC-GCLs versus batch aging time.....	64
Figure 5.12. Hydraulic conductivity of batch aged BPC-GCLs versus flow stress of the corresponding polymer gel.....	65
Figure 5.13. Hydraulic conductivity of batch aged BPC-GCLs versus polymer loading of the BPC-GCL after batch aging.....	65
Figure 5.14. Plates constraining samples in (A) batch aging containers and (B) permeameters. The batch aging container contains 49 holes (3 mm diameter) in both the top and bottom plates, all of which are continuously open. The permeameter plate contains two holes (6.4 mm diameter) – one for effluent to flow through, and the other is only opened to facilitate clearing of clogs when necessary.....	66
Figure 6.1. Geometry employed in each of the models, consisting of two NaB granules and a single polymer gel positioned just below the pore space between the NaB granules.....	72
Figure 6.2. Velocity profiles of preliminary testing model using (A) laminar and (B) creeping flow physics.....	73
Figure 6.3. Viscosity (η) of polymer P1 (A) and P3 (B) gels at moisture contents of 500%, 1000%, and 2000%.....	74
Figure 6.4. Distribution of the polymer at $t = 0$ (A), and $t = 5$ for $\eta = 1 \times 10^6$ Pa·s (B), $\eta = 3 \times 10^3$ Pa·s (C), and $\eta = 1 \times 10^2$ Pa·s (D). The polymer is indicated in blue, the permeant solution is indicated in red, and the NaB granules are indicated in white.....	75
Figure 6.5. Velocity profiles when polymer is in the pore space (A; corresponding to Fig. 6.4B), and after polymer elutes from the pore space (B; corresponding to Fig. 6.4D).....	76
Figure 6.6. Shear rate, $\dot{\gamma}$, measured at various points for $\eta = 1 \times 10^6$ Pa·s.....	77
Figure 6.7. Hydraulic conductivity (A) of BPC-GCL-P1 and P3 to 50 mM CaCl ₂ , and and flow stress (B) of the corresponding polymer gels.....	79

List of Abbreviations

BPC Bentonite-polymer composite

GCL Geosynthetic clay liner

NaB Sodium bentonite

CaB Calcium bentonite

LOI Loss on ignition

TC Total carbon

TOC Total organic carbon

Chapter 1: Introduction

Geosynthetic clay liners (GCLs) are commonly used in waste containment system liners due to their low cost, ease of installment, and effectively low hydraulic conductivity compared to compacted clay liners. In conventional GCLs, two geotextiles constrain a layer of sodium bentonite (NaB) that swells when hydrated with a low-strength, neutral solution (Fig. 1.1). Bentonite-polymer composite geosynthetic clay liners (BPC-GCLs) are alternatives to conventional NaB-GCLs for lining containment facilities with aggressive leachates. BPC-GCLs offer several benefits over NaB-GCLs, including lower hydraulic conductivity to aggressive solutions (Scalia et al. 2011; Athanassopoulos et al. 2015; Tian et al. 2016a; Donovan et al. 2017; Tian and Benson 2018; Chen et al. 2019), greater resistance to internal erosion (Ashe et al. 2015; Rowe et al. 2016a; b), and greater self-healing capacity (De Camillis et al. 2016, 2017; Prongmanee and Chai 2019; Chai and Prongmanee 2020). BPC-GCLs can be employed to contain aggressive waste streams from mining and ore beneficiation, energy production, and industrial applications (Athanassopoulos et al. 2015; Tian et al. 2016a; Donovan et al. 2017; Tian and Benson 2018; Chen et al. 2019). Due to the risks posed by these leachates to human and environmental health, the service lives of BPC-GCLs used in these applications may need to be guaranteed for extended periods of time, up to 1,000 years or more for radioactive waste containment (Tian et al. 2017).

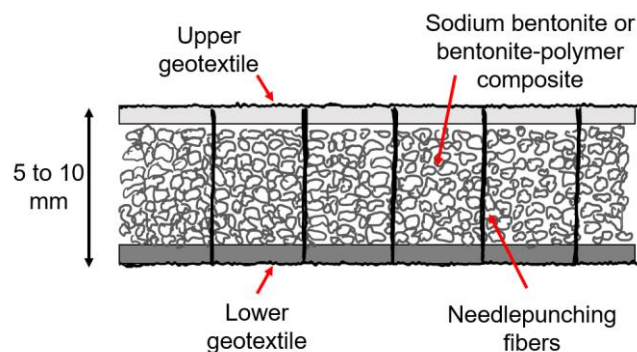


Figure 1.1. Schematic illustration of a geosynthetic clay liner.

The service life of a BPC-GCL ends when the hydraulic conductivity exceeds some maximum threshold. BPC-GCLs maintain low hydraulic conductivity as long as sufficiently narrow and tortuous pores are maintained. Narrow and tortuous pores can be achieved by swelling of the NaB component and/or by retention of the hydrated polymer component between NaB granules (Scalia et al. 2014; Tian et al. 2016a; b). The pore-filling mechanism of the polymer gels is particularly important for maintaining low hydraulic conductivity to aggressive leachates, because NaB swell is limited when the hydrating solution has high ionic strength, polyvalent cations, $\text{pH} < 3$, or $\text{pH} > 12$ (Jo et al. 2001; Shackelford et al. 2010; Bouazza and Gates 2014; Chen et al. 2019). When pores are filled with polymer, flow paths through the BPC-GCL are narrow and tortuous, similar to those in an NaB-GCL hydrated with non-aggressive solution. The polymer component of BPC-GCLs may elute during permeation, changing the properties of the remaining gels in the pore spaces (Tian et al. 2019). If sufficient polymer is eluted, flow paths can widen, increasing the hydraulic conductivity of the BPC-GCL and ending the service life.

This dissertation explores methods for quantifying and predicting polymer elution and degradation in BPC-GCLs. The goal of this research is to develop empirical and computational methods that can be used to predict the hydraulic conductivity and service life of BPC-GCLs.

This dissertation is divided into seven chapters and one appendix, including this introductory chapter. The remaining chapters are divided as follows:

Chapter 2 presents a review of the literature pertaining to hydraulic performance of BPC-GCLs and other polymer-amended bentonites. This chapter delves into the effects of both BPC-GCL components and application conditions on hydraulic conductivity.

Chapter 3 presents a bench-scale study of BPC-GCLs permeated with CaCl_2 solutions, in which the mechanisms controlling hydraulic conductivity are closely examined.

In Chapter 4 an index test is developed based on properties of the polymer and NaB components of BPC-GCLs. To date, there are no standardized or widely used methods to screen for BPC-GCLs that will maintain low hydraulic conductivity against aggressive solutions. Therefore, the index proposed in this chapter may be of great use for assessing appropriate BPC-GCLs for landfill design applications.

Chapter 5 assesses the effects of elevated temperatures on the hydraulic conductivity of BPC-GCLs. Landfill liner temperatures vary depending on geographic location, waste type, and waste degradation; as such, the effects of temperature should be considered when predicting hydraulic conductivity or service life.

In Chapter 6 computational models are developed that simulate the movement of a polymer gel through a pore space in a BPC-GCL, and the modeling results are compared to experimental observations described in the preceding chapters.

Chapter 7 summarizes the findings of this dissertation and the practical implications of the research presented herein. Recommendations for future research are also provided.

To complete the bench-scale studies included in this dissertation, a reliable method for measuring polymer loading in BPC-GCLs was necessary. Appendix A presents a detailed assessment of methods used to determine polymer loading in BPC-GCLs, including practical recommendations for measuring polymer loading for either for quality control (e.g., in construction or manufacturing), and forensic assessment of BPC-GCLs (e.g., in academic research).

Chapter 2: Performance of Bentonite-Polymer Composite Geosynthetic Clay Liners

2.1 INTRODUCTION

Bentonite-polymer composite geosynthetic clay liners (BPC-GCLs) are employed for lining containment systems with leachates that are too aggressive for conventional sodium bentonite (NaB) GCLs to maintain suitably low hydraulic conductivity. BPC-GCLs contain a variety of polymer amendments, each of which may interact differently with various leachates. In addition to differences in polymer chemistry and structure, BPC-GCLs may differ in polymer loading (g polymer/kg BPC), bentonite source and/or type (e.g., natural versus activated NaB, granular versus powdered), or the type and number of geotextiles (e.g., the inclusion of a woven “slit film” between the BPC and the lower non-woven geotextile). Leachates contained by BPC-GCLs can vary from extremely acidic solutions (e.g., copper mining wastes) to extremely alkaline solutions (e.g., bauxite liquor from “red mud”) with various ionic strengths and compositions. Additionally, landfill liner temperatures may vary significantly depending on the location, waste type, and waste decomposition state. This chapter synthesizes findings of available literature on the effects of BPC-GCL components and application conditions on the hydraulic conductivity of BPC-GCLs.

BPC-GCLs are part of a larger category of “polymer-amended bentonites” which also includes polymer-modified bentonites. BPCs are comprised of dry mixtures of bentonites and polymers, whereas polymer-modified bentonites are produced through polymer treatment of the mineral surface or intercalation of polymer within the interlayer of montmorillonite. This review includes discussion of both BPCs and polymer-modified bentonites.

2.2 BPC-GCL COMPONENTS

2.2.1 Polymer Chemistry and Structure

The polymers contained in BPC-GCLs and polymer-modified bentonites have various chemistries and structures, including linear or cross-linked polymers, and cationic or anionic polymers. The structure or chemistry of the polymers may influence their interactions with NaB or with the permeant solution, in turn affecting the hydraulic conductivity of the BPC-GCL. Polymers that have been used in polymer amended bentonites include polyacrylamide (Scalia et al. 2011, 2014; Tian et al. 2016a; Chen et al. 2019; Ören et al. 2019; Yu et al. 2020), sodium polyacrylate (Prongmanee et al. 2018b; a; Ören et al. 2019; Prongmanee and Chai 2019; Salemi et al. 2019; Chai and Prongmanee 2020) and sodium carboxymethyl cellulose (Di Emidio et al. 2011, 2015; De Camillis et al. 2016, 2017). Other various proprietary polymers, for which limited characteristics are publicly identified, are also commonly used in commercially available BPC-GCLs (Razakamanantsoa et al. 2012; Razakamanantsoa and Djeran-Maigre 2016; Tian et al. 2016a, 2019; Chen et al. 2019; Gustitus et al. 2020).

Some polymers, known as polyelectrolytes, have a high density of electrostatically charged functional groups along the base chain. The charged functional groups can interact strongly with electrostatic charges in the solutions surrounding them (e.g., high ionic strength leachates) or at the surface of other particles (e.g., edge charges of montmorillonite, the primary mineral in NaB). Polyelectrolyte chains in dilute solutions tend to have elongated structures due to repulsion between the charged functional groups. However, in concentrated solutions abundant counter-ions can neutralize charges along the chain, causing the polymer to coil up in what is known as the polyelectrolyte effect (Young and Lovell 2011). Contraction of charged polymer chains affects the

mobility of polymers, and has been suggested as a cause of increased hydraulic conductivity for BPC-GCLs permeated with high ionic strength solutions (Tian et al. 2016b, 2017).

Cationic and anionic polyelectrolytes have both been shown to be effective amendments for maintaining lower hydraulic conductivity than unamended NaB (Razakamanantsoa et al. 2012; Özhan 2018). Razakamanantsoa et al. (2012) found that BPCs with cationic and anionic polymers both maintained hydraulic conductivity approximately one order of magnitude lower than the unamended activated calcium bentonite (CaB) when permeated with synthetic MSW leachate. However, the BPC with a cationic polymer had significantly greater swelling and water retention than the unamended activated CaB, while a BPC with an anionic polymer did not. Ozhan (2018) found that for BPCs permeated with MgCl_2 solutions at 20 and 40 °C, a BPC containing an anionic polymer consistently maintained lower hydraulic conductivity than a BPC containing a cationic polymer. At 60°C the BPC with the cationic polymer had a slightly lower hydraulic conductivity against a lower strength solution (0.1 M MgCl_2) while the BPC with the anionic polymer had a lower hydraulic conductivity against a higher strength solution (0.5 M MgCl_2). Several studies have assessed the performance of HYPER clay (a polymer-modified bentonite prepared by stirring bentonite in an anionic sodium carboxymethyl cellulose solution ,then drying) which maintains a lower hydraulic conductivity than unamended NaB when permeated with salt solutions (Di Emidio et al. 2011, 2015; De Camillis et al. 2016, 2017). When permeated with very strong salt solutions (e.g., 1 M), polymer-modified bentonites may have hydraulic conductivity comparable to that of unamended NaB, regardless of polymer charge (McRory and Ashmawy 2005), which may be a result of contracting polymer chains in concentrated solutions, as observed by Tian et al. (2016b).

Polymer behavior can also be affected by the structural arrangement of the polymer chains. Polymer structures can be categorized as linear, cyclic, branched, or network structures. Network

polymers are unique for their three dimensional structures which are a result of bonding polymer chains through crosslinking. The three dimensional structure of network polymers leads to unique properties, such as swelling in compatible solutions rather than dissolving (Young and Lovell 2011). Network polymers that swell to hold many times their mass in water or solution are classed as “hydrogels” or “superabsorbant polymers” (Ahmed 2015). Figure 2.1 shows examples of a crosslinked hydrogel (polymer P2 in subsequent chapters) and a linear polymer (polymer P3 in subsequent chapters) that are used in commercially available BPC-GCLs. To date, properties such as degree of cross-linking have not been specifically studied with respect to BPC-GCLs.

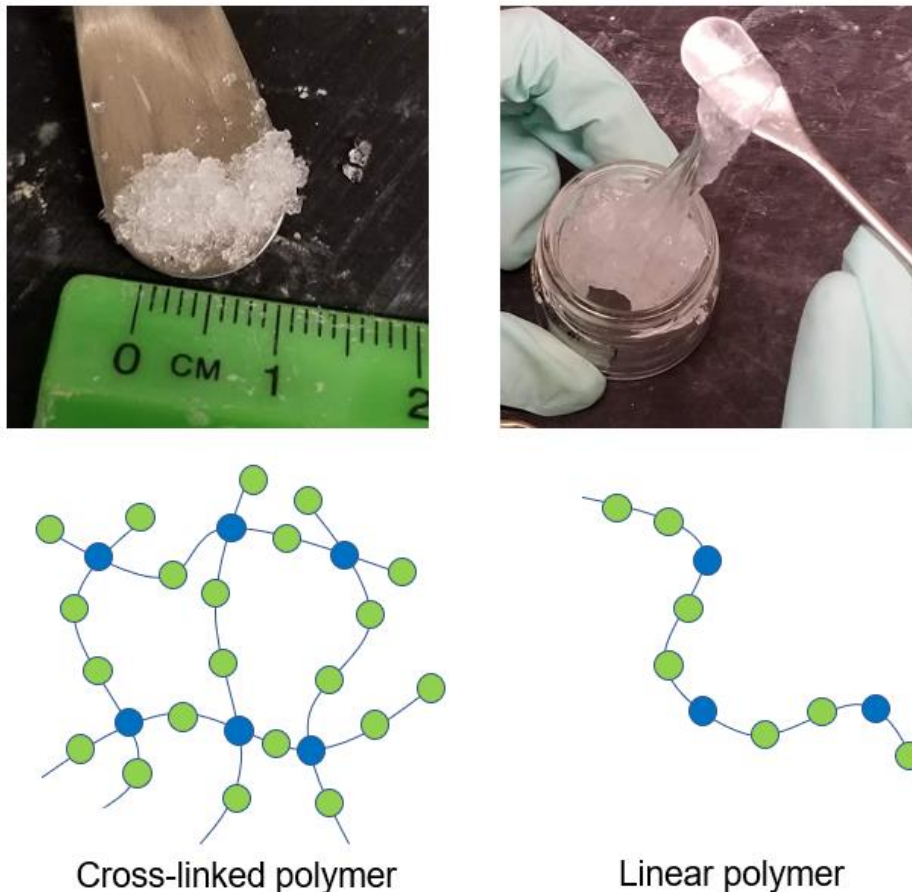


Figure 2.1. Cross-linked polymer, P1 (left) and linear polymer, P2 (right) are two proprietary polymers investigated in subsequent chapters.

2.2.2 Polymer Loading

Polymer loading in polymer-modified bentonites may vary from 10 g polymer/kg BPC (1%) or less (Özhan 2018; Chen et al. 2019; Ören et al. 2019) up to 160 g polymer/kg BPC (15%) (Di Emidio et al. 2015). The hydraulic conductivity of BPC-GCLs decreases with increasing polymer loading, all else equal (Chen et al. 2019; Salemi et al. 2019). However, Chen et al. (2019) also showed that hydraulic conductivity can vary by up to five orders of magnitude for BPC-GCLs that have the same polymer loading, but are permeated with different solutions and/or contain different proprietary polymers. Polymer loading may vary by design or as polymer is eluted during permeation (Chen et al. 2019; Tian et al. 2019). Chen et al. (2019) demonstrated that high hydraulic conductivity resulted from preferential flow through an area with the lowest polymer loading on a BPC-GCL sample permeated with high strength Trona leachate.

The effects of polymer loading on other physical properties of polymer-amended bentonites are dependent on polymer type. Di Emidio et al. (2015) showed that the liquid limit, plastic limit, and plasticity index of HYPER clay increased with increasing loading of sodium carboxymethyl cellulose from 20 to 160 g polymer/kg HYPER clay. In contrast, Salemi et al. (2019) found only negligible differences in Atterberg limits for NaB compared to BPCs with sodium polyacrylate loading varying from 30 to 70 g polymer/kg BPC.

2.2.3 Bentonite Type

NaB is the most commonly used bentonite in GCLs, primarily because NaB undergoes both crystalline and osmotic swelling, whereas bentonites with multivalent ions in the interlayer (e.g., CaB) only undergo crystalline swelling (Norrish and Quirk 1954; Scalia et al. 2018). Osmotic swelling of NaB leads to smaller pore paths, and therefore lower hydraulic conductivity. When

GCLs are permeated with low ionic strength, neutral solutions (e.g., deionized water) that don't negatively impact the osmotic swelling of NaB, the hydraulic conductivity of NaB-GCLs may be comparable to that of polymer-modified bentonites (De Camillis et al. 2016).

The charge of the mineral edge surface may attract or repel ionic polymers, affecting how well the polymer adsorbs to the clay. For example, Heller and Keren (2003) found negatively charged polyacrylamide (PAM) had a greater tendency to adsorb to pyrophyllite, which has an uncharged basal surface, than montmorillonite, which has a negatively charged basal surface. The cation exchange capacity (CEC) also affects polymer adsorption. Stutzmann and Siffert (1977) found that adsorption of acetamide on montmorillonite increases with increasing polarization power of the cation in the interlayer.

BPC-GCLs and polymer-modified bentonites may contain either granular or powdered bentonite. Unamended granular NaB takes longer to hydrate and swell than unamended powdered NaB, and may have hydraulic conductivity comparable to coarse-grained materials when permeated with a swell-limiting aggressive solution (Shackelford et al. 2000). The hydraulic conductivity of powdered bentonite is sensitive to temperature regardless of void ratio, whereas the hydraulic conductivity of granular bentonites is more sensitive to temperature at lower void ratios (Abuel-Naga et al. 2013). To date, no studies have been published directly comparing BPC-GCLs that differ only in bentonite form.

2.2.4 Geotextile Type

BPC-GCLs typically consist of a layer of BPC sandwiched between two geotextiles that are bound together by needle-punching, whereby bundles of threads punched through the entire thickness of the GCL bind the geotextiles at a set distance apart. Generally, the BPC swells

sufficiently around the fiber bundles, preventing preferential flow paths; however, in some cases flow can be conducted primarily through the fiber bundles if the stress is too low to adequately seal them (Conzelmann et al. 2017). Both NaB and polymer can be extruded through the geotextiles when sufficient overburden stress is applied (Chen et al. 2017), and polymer can be eluted through the bottom-most geotextile as polymer-laden effluent exits the BPC-GCL (Scalia et al. 2014; Tian et al. 2019). In some BPC-GCLs a third, woven geotextile referred to as a “slit-film” is included between the BPC and the bottom-most geotextile to reduce polymer elution. The inclusion of a slit-film has been demonstrated to lower hydraulic conductivity of a BPC-GCL by promoting the retention of polymer within the BPC (Tian et al. 2019).

2.3 BPC-GCL APPLICATIONS

2.3.1 Solution Chemistry

BPC-GCLs and polymer-modified bentonites are primarily employed in situations where NaB-GCLs are incompatible with the solution that needs to be contained. Specifically, NaB-GCLs may have high hydraulic conductivity when permeated with extremely acidic ($\text{pH} < 3$), alkaline ($\text{pH} > 12$), or high ionic strength ($> 1 \text{ M}$) solutions (Jo et al. 2001; Shackelford et al. 2010; Bouazza and Gates 2014; Chen et al. 2019).

2.3.1.1 Extreme pH Solutions

BPC-GCLs may be used to contain leachates with extreme pH. For example, copper and uranium are often extracted through a sulfuric acid leaching process, resulting in waste solutions that may have $\text{pH} < 1$ (Hornsey et al. 2010; Ghazizadeh et al. 2018), while the processing of bauxite into alumina results in highly alkaline bauxite liquor with pH up to 13 (Hornsey et al. 2010;

Athanassopoulos et al. 2015; Ghazizadeh et al. 2018; Tian and Benson 2018). The hydraulic conductivities of NaB-GCLs permeated with extreme pH solutions are several orders of magnitude higher than the hydraulic conductivity of the same NaB-GCL permeated with water (Benson et al. 2010; Shackelford et al. 2010; Liu et al. 2015).

BPC-GCLs and polymer-modified bentonites can maintain low hydraulic conductivity to extreme pH solutions that adversely affect NaB-GCLs. Prongmanee and Chai (2019) found that sodium polyacrylate-modified bentonite maintained lower hydraulic conductivity than NaB-GCLs for solutions with pH of 1 and 13. BPC-GCLs and polymer-modified bentonites containing polyacrylate have been shown to maintain hydraulic conductivity on the order of 10^{-11} m/s for solutions of CuCl_2 with pH= 4 (Ören et al. 2019), NaOH with pH = 13.1, and HNO_3 with pH = 0.3 (Scalia et al. 2014). Multiple studies have demonstrated that BPC-GCLs can maintain hydraulic conductivity on the order of 10^{-12} to 10^{-11} m/s to highly alkaline bauxite liquor (Athanassopoulos et al. 2015; Donovan et al. 2017; Tian and Benson 2018).

2.3.1.2 High Ionic Strength Solutions

Solutions with high ionic strength and/or a prevalence of polyvalent cations limit the amount that NaB swells, resulting in larger pore paths and higher hydraulic conductivity in NaB-GCLs. When Na^+ ions occupy the interlayer of montmorillonite (the primary mineral in bentonite), adjacent layers interact weakly, which allows for significant water sorption into the interlayer, separating the space and causing dramatic swelling (Mitchell and Soga 2005; Bouazza and Gates 2014). However, when Na^+ ions are exchanged with polyvalent cations that are less favorable to swelling, hydraulic conductivity of NaB-GCLs can increase by an order of magnitude or more (Jo et al. 2001, 2005; Kolstad et al. 2004).

BPC-GCLs and polymer-modified bentonites have been shown to maintain lower hydraulic conductivity than NaB-GCLs for a number of high ionic strength solutions. Scalia et al. (2014) demonstrated that a BPC containing Na-polyacrylate maintained hydraulic conductivity $<10^{-10}$ m/s for CaCl_2 solutions up to 500 mM for over two years. HYPER clay has been shown to maintain lower hydraulic conductivity and increased self-healing capacity compared to untreated NaB when exposed to seawater (De Camillis et al. 2016, 2017). Chen et al. (2019) demonstrated that commercially available BPC-GCLs containing proprietary polymers could maintain hydraulic conductivities approaching 10^{-12} m/s when permeated with coal combustion product leachates with ionic strength approaching 1 M.

There are limitations to the compatibility of BPC-GCLs with high ionic strength solutions. Similar to NaB-GCLs, the hydraulic conductivity of BPC-GCLs may increase with increasing ionic strength (Özhan 2018) or replaceability power of the cations (McRory and Ashmawy 2005). For very high ionic strength solutions (~ 1 M), polymer-amended bentonites may have comparable hydraulic conductivity to NaB-GCLs when hydrated directly with the salt solution, but lower hydraulic conductivity than NaB-GCLs when pre-hydrated with DI water (McRory and Ashmawy 2005; Chen et al. 2019).

2.3.2 Landfill Liner Temperature

Wastes that require the use of BPC-GCLs may exhibit elevated temperatures (Klein et al. 2001; Koerner and Koerner 2006; Yeşiller et al. 2015). For example, mining wastes may exhibit elevated temperatures up to 65°C , and MSW incinerator ash may reach temperatures up to 87°C (Yeşiller et al. 2015). The temperature in the bulk of the waste can affect the temperature at the

landfill liner. For example, for an MSW incinerator ash landfill with a maximum temperature of 70 °C in the bulk of the waste, the liner reached a maximum temperature of 46 °C (Klein et al. 2001). Elevated liner temperatures affect the swelling and sorption properties of NaB (Villar and Lloret 2004; Rowe et al. 2005; Abuel-Naga and Bouazza 2013; Bag and Rabbani 2017); the degradation of polymeric components, such as HDPE geomembranes and leachate pipes (Rowe and Islam 2009; Rowe et al. 2009; Krushelnitzky and Brachman 2013; Abdelaal and Rowe 2014; Ewais and Rowe 2014; Tian et al. 2017); and moisture migration in liners (Southen and Rowe 2005; Azad et al. 2011, 2012; Bouazza et al. 2014). Prolonged exposure to elevated temperatures may detrimentally impact the hydraulic conductivity, contaminant transport, and longevity of a liner (Rowe 2005).

Hydraulic conductivity of NaB-GCLs may increase by an order of magnitude or more when the temperature is increased from 20 to 60 °C (Ishimori and Katsumi 2012; Özhan 2018). Decreased hydraulic conductivity in NaB-GCLs at high temperatures may be attributed to reduced swelling of bentonite due to changes in the thickness of the diffuse double layer (Mitchell and Soga 2005; Hornsey et al. 2010) and/or a decrease in permeant viscosity (Mitchell and Soga 2005; Bouazza et al. 2008; Özhan 2017, 2018). Ishimori and Katsumi (2012) found that despite increased free swell, a NaB-GCL exhibited a decrease in diffuse double layer thickness and had a higher intrinsic permeability and hydraulic conductivity at 60 °C than at 20 °C. Özhan (2018) demonstrated that the hydraulic conductivity of BPC-GCLs containing anionic or cationic polymers increased with increasing temperature when permeated with MgCl₂ solutions. In contrast, Yu et al. (2020) report that a BPC containing polymacrylamide had reduced healing capacity and higher hydraulic conductivity than unamended NaB when exposed to temperatures from 40 to 78 °C and permeated with brine.

In addition to the effects of temperature on NaB, changes to the degradation and flow properties of viscoelastic polymer gels in BPC-GCLs may impact hydraulic conductivity. For example, when polymers in BPC-GCLs dissolve in permeating solutions, the viscosity of the permeant increases (Scalia et al. 2014; Geng et al. 2016; Tian et al. 2016a, 2019; Özhan 2017, 2018), and changes in permeant viscosity with temperature impact hydraulic conductivity (Cho et al. 1999; Geng et al. 2016; Özhan 2017, 2018).

2.4 CONCLUSIONS

The hydraulic conductivity of BPC-GCLs and polymer-modified bentonites varies depending on the components of the BPC-GCL (i.e., polymer, bentonite and geotextiles) as well as the environmental conditions of the application (i.e., leachate chemistry and temperature). A plethora of BPC-GCL/application pairs are possible, especially as the market expands with additional proprietary polymers. Therefore, to facilitate effective design of containment systems, index tests are needed to assess the hydraulic performance and longevity of BPC-GCLs. This dissertation delves into the mechanisms controlling hydraulic conductivity of BPC-GCLs, then explores recommended testing and procedures for estimating the hydraulic conductivity and service life of BPC-GCLs under various conditions.

Chapter 3: Polymer Elution and Hydraulic Conductivity of Bentonite-Polymer Composite Geosynthetic Clay Liners Permeated with Aggressive Solutions

This chapter is an excerpt of work published in the proceedings of GeoAmericas 2020, the 4th Pan American Conference on Geosynthetics. The citation is as follows:

Gustitus, S.A., & Benson, C.H. (2020). Using Flow Stress to Assess Polymer Elution and Hydraulic Conductivity of Bentonite-Polymer Composite Geosynthetic Clay Liners Permeated with Aggressive Solutions. GeoAmericas Online 2020. Oct 26-31, 2020.

3.1 INTRODUCTION

Geosynthetic clay liners (GCLs) are used for lining containment systems, such as solid waste landfills, waste impoundments, lagoons, and tailing impoundments. Conventional GCLs are traditionally composed of a layer of granular or powdered sodium bentonite (NaB) bound between two geotextiles. Montmorillonite, the primary mineral component of NaB, swells appreciably when hydrated, which reduces the size of pores through which flow is conveyed to create a low hydraulic conductivity barrier (Kolstad et al. 2004; Mitchell and Soga 2005). However, swelling of NaB can be suppressed by aggressive solutions that have high ionic strength or extreme pH (pH<3 or pH>12), leading to hydraulic conductivity that is 3-4 orders of magnitude higher than that of NaB permeated with more dilute solutions (Jo et al. 2001; Shackelford et al. 2010; Chen et al. 2019). Consequently, NaB-GCLs may not be appropriate for containment systems with more aggressive leachates.

Bentonite-polymer composite (BPC) GCLs can maintain low hydraulic conductivity in applications where NaB-GCLs are too permeable (Trauger and Darlington, 2000; Ashmawy et al. 2002; Benson et al. 2010; Scalia et al. 2011, 2014; Athanassopoulos et al. 2015; Scalia and Benson,

2016). Applications of BPC-GCLs include containment of mining and industrial process wastes (e.g., bauxite, also known as red mud) and coal combustion products (Athanasopoulos et al. 2015; Donovan et al. 2017; Tian and Benson, 2018; Chen et al. 2019). Unlike NaB-GCLs, which are sensitive to aggressive solutions, BPC-GCLs can maintain low hydraulic conductivity (10^{-13} to 10^{-10} m/s) to solutions with high ionic strength and extreme pH (Athanasopoulos et al. 2015; Donovan et al. 2017; Scalia et al. 2018, 2014; Tian and Benson, 2018; Chen et al. 2019).

Different mechanisms control the hydraulic conductivity of NaB- and BPC-GCLs, as shown in Fig. 3.1. In NaB-GCLs, intergranular pores close when the bentonite granules swell, resulting in small and tortuous flow paths that correspond to low hydraulic conductivity. For this reason, swelling is a key indicator of hydraulic conductivity of traditional NaB-GCLs (Scalia et al. 2011; Tian et al. 2016a, 2017). For BPCs, the permeant solution hydrates the polymer to create a polymer hydrogel that fills pores between the bentonite granules, creating tortuous flow paths that are responsible for low hydraulic conductivity regardless of whether the NaB component swells (Scalia et al. 2014; Tian et al. 2016a, 2016b). Consequently, swell is not an effective indicator of hydraulic conductivity for BPC-GCLs (Chen et al. 2019).

BPCs maintain low hydraulic conductivity provided the polymer fills the pores in a BPC-GCL. However, the polymer may elute in a viscous effluent while a BPC-GCL is in service (Scalia et al. 2014; Tian et al. 2017a). As elution continues, pores initially filled with polymer are opened and the hydraulic conductivity increases (Tian et al. 2017, 2019). The propensity for polymer elution and the corresponding increase in hydraulic conductivity are influenced by the chemistry of the permeant solution (Tian et al. 2016b, 2017). Commercially available BPC-GCLs contain numerous proprietary polymers, each of which interacts differently with leachates and therefore

has different chemical compatibility. In this study, the relationship between the hydraulic conductivity of BPC-GCLs and polymer elution was investigated.

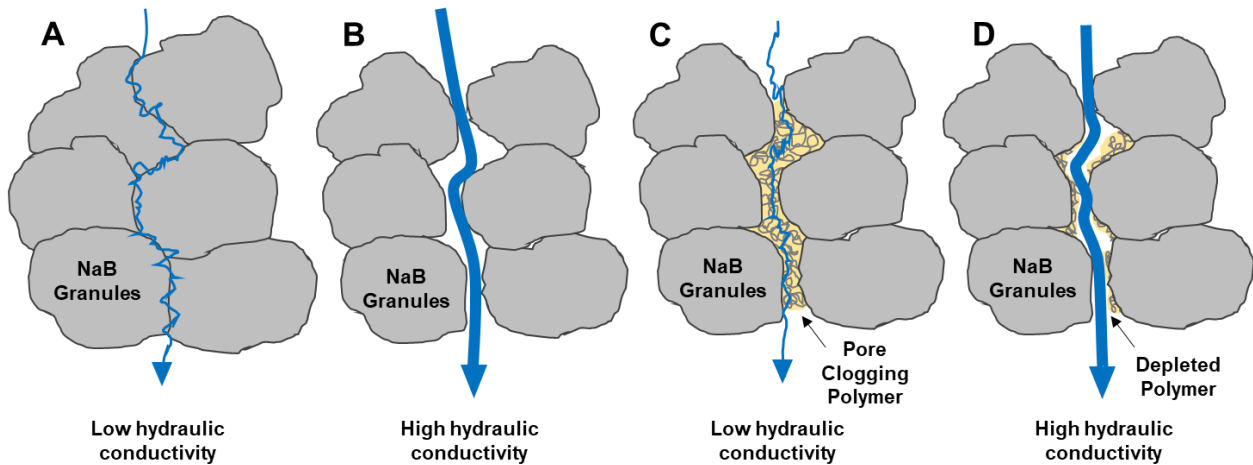


Figure 3.1. (A) NaB granules swell in leachate with low to modest ionic strength, closing inter-granular pores and resulting in low hydraulic conductivity; (B) NaB granules permeated with aggressive leachate do not swell, resulting in larger inter-granular pores and higher hydraulic conductivity; (C) polymer component of BPC fills inter-granular pores, creating a low hydraulic conductivity barrier; (D) elution of polymer results in BPC with higher hydraulic conductivity.

3.2 MATERIALS AND METHODS

Two commercially available BPC-GCLs were used in this study: BPC-GCL-N and BPC-GCL-S. The BPC-GCLs contained proprietary polymers, NaB, and nonwoven upper and lower geotextiles bonded by needlepunching. BPC-GCL-S contained a woven slit film geotextile on the interior to promote polymer retention.

Hydraulic conductivity testing on each BPC-GCL was conducted in flexible-wall permeameters using the falling headwater, constant tailwater method in accordance with ASTM D6766. The average effective stress was 29 kPa and the average hydraulic gradient was 115. BPC-GCLs were hydrated with the permeant solution in the permeameter with the stress applied and

the outflow line closed for 48 h prior to permeation. No backpressure was used to preclude geochemical changes that would not occur at natural porewater pressures. All tests were conducted until the termination criteria in D6766 were satisfied. Effluent from each hydraulic conductivity test was collected in 60 mL HDPE bottles. Polymer content of the effluent was determined based on total carbon (TC) analysis using the solid-state module of a TOC analyzer (Shimadzu TOC-L, Kyoto, Japan). Viscosity of effluent was measured using a rotational viscometer (Brookfield LVE, Middleboro, MA) paired with a low viscosity adapter.

Scanning electron microscopy (SEM) was used to assess structures of polymers in the pore space. Samples approximately 10 mm x 30 mm were cut from each BPC-GCL specimen after permeation and prepared following Tian et al. (2016b). The samples were flash frozen in liquid nitrogen and lyophilized (Labconco Model 7740020, Kansas City, MO). Smaller samples approximately 2 mm thick were removed from the freeze-dried material with a surgical scalpel and sputter-coated with gold. Images were obtained using a FEI Quanta 650 SEM (ThermoFisher Scientific, Hillsboro, Oregon).

3.3 RESULTS AND DISCUSSION

An initial set of duplicate hydraulic conductivity tests was conducted with BPC-GCL-N and BPC-GCL-S using 20 and 100 mM CaCl₂ solutions. The initial hydraulic conductivity of BPC-GCL-N was less than 1×10^{-11} m/s with 20 and 100 mM CaCl₂, whereas the initial hydraulic conductivity of BPC-GCL-S was less than 1×10^{-10} m/s with 20 mM CaCl₂ and less than 6×10^{-10} m/s with 100 mM CaCl₂ (Fig. 3.2). With the exception of BPC-GCL-N with 20 mM CaCl₂, which maintained hydraulic conductivity below 10^{-11} m/s throughout the duration of testing, all specimens eventually reached a hydraulic conductivity greater than 10^{-8} m/s.

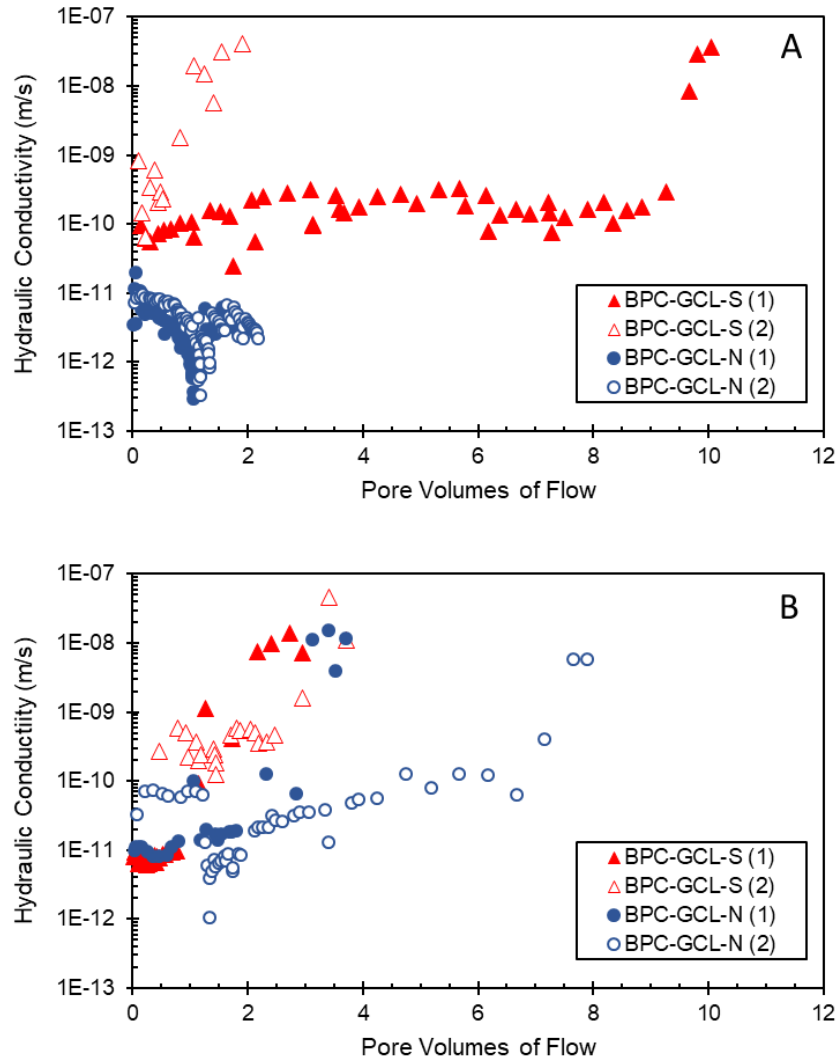


Figure 3.2. Hydraulic conductivity of BPC-GCL-S and BPC-GCL-N permeated with (A) 20 mM CaCl₂ and (B) 100 mM CaCl₂. Numbers in parentheses indicate replicates.

Throughout the duration of testing, polymer content of the effluent was determined by TC analysis. The relationship between hydraulic conductivity and polymer content of the effluent is shown in Fig. 3.3. Polymer content of the effluent decreases as the hydraulic conductivity increases, which can be explained conceptually by elution of polymer from the pore space, as shown in Fig. 3.4. Initially, when the hydraulic conductivity is low, the flow rate is low and small

volumes of effluent with high concentrations of dissolved polymer are produced. The polymer concentration is high because there is a high ratio of polymer to solution in the pore space and the retention time is long, allowing polymer to dissolve into the flowing pore water (Fig. 3.4A). In contrast, when the hydraulic conductivity is high, larger volumes of effluent are conducted that have lower polymer concentration because the solution moves quickly through pore spaces depleted of polymer, reducing the amount of polymer contacted by solution and the contact time (Fig. 3.4B).

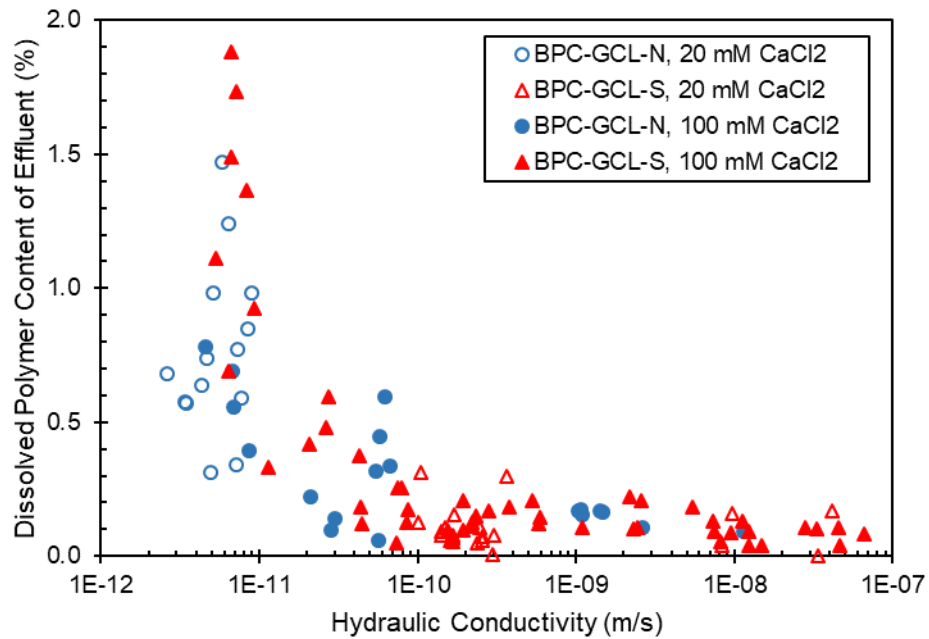


Figure 3.3. Dissolved polymer content of effluent as a function of hydraulic conductivity when the effluent was collected.

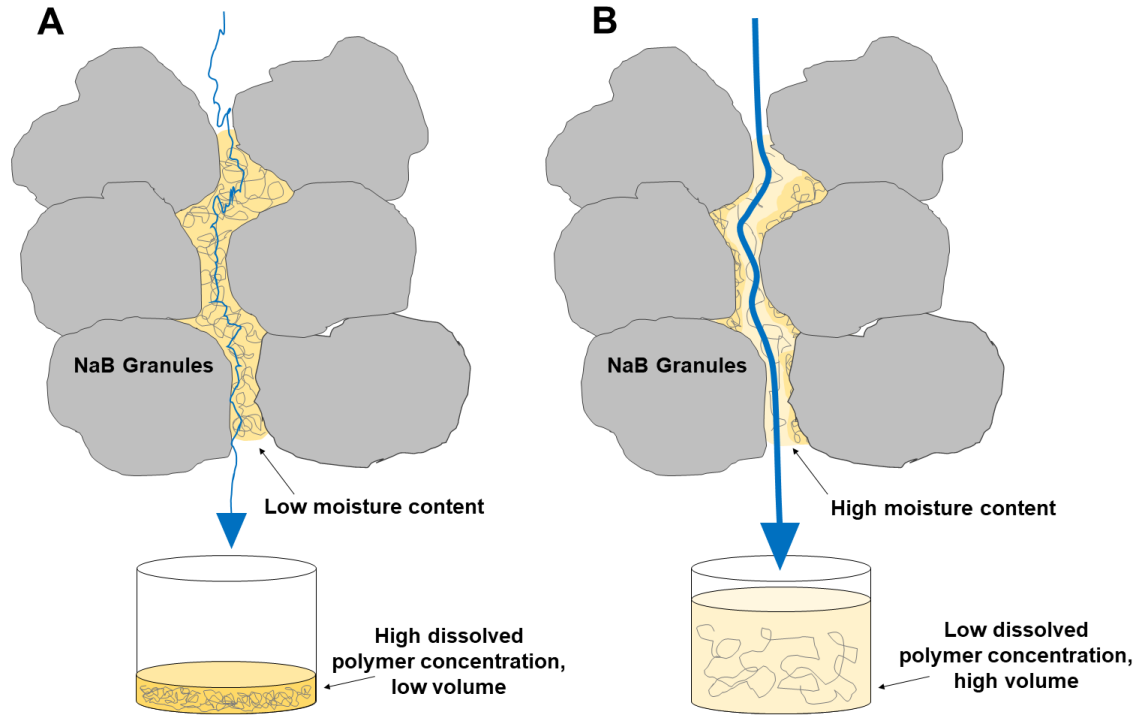


Figure 3.4. Conceptual model showing how properties of the polymer hydrogel and effluent change during polymer elution from a BPC-GCL. (A) High polymer to solution ratio in the pore space at low hydraulic conductivity leads to increased contact between the pore water and the polymer gel, and higher polymer content of the effluent; (B) Lower polymer to solution ratio when the hydraulic conductivity is higher leads to less contact between the pore water and the polymer gel, and lower polymer content of the effluent.

Changes in hydraulic conductivity occur in response to changes in the porous medium and/or the fluid properties. To evaluate which mechanism is responsible for the alterations in hydraulic conductivity shown in Figs. 3.2 and 3.3, intrinsic permeability was calculated using the viscosity of the effluent:

$$k = \frac{k_i \rho g}{\mu} \quad [3.1]$$

where k is the hydraulic conductivity, k_i is the intrinsic permeability, ρ is the density of the eluent, g is the acceleration due to gravity, and μ is the measured dynamic viscosity. Intrinsic permeability represents the geometry of the pore space (size, shape, and tortuosity) and is independent of the hydrodynamic properties of the permeant liquid.

An example of changes in intrinsic permeability as a function of pore volumes of flow (PVF) is shown in Fig. 3.5 for BPC-GCL-S permeated with 20 mM CaCl₂. The intrinsic permeability increases concomitantly with hydraulic conductivity, indicating that the change in hydraulic conductivity is predominantly due to opening of the pore space due to polymer elution.

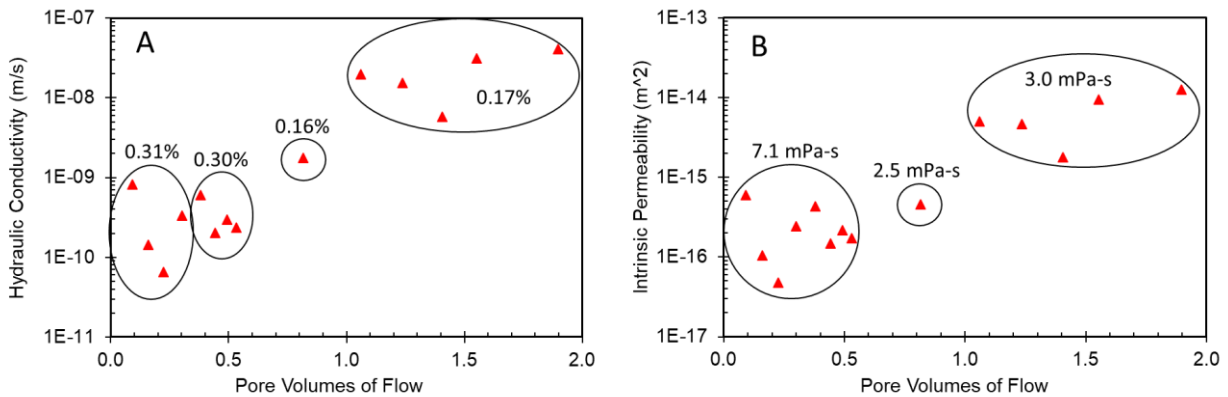


Figure 3.5. (A) Hydraulic conductivity and (B) intrinsic permeability of BPC-GCL-S permeated with 20 mM CaCl₂. Called out data represent (A) dissolved polymer content and (B) viscosity of effluent.

The opening of large pores results in preferential flow paths through which the majority of flow passes, yielding high hydraulic conductivity. Specimens that had hydraulic conductivity greater than 5×10^{-9} m/s were permeated with rhodamine dye, disassembled, and visually inspected for stained flow paths. Flow paths on the order of 1 to 10 mm wide were present in isolated locations in each specimen (Fig. 3.6). The number of flow paths per specimen ranged from 1 to 5,

with several specimens having only 1 to 2 preferential flow paths. The low number of flow paths indicates that polymer is eluted from isolated locations rather than uniformly across the BPC-GCL.

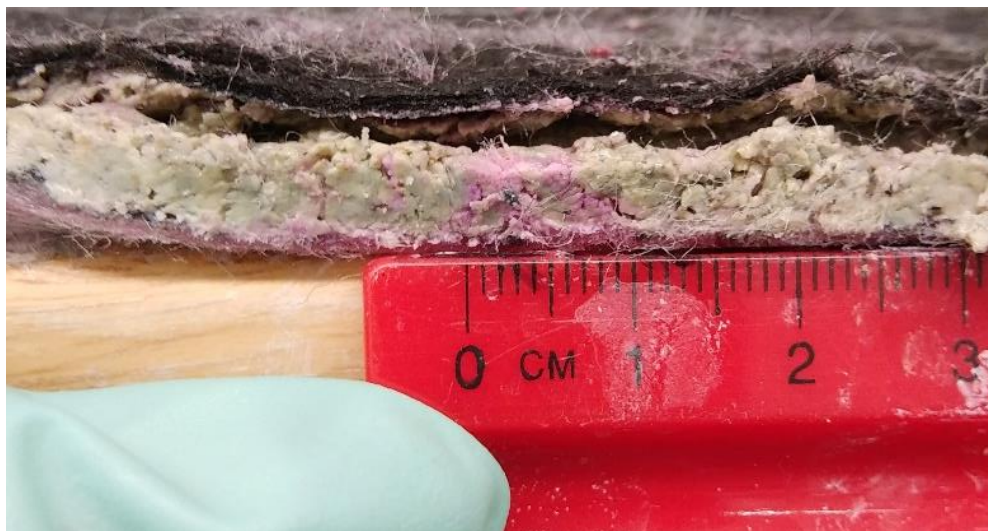


Fig. 3.6. Example of preferential flow path dyed pink in BPC-GCL-N.

To further investigate changes in the polymer arrangement, the BPC-GCLs were analyzed using SEM. BPC-GCL specimens that were hydrated, but not permeated, were used to examine initial conditions. Two polymer structures were observed in the initial conditions: sheets (Fig. 3.7A) and honeycombs (Fig. 3.7B). Stringy structures (Fig. 3.7C) were observed in addition to sheet and honeycomb structures in BPC-GCLs that had been permeated and underwent an increase in hydraulic conductivity. The stringy structures appear to be remnants of the sheet or honeycomb structures. The sheet and honeycomb structures appear to completely fill the pore space, whereas the stringy structures do not. All three structures could be found in the same specimen after permeation, but stringy structures were never present prior to permeation. The presence of all three structures in the specimens with high hydraulic conductivity indicates that polymer loss does not occur uniformly across a BPC-GCL.

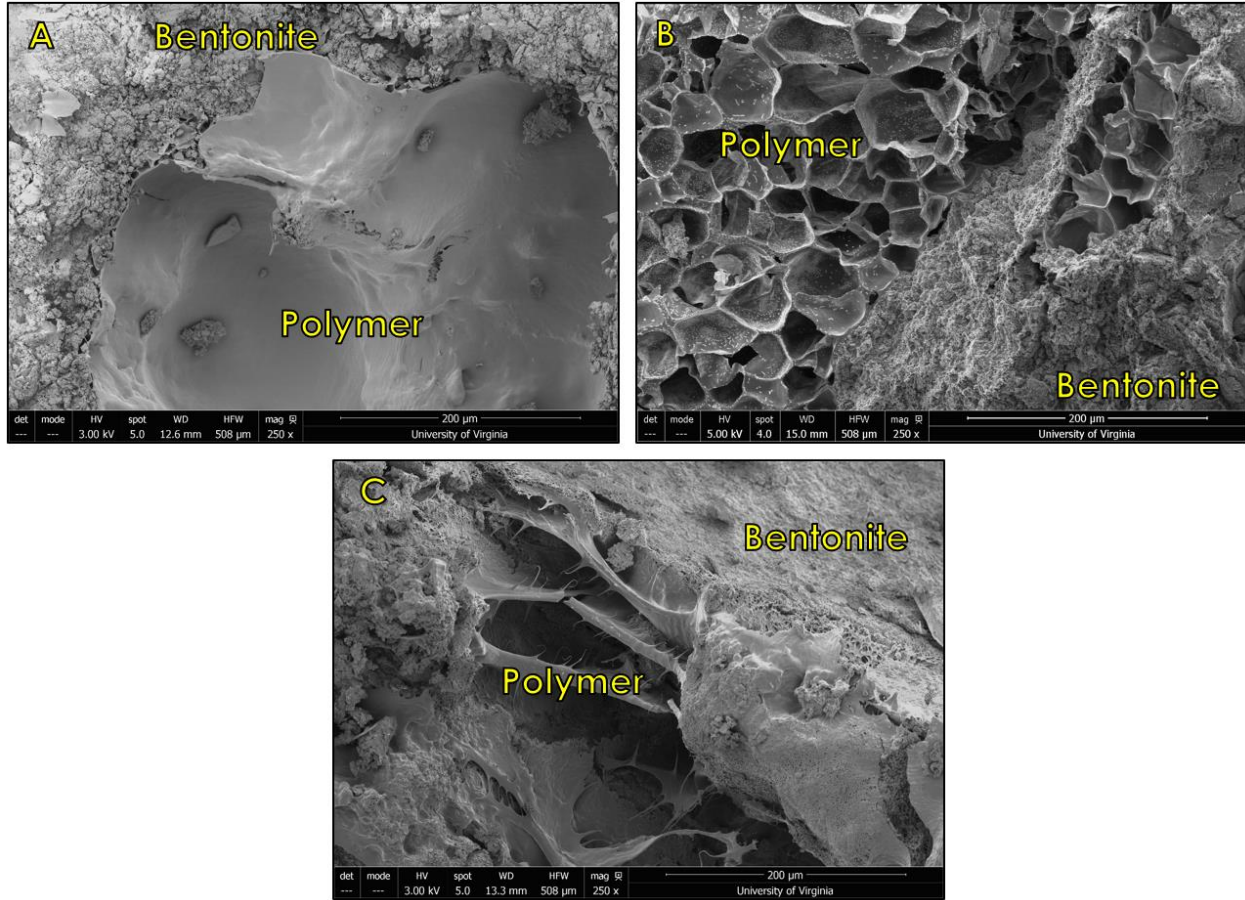


Figure 3.7. (A) Sheet, (B) honeycomb, and (C) string polymer structures found in BPC-GCLs.

3.4 SUMMARY AND CONCLUSIONS

Tests were conducted to evaluate the relationship between hydraulic conductivity and polymer elution from BPC-GCLs. The findings illustrate that the hydraulic conductivity of BPC-GCLs is controlled by polymer gels in the pore space when aggressive leachates suppress swelling of the bentonite fraction. When the polymer forms a gel that fills pores between bentonite granules, and that gel is retained in the pores in the presence of leachate, low hydraulic conductivity is maintained. If the polymer gel is eluted, the hydraulic conductivity increases as larger pores open for flow. Elution of polymer generally occurs in localized regions, forming preferential flow paths

that are responsible for high hydraulic conductivity. SEM images demonstrated that polymer that originally fills the pore space is altered by elution during permeation, and dye studies confirmed that polymer elution results in the preferential flow paths in BPC-GCLs with high hydraulic conductivity.

Chapter 4: Flow-Swell Index for Predicting Long-Term Hydraulic Conductivity of Bentonite-Polymer Composite Geosynthetic Clay Liners

4.1 INTRODUCTION

Bentonite polymer composite (BPC) geosynthetic clay liners (GCLs) are used to contain aggressive solutions for which traditional sodium bentonite (NaB) GCLs are too permeable. BPC-GCLs are comprised of a dry blend of NaB and polymer contained between two geotextiles bonded by needlepunching. BPC-GCLs are used to contain wastes in applications where conventional NaB GCLs may be incompatible, such as mining and ore beneficiation, petroleum exploration and production, environmental restoration of uranium and plutonium production, and coal combustion products (Athanasopoulos et al. 2015; Tian et al. 2016a; Donovan et al. 2017; Tian and Benson 2018; Chen et al. 2019).

Mechanisms controlling the hydraulic conductivity of NaB- and BPC-GCLs are illustrated in Fig. 4.1. The hydraulic conductivity of conventional NaB-GCLs is controlled by constriction of intergranular pores as the NaB granules swell during hydration. Low hydraulic conductivity is achieved when swelling of the granules is sufficient to create narrow and tortuous flow paths. With adequate swelling, NaB has hydraulic conductivities on the order of 10^{-11} m/s (Gleason et al. 1997; Petrov et al. 1997; Kolstad et al. 2004; Mitchell and Soga 2005). However, if swelling is suppressed when the NaB is hydrated or permeated with aggressive solutions (i.e., solutions with high ionic strength, polyvalent cations, $\text{pH} < 3$, or $\text{pH} > 12$), larger and less tortuous pores remain, resulting in hydraulic conductivities two to four orders of magnitude higher (Jo et al. 2001; Hornsey et al. 2010; Shackelford et al. 2010; Chen et al. 2019; Prongmanee and Chai 2019; Wang et al. 2019). For this reason, the hydraulic conductivity of NaB GCLs is strongly and inversely

related to swell index measured with ASTM D5890 using the permeation solution for hydration (Standard Test Method for Swell Index of Clay Mineral Component of Geosynthetic Clay Liners).

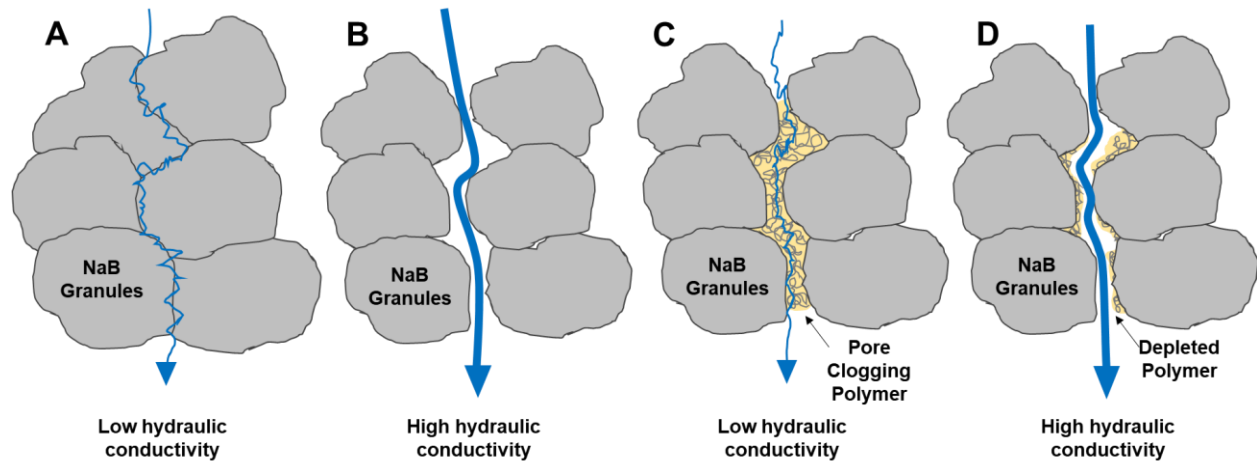


Figure 4.1. (A) Bentonite with swollen granules and narrow and tortuous flow paths that yield low hydraulic conductivity; (B) bentonite with suppressed granule swelling and are larger and less tortuous flow paths that yield high hydraulic conductivity; (C) bentonite-polymer composite with polymer gel filling intergranular pores, yielding low hydraulic conductivity; and (D) bentonite-polymer composite after elution of polymer gel, with larger and less tortuous flow paths and high hydraulic conductivity.

Hydraulic conductivity of BPC-GCLs is controlled by swelling of the NaB component and pore clogging by the viscoelastic polymer gels that form during hydration (Scalia et al. 2011; Chen et al. 2019). Even when NaB swell is limited, BPC-GCLs can maintain low hydraulic conductivity provided the polymer loading is sufficient to fill the intergranular pores and the gel remains within the pore space, creating narrow and tortuous flow paths similar to those found in highly swollen NaB (Scalia et al. 2014; Tian et al. 2016a; b; Özhan 2018). However, if a sufficient amount of the polymer elutes from the pore space, preferential flow paths form and the hydraulic conductivity of BPC-GCLs can increase dramatically (Tian et al. 2019; Gustitus and Benson 2020). Swell index measured with ASTM D5890 does not capture the pore clogging and elution mechanisms associated with the polymer. Therefore, correspondence does not exist between the hydraulic

conductivity of BPC-GCLs and swell index (McRory and Ashmawy 2005; Scalia et al. 2011, 2014; Salihoglu et al. 2016; Chen et al. 2019).

No standardized indices currently exist to screen BPC-GCLs for chemical compatibility. Indices that have been proposed include water vapor sorption (Akin et al. 2017), rapid fluid indicator testing (Norris et al. 2019), and viscosity of the BPC hydrated with the permeant solution (Geng et al. 2016). General correspondence between hydraulic conductivity and these indices has not yet been demonstrated or their generality has yet to be proven (Geng et al. 2016; Akin et al. 2017; Norris et al. 2019). In a manner similar to the correspondence between the hydraulic conductivity of NaB GCLs and swell index, an effective index for evaluating the compatibility of BPC-GCLs and permeant solutions should represent the mechanisms controlling hydraulic conductivity of a BPC, namely retention of polymer in the pore spaces between NaB granules and swelling of the NaB granules.

In this study, two indices of compatibility were evaluated that are related to these mechanisms: flow stress, the shear stress at which the polymer gel transitions to flow like a liquid rather than deforming as an elastic solid (Mezger 2015), and swell index of the NaB component. These indices were evaluated independently and in conjunction with each other.

4.2 MATERIALS

Five commercially available BPC-GCLs were used in this study: BPC-GCL-P1, BPC-GCL-P2, BPC-GCL-P3L, BPC-GCL-P3H, and BPC-GCL-P4. The polymer and polymer loading in each BPC-GCL is summarized in Table 4.1. All five BPC-GCLs consisted of BPC constrained by upper and lower nonwoven geotextiles bound by needlepunching. BPC-GCL-P3H contained a woven slit-film geotextile between the bentonite and the lower non-woven geotextile. The same granular NaB was used as the bentonite component for each BPC-GCL. Four different polymers

were used: P1-P4. All of the polymers are synthetic and water-soluble or water-swellaable, and are proprietary to the manufacturers; therefore, their exact chemical formulations are not available.

Table 4.1. Characteristics of the polymers contained in the BPC-GCLs used in this study.

BPC-GCL	Avg polymer loading (g polymer/kg BPC)	Polymer	Polymer structure	Polymer application
BPC-GCL-P1	6.5	P1	Cross-linked	Alkaline solutions
BPC-GCL-P2	6.0	P2	Cross-linked	Acidic solutions
BPC-GCL-P3L	2.5	P3	Linear	Neutral or alkaline solutions
BPC-GCL-P3H	4.0			
BPC-GCL-P4	4.5	P4	Mixture of cross-linked and linear	High ionic strength solutions

Quantitative X-ray diffraction (XRD) conducted using the methods in Moore and Reynolds (1989) and Scalia et al. (2014) indicate that the montmorillonite content of the bentonite is 75% and the cristobalite content is 16%. The bentonite also contains measurable quantities of tridymite (3%), oligoclase (3%), quartz (1%), calcite (1%) and gypsum (1%). Granule size distribution measured following ASTM D6913 indicates that 100% of the NaB was finer than a US No. 10 (2 mm) sieve, 39% was finer than a US No. 20 (0.841 mm) sieve, and 0.9% was finer than a US No. 200 (0.074 mm) sieve.

Five solutions were used as permeants: 50 mM CaCl₂ (electrical conductivity, EC = 1.0 S/m; pH 5.8), 100 mM CaCl₂ (EC = 1.5 S/m), synthetic bauxite liquor (EC = 6.6 S/m; pH 13.5), the European Comité Européen de Normalisation (CEN) standard alkaline solution (EC = 1.4 S/m; pH 12.4), and the CEN standard acidic solution (EC = 1.4 S/m, pH 1.8). The CEN solutions are described in EN 14030:2001. The synthetic bauxite liquor contained 287.2 mM NaOH, 0.06 mM

CaCl₂, 3.0 mM KCl, 0.3 mM Na₃PO₄, 0.4 mM NaNO₃, 54.2 mM Na₂O-Al₂O₃, 19.1 mM NaCl, and 5.0 mM Na₂SO₄.

4.3 METHODS

4.3.1 Hydraulic Conductivity

Hydraulic conductivity was determined using the falling headwater, constant tailwater method with flexible-wall permeameters in accordance with ASTM D6766. The average effective stress was 29 kPa and the average hydraulic gradient was 115. No backpressure was used to preclude geochemical changes that would not occur at natural porewater pressures. Prior to permeation, GCLs were hydrated with the permeant solution in the permeameter with the stress applied and the outflow line closed for 48 h. Tests were conducted until the hydraulic conductivity was steady, inflow equaled outflow, and the EC of the influent and effluent were within 10%.

4.3.2 In-Situ Gel Moisture Content

Flow stress of a polymer gel depends on the moisture content of the gel. However, in-situ moisture content of the polymer gels in BPCs cannot be measured directly because the polymer component cannot be separated from the bentonite component in a hydrated BPC. A bentonite-polymer moisture affinity test was developed to estimate the in-situ moisture content of both components. The bentonite-polymer moisture affinity test allows the polymer and NaB components to compete for moisture in a manner similar to hydration in a BPC, while still remaining readily separable for moisture content analysis.

A depiction of the bentonite-polymer moisture affinity test is shown in Fig. 4.2. The test is completed in a sealable hydration container with 7-mm-wide test compartments. Within a

compartment, oven-dry NaB and oven-dry polymer are added to opposite sides of a 5 μm polyester filter. A polymeric filter was used to minimize moisture uptake by the filter. Twelve grams of bentonite and polymer were used in proportion to the polymer loading of the BPC-GCL. Each component was evenly distributed across the face of the filter using a small spatula. Solution (12 g) was added to the filter using a bulb dropper to achieve a target moisture content of 100%. The container was then sealed for at least 48 hr, after which the hydrated polymer and NaB were removed and placed in separate drying containers. Moisture content of each hydrated component was measured in accordance with ASTM D2216.

Triplicate tests were performed for each BPC. To avoid cross-contamination from the polymer, bentonite was not collected within 1 mm of the edge of the filter (Fig 4.3). Cross-contamination of the polymer with bentonite was visually identifiable, and any such spots were avoided. Even hydration of the components was confirmed via visual inspection on completion of the test.

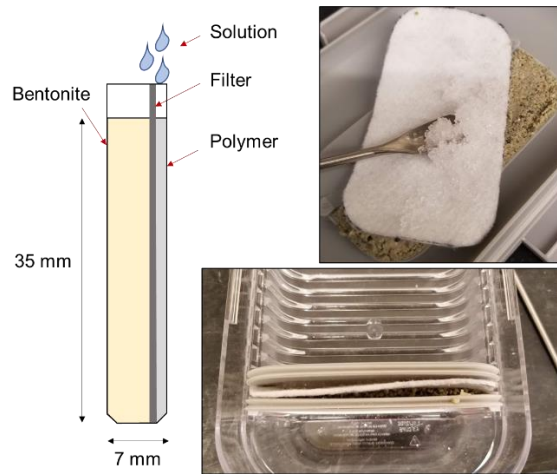


Figure 4.2. Schematic illustration of bentonite-polymer moisture affinity test (left), hydrated polymer and bentonite components at end of test (top right), and top view of filled test compartment (bottom right).

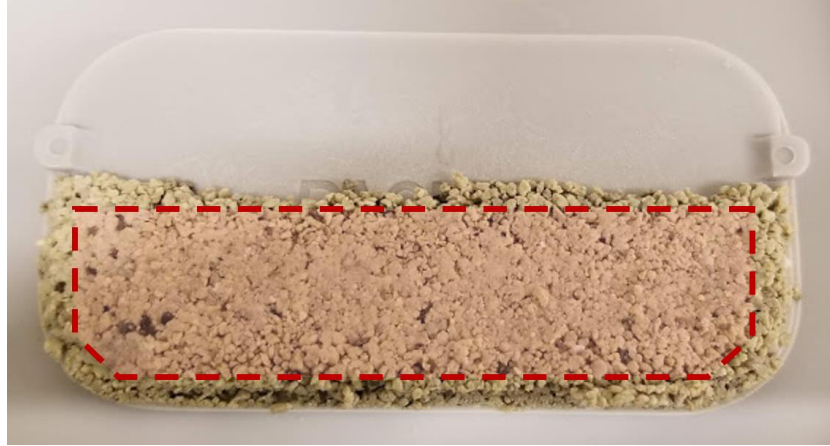


Figure 4.3. Hydrated bentonite after termination of a bentonite-polymer moisture affinity test. Red box outlines portion of bentonite removed to determine moisture content.

4.3.3 Viscoelastic Properties of Polymer Gels

Storage and loss moduli of polymer gels were measured using shear-strain-amplitude sweeps with controlled-shear deformation on an Anton Paar MCR 302 rheometer (Anton Paar, Austria). Amplitude sweeps were completed over a range of 0.01 to 10,000% shear strain using a 25-mm-diameter sandblasted parallel plate. Flow stress of the hydrated polymer gels was determined as the cross-over point of the storage modulus and loss modulus. Polymer gels used in the test were hydrated to moisture contents of 200%, 500%, 1000% and 2000%, encompassing the range of moisture contents determined using the bentonite-polymer moisture affinity tests.

4.3.4 Polymer Loading

Polymer loading of BPC-GCLs and concentration of polymer in effluent from the hydraulic conductivity tests was determined using total carbon analysis following the methods in Gustitus et al. (2020). A Shimadzu TOC-L analyzer (Kyoto, Japan) paired with a solid sample module (SSM) was used for analysis.

4.4 RESULTS

4.4.1 Hydraulic Conductivity

Hydraulic conductivities of the BPC-GCLs are summarized in Table 4.2. Two hydraulic conductivities are reported for each GCL corresponding to “early equilibrium” and “longer-term equilibrium” hydraulic conductivity. Early equilibrium is the first hydraulic conductivity for which the flow is stable (three or more measurements of hydraulic conductivity are between 0.75 to 1.25 times the average), and the ratio of inflow to outflow rate is between 0.75 to 1.25, and effluent EC is within 10% of influent EC (per termination criteria for ASTM D6766). Longer-term hydraulic conductivity is the final hydraulic conductivity (BPC-GCLs that had hydraulic conductivity $>1 \times 10^{-9}$ m/s), or the hydraulic conductivity at the time of writing (BPC-GCLs that have maintained hydraulic conductivity below 1×10^{-9} m/s). Both early and longer-term hydraulic conductivities are reported because equilibrium conditions and termination criteria for BPC-GCLs have not yet been identified. Early hydraulic conductivities may satisfy the termination criteria in ASTM D6766, but may not reflect the actual equilibrium hydraulic conductivity. The elapsed testing time and the pore volumes of flow (PVF) corresponding to both conditions are summarized in Table 4.2.

Table 4.2. Hydraulic conductivities of GCLs. Early equilibrium refers to the first time a GCL met the termination criteria prescribed in ASTM D6766, and late equilibrium or current status refers to the final equilibrium of the GCL or the status at the time of writing. PVF is pore volumes of flow (estimated for samples currently running).

GCL	Permeant Solution	Early Equilibrium			Longer-Term Equilibrium or Current Status		
		Hydraulic Conductivity (m/s)	Pore Volumes of Flow	Elapsed Time (days)	Hydraulic Conductivity (m/s)	Pore Volumes of Flow	Elapsed Time (days)
BPC-GCL-P1	50 mM CaCl ₂	5.6 x 10 ⁻¹²	0.8	50	4.2 x 10 ⁻⁸	2.9	62
	100 mM CaCl ₂	4.4 x 10 ⁻⁸	3.7	0.1	4.4 x 10 ⁻⁸	3.7	0.1
	CEN Alkaline Standard	4.4 x 10 ⁻¹²	2.5	181	6.8 x 10 ⁻¹²	6.6	579
	Synthetic Bauxite	4.1 x 10 ⁻¹²	2.2	150	2.5 x 10 ⁻¹²	5.1	576
BPC-GCL-P2	50 mM CaCl ₂	2.5 x 10 ⁻⁸	3.2	0.2	2.5 x 10 ⁻⁸	3.2	0.2
	CEN Acidic Standard	2.4 x 10 ⁻¹¹	2.3	41	1.4 x 10 ⁻¹⁰	32.2	293
BPC-GCL-P3L	50 mM CaCl ₂	6.3 x 10 ⁻⁹	3.3	0.4	6.3 x 10 ⁻⁹	3.3	0.4
BPC-GCL-P3H	50 mM CaCl ₂	7.6 x 10 ⁻⁹	2.6	0.2	6.0 x 10 ⁻⁹	3.9	0.3
	100 mM CaCl ₂	2.0 x 10 ⁻⁸	2.8	0.1	2.0 x 10 ⁻⁸	2.8	0.1
	CEN Alkaline Standard	1.3 x 10 ⁻¹²	1.0	164	1.3 x 10 ⁻¹²	1.0	164
	Synthetic Bauxite	2.2 x 10 ⁻¹²	4.1	286	6.7 x 10 ⁻¹²	10.6	458
BPC-GCL-P4	50 mM CaCl ₂	3.4 x 10 ⁻⁹	4.6	0.6	3.4 x 10 ⁻⁹	4.6	0.6

Hydraulic conductivities of the BPC-GCLs ranged from 1.3 x 10⁻¹² m/s for BPC-GCL-P3H with the CEN alkaline standard solution to 4.4 x 10⁻⁸ m/s for BPC-GCL-P1 with 100 mM CaCl₂. Some BPC-GCLs maintained relatively consistent hydraulic conductivity throughout permeation, while others varied significantly (Fig 4.4).

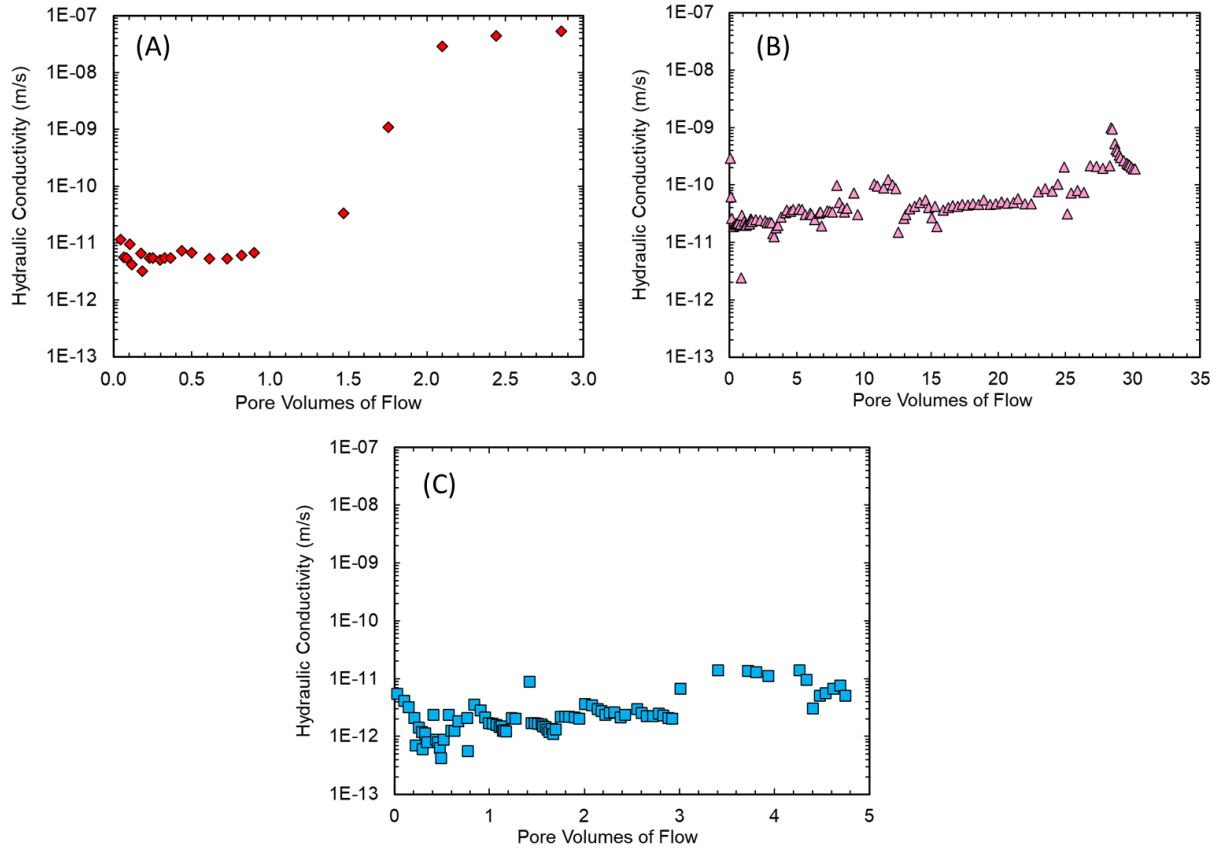


Figure 4.4. Hydraulic conductivity vs. pore volumes of flow for (A) BPC-GCL-P1 permeated with 50 mM CaCl₂ illustrating a sudden jump in hydraulic conductivity; (B) BPC-GCL-P2 permeated with CEN acidic standard solution illustrating gradual increase in hydraulic conductivity and (C) BPC-GCL-P3H permeated with synthetic bauxite solution that retained relatively consistent hydraulic conductivity.

4.4.2 Moisture Content

Moisture contents of the polymer gel and NaB components within each BPC-GCL estimated from the moisture affinity tests are summarized in Table 4.3. Total BPC moisture content from the competitive hydration test was confirmed to be between 90-110%, which is comparable to the total moisture content of 100% that is used to determine the masses of NaB, polymer, and solution used in the test. The total moisture content (~100%), compartment width (7 mm), and BPC loading (~3 kg/m²) are representative of typical conditions for the BPC-GCLs used in this

study. Actual widths varied from 6 to 9 mm, and actual total moisture contents ranged from 80 to 120%. The hydrated polymer gels appeared visually similar to the gels observed in hydrated BPC-GCLs.

Table 4.3. Moisture content and flow stress of in-situ polymer gel from bentonite-polymer moisture affinity test; swell indices of NaB and BPC for each GCL; flow-swell index defined as product of polymer flow stress and NaB swell index.

GCL	Permeant Solution	Polymer Gel Moisture Content (%)	Polymer Gel Flow Stress (kPa)	NaB Swell Index (mL/2g)	BPC Swell Index (mL/2g)	Flow-Swell Index (kPa·mL/2g)
BPC-GCL-P1	50 mM CaCl ₂	613	1.23	11	11	13.5
	100 mM CaCl ₂	603	1.67	10	10	16.7
	CEN Alkaline Standard	685	1.07	31	29	33.2
	Synthetic Bauxite	405	1.21	11	13	13.3
BPC-GCL-P2	50 mM CaCl ₂	569	0.61	11	14	6.7
	CEN Acidic Standard	682	0.85	19	27	16.2
BPC-GCL-P3L	50 mM CaCl ₂	780	0.79	11	12	8.6
BPC-GCL-P3H	50 mM CaCl ₂	667	1.07	11	11	11.7
	100 mM CaCl ₂	621	1.12	10	12	11.2
	CEN Alkaline Standard	573	1.36	31	41	42.1
	Synthetic Bauxite	563	2.24	11	13	24.6
BPC-GCL-P4	50 mM CaCl ₂	983	0.45	11	17	5.0

The moisture contents in Table 4.3 represent expected in-situ moisture contents for the polymer immediately following hydration of the BPC. Gel moisture content ranged from 405% for BPC-GCL-P1 with synthetic bauxite liquor to 780% for BPC-GCL-P3L with 50 mM CaCl₂. Moisture content of the hydrated NaB ranged from 51% for BPC-GCL-P1 with CEN alkaline solution to 80% for BPC-GCL-P3L with 50 mM CaCl₂. For each BPC-GCL, the moisture contents of the components varied with the hydrating solution (Fig 4.5). For example, the moisture content

of polymer P1 in BPC-GCL-P1 varied from 405% with synthetic bauxite solution to 685% with the CEN alkaline standard solution.

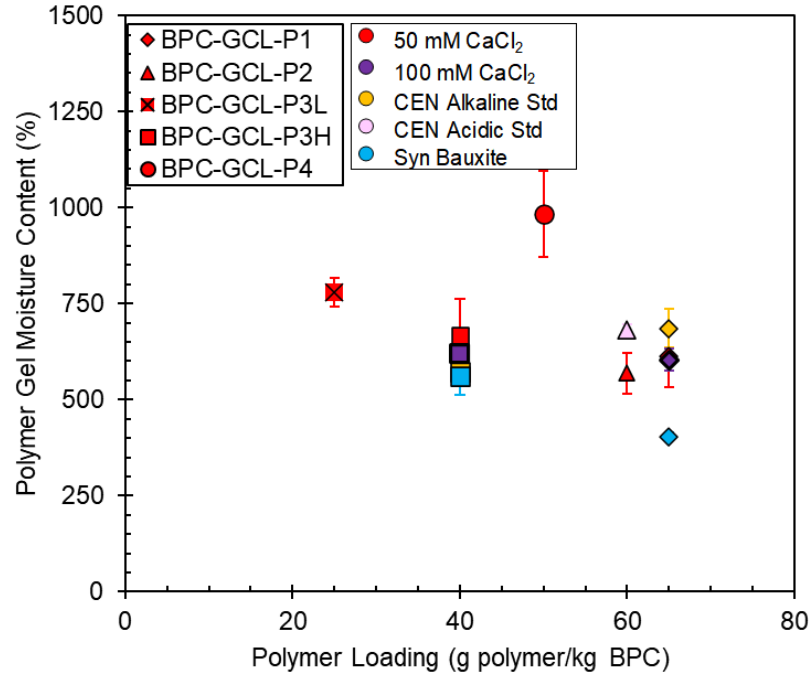


Figure 4.5. Polymer gel moisture content from bentonite-polymer moisture affinity test as a function polymer loading for each BPC hydrated in varying solutions at the same polymer loading as the BPC-GCL.

Polymer loading may vary either temporally as a result of elution during permeation, or spatially as a result of inconsistent polymer distribution across a BPC-GCL. Polymer loading may also vary by design (e.g., BPC-GCL-P3L contains a lower concentration of the same polymer as BPC-GCL-P3H). To assess the effect of variations in polymer loading, BPCs with polymer loading varying from 20 g polymer/kg BPC to the average polymer loading in the corresponding BPC-GCL were hydrated with 50 mM CaCl₂. Gel moisture content decreased with increasing polymer loading for each BPC, hydrated with 50 mM CaCl₂ (Fig. 4.6), as the water available per mass of polymer diminishes as the polymer loading increases.

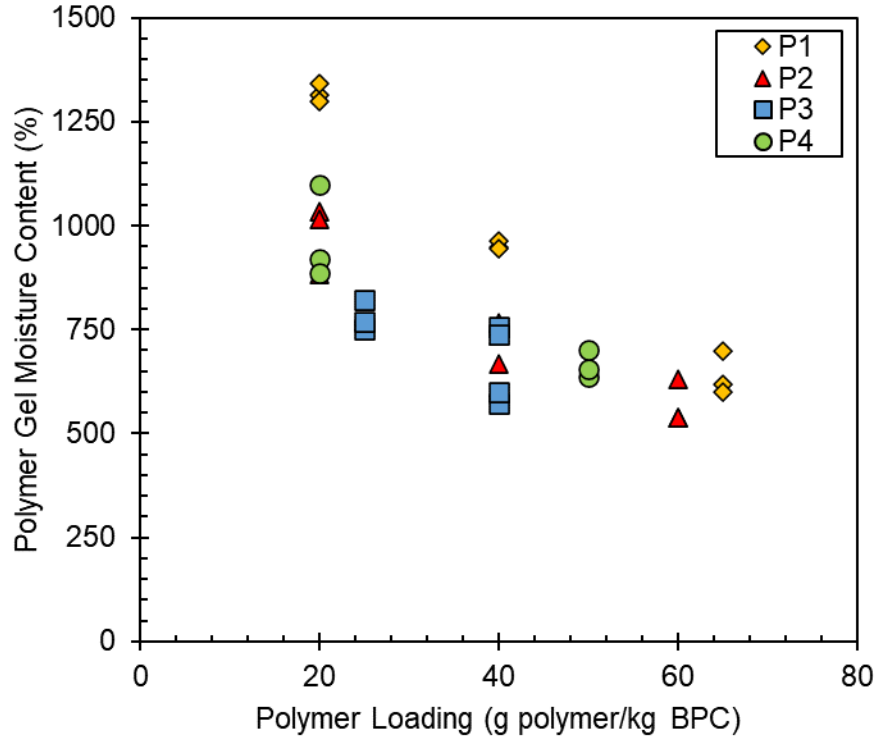


Figure 4.6. Polymer gel moisture content from bentonite-polymer moisture affinity test as a function polymer loading for each BPC hydrated in 50 mM CaCl₂ at various polymer loadings at and below the loading in the BPC-GCL.

4.4.3 Flow Stress of Hydrated Polymer Gels

Flow stress (τ_f) of each gel decreased with increasing moisture content, as shown in Fig. 4.7. The relationship between flow stress and moisture content was unique for each polymer-solution pair, but all followed the power function:

$$\tau_f = \alpha w^\beta$$

where w is the moisture content and α and β are empirically derived parameters. The relationship between flow stress and moisture content depends on both type of polymer (Fig. 4.7A) and the permeant solution (Fig. 4.7B). The relationship between flow stress and moisture content is more sensitive to solution chemistry (e.g., CaCl₂ solution vs. CEN alkaline standard) than to solution concentration (e.g., 50 vs 100 mM CaCl₂). This may indicate that the polymer functional groups

were approaching saturation, resulting in minimal differences in polymer conformation as the solution concentration increased.

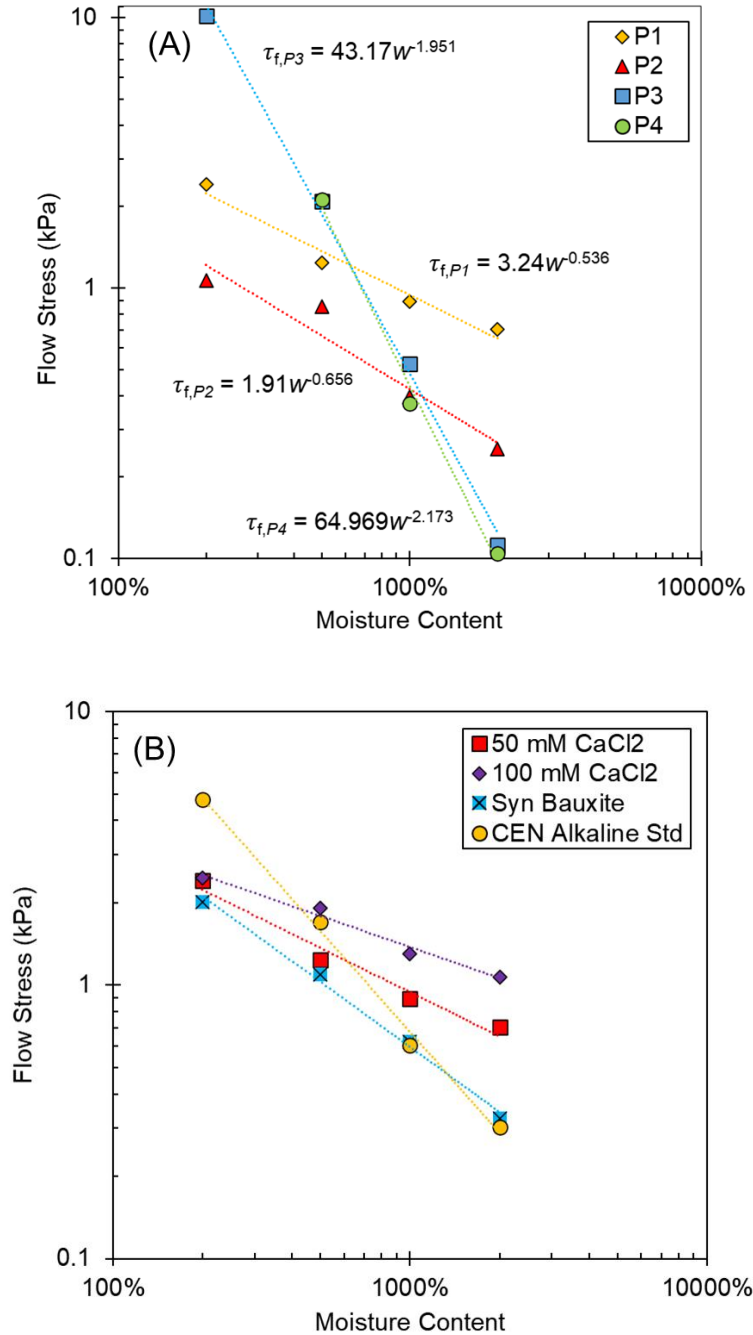


Figure 4.7. Flow stress (τ_f) of hydrated polymer gels as a function of moisture content (w) for each of the polymers hydrated with 50 mM CaCl₂ (A) and polymer P1 hydrated with various permeant solutions (B).

Flow stresses of the gels at the in-situ moisture content are summarized in Table 4.3, and ranged from 0.6 kPa for BPC-GCL-P2 with 50 mM CaCl₂ to 2.2 kPa for BPC-GCL-P3H with synthetic bauxite solution. The moisture content of the polymer, and therefore the flow stress, may vary between pores due to spatial variability of pore size and polymer loading. For example, if two identically sized pores contain slightly different amounts of polymer, the ratio of polymer to solution would be higher in the pore with more polymer, and the resulting gel would have a higher flow stress. Therefore, while the flow stresses reported here are expected to be representative of typical gels in the pore space, gels may also exist with higher or lower flow stress in individual pores.

4.4.4 Swell Index

Swell indices of the NaB and each BPC in the permeant solutions are summarized in Table 4.3. Swell indices of the NaB range from 9 mL/2g in the synthetic high salt solution to 31 mL/2g with the CEN alkaline standard solution. For all of the solutions except the CEN alkaline standard solution, the swell index ranges between 9-12 mL/2 g. Thus, most of the solutions suppress osmotic swelling of the bentonite component, which generally leads to higher hydraulic conductivity. Swell indices of the BPCs ranged from 10 mL/2g for BPC-GCL-P1 with 100 mM CaCl₂ solution to 41 mL/2g for BPC-GCL-P3H with the CEN alkaline standard solution. Swell indices of the BPCs are similar to or higher than the swell index of NaB hydrated in the same solution.

4.4.5 Polymer Elution

Polymer was observed in the effluent of all BPC-GCLs tested in this study. Polymer concentration in the effluent was measured for each BPC-GCL permeated with the 50 mM CaCl₂ solution. For these GCLs, the concentration of polymer in the effluent decreased as hydraulic conductivity increased (Fig 4.8A), but the flux of eluted polymer increased with increasing hydraulic conductivity despite lower polymer concentration (Fig 4.8B).

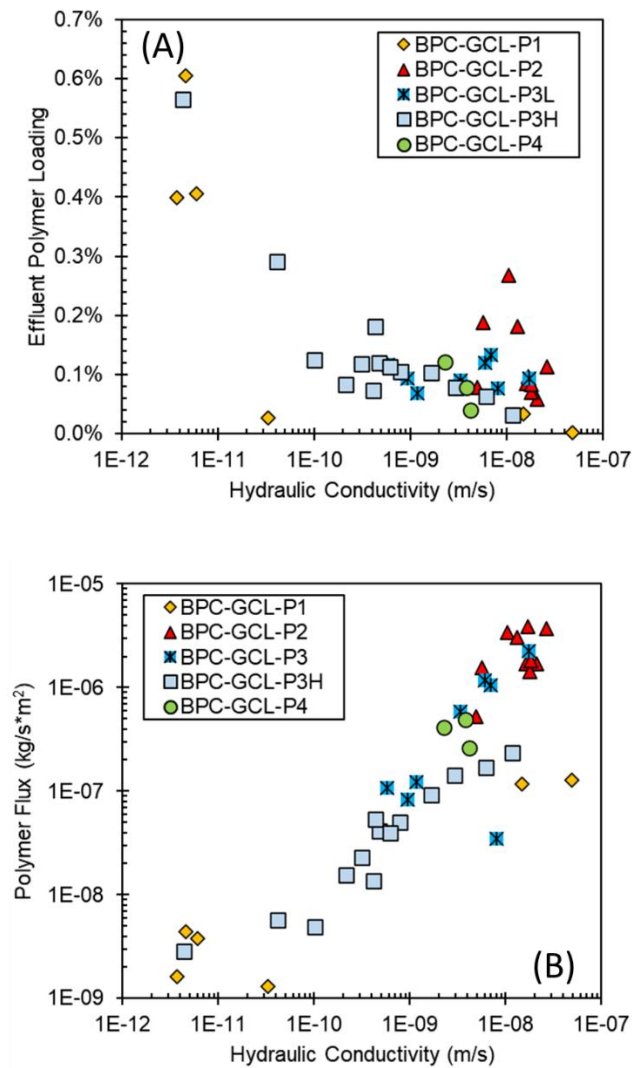


Figure 4.8. Polymer concentration of effluent (A) and polymer flux (B) versus average hydraulic conductivity of the BPC-GCL during the time that the effluent was collected.

4.5 DISCUSSION

Hydraulic conductivity is shown versus flow stress in Figure 4.9A, and versus BPC swell index in Figure 4.9B. No correspondence exists between hydraulic conductivity and either index. For examples, BPC-GCLs with polymer flow stress below 1.5 kPa have hydraulic conductivities ranging from 1.3×10^{-12} to 4.2×10^{-8} m/s. Similarly, BPC-GCLs with a BPC swell index less than 14 mL/2 g have hydraulic conductivities ranging from 2.5×10^{-12} to 4.4×10^{-8} m/s (Fig. 4.9B). Correspondence is lacking for both indices and because neither index accounts for both mechanisms controlling the hydraulic conductivity of BPCs. The narrow tortuous flow paths that yield hydraulic conductivity can be achieved by bentonite granules swelling, polymer clogging intergranular pores, or combination of both mechanisms.

Hydraulic conductivity is shown in Fig 4.10 vs. the product of flow stress of the polymer gel at the in-situ gel moisture content from the bentonite-polymer moisture affinity test and the swell index of the NaB. This product is referred to as the flow-swell index. BPC-GCLs with a flow-swell index less than 11 kPa·mL/2g have high hydraulic conductivity ($>1 \times 10^{-9}$ m/s), whereas BPC-GCLs with a flow-swell index greater than 20 kPa·mL/2g have low hydraulic conductivity ($<1 \times 10^{-11}$ m/s). There is a transition zone corresponding to flow-swell indices ranging from 11 to 20 kPa·mL/2g where the hydraulic conductivity of the BPC-GCLs ranges by approximately four orders of magnitude (from 2.5×10^{-12} m/s for BPC-GCL-P1 with synthetic bauxite liquor to 4.4×10^{-8} m/s for BPC-GCL-P1 with 100 mM CaCl_2).

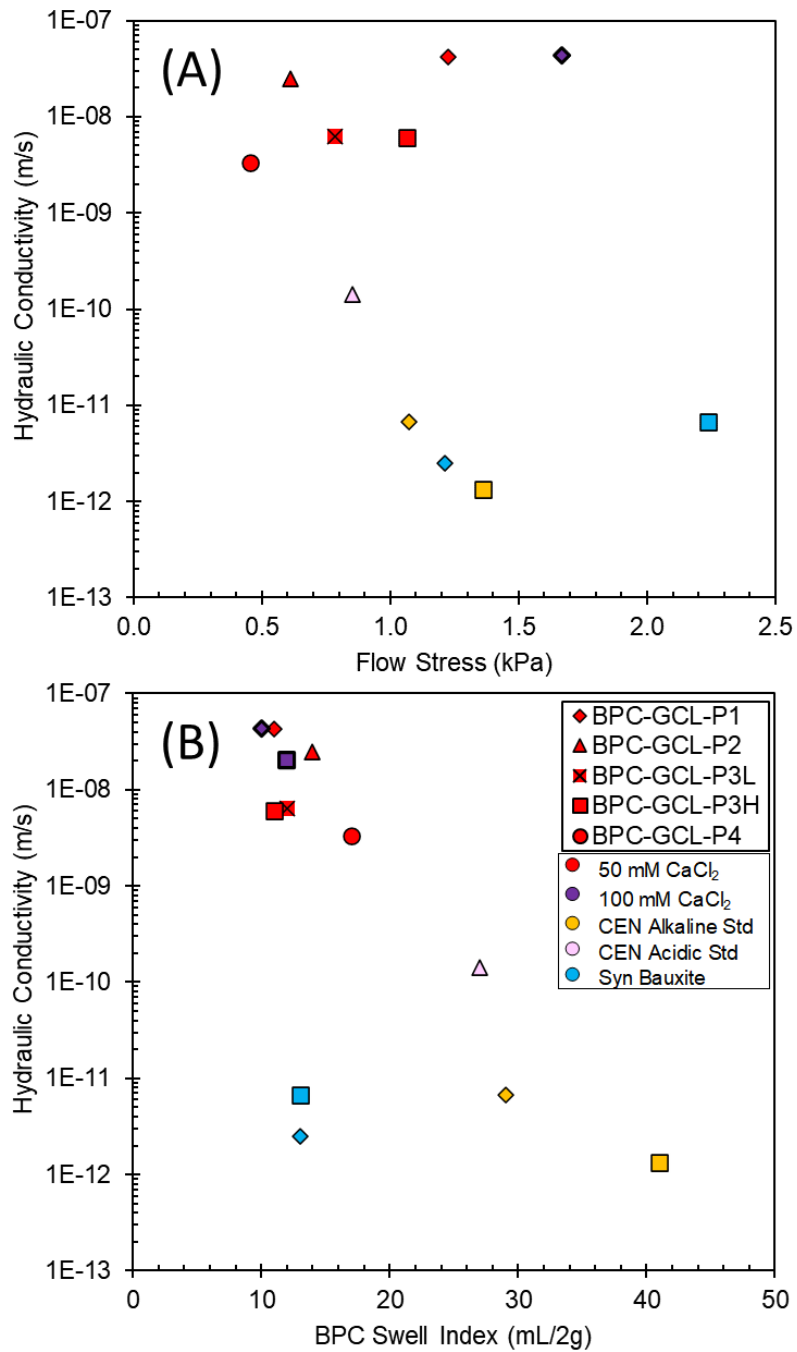


Figure 4.9. Longer term hydraulic conductivity versus the (A) flow stress of the initial condition in-situ hydrated polymer gel and (B) swell index of the BPC.

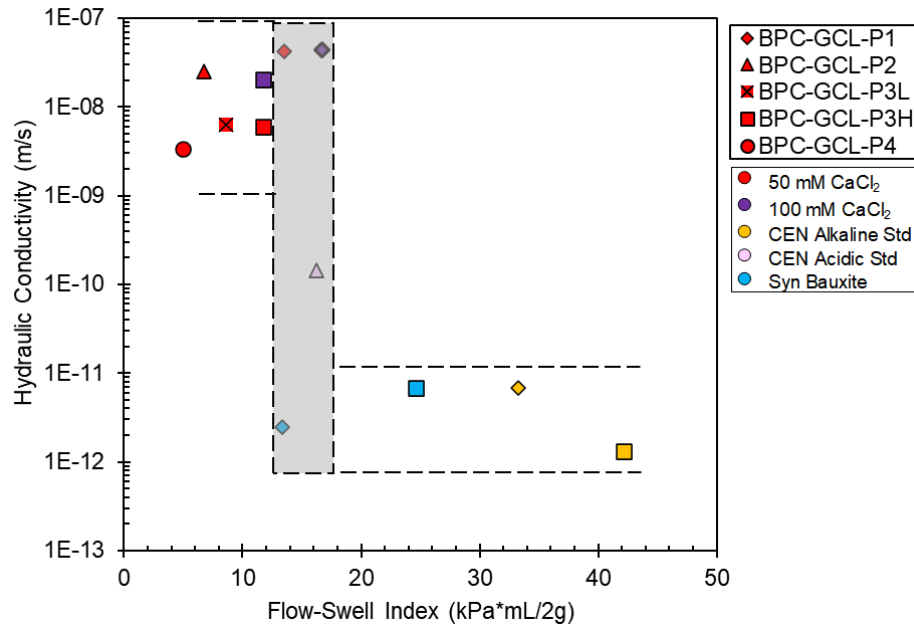


Figure 4.10. Longer term hydraulic conductivity vs. flow-swell index, defined as product of polymer flow stress and NaB swell index with permeant solution.

Flow-swell index provides discrimination between low and high hydraulic conductivity because the index represents both mechanisms controlling the hydraulic conductivity of BPCs: pore clogging by the polymer and swelling of the bentonite granules. When swelling of the bentonite granules is lower, the intergranular pores are larger and the polymer gel must be more resistant to flow (higher flow stress). Conversely, when more swelling of the bentonite granules occurs, the intergranular pores are smaller and a polymer gel can resist flow even with a lower flow stress, which ensures that the intergranular pores remain clogged. Swell index of the bentonite is used rather than swell index of the BPC, as hydraulic conductivity of BPCs is not controlled by the swelling mechanism (McRory and Ashmawy 2005; Scalia et al. 2011, 2014; Salihoglu et al. 2016; Chen et al. 2019).

The hydraulic conductivities in Fig. 4.10 correspond to the longer-term hydraulic conductivities measured in this study which are believed to represent the equilibrium condition

between the BPC and the permeant solution. As indicated previously, the hydraulic conductivity of some BPC-GCLs increased significantly after an initial stable period. For example, BPC-GCL-P1 permeated with 50 mM CaCl₂ (Fig. 4.4A) initially maintained a hydraulic conductivity of 5.6×10^{-12} m/s through 0.8 PVF, but the hydraulic conductivity increased dramatically at 0.9 PVF, eventually reaching 4.2×10^{-8} m/s at 2.9 PVF. Permeation with rhodamine dye revealed that for samples with high hydraulic conductivity flow was primarily directed through narrow preferential flow paths ranging in width from 1 to 20 mm. The opening of preferential pore paths is consistent with the observed decrease in effluent polymer concentration with increasing hydraulic conductivity (Fig 4.8A; Gustitus and Benson 2020). As polymer is depleted along a given pore path, the permeant will contact and dissolve less polymer. Additionally, as hydraulic conductivity increases the permeant moves through pores more rapidly, decreasing contact time with the polymer. As the permeant contacts less polymer over a shorter time, polymer concentration in the effluent decreases. However, significantly more effluent is produced as hydraulic conductivity increases by orders of magnitude, leading to an overall increase in polymer flux out of the BPC-GCL.

If polymer elution opens preferential flow paths, a low hydraulic conductivity upon reaching the termination criteria prescribed in ASTM D6766 may not be representative of the long-term hydraulic conductivity for BPC-GCLs. The data in Fig. 4.10 indicate that BPC-GCLs with a flow-swell index > 20 kPa·mL/2g are likely to maintain low hydraulic conductivity, whereas BPC-GCLs with flow-swell index < 20 kPa·mL/2g may become more permeable due to elution of polymer.

4.6 SUMMARY AND CONCLUSIONS

Swell index of the BPC and the NaB component of BPC-GCLs were measured with each permeant solution to evaluate how the intergranular pore space in the BPCs likely varied between the permeant solutions. Flow stress of the polymer gel component was determined to evaluate the propensity for the polymer gel be effective in clogging intergranular pores under a hydraulic gradient. Swell index and flow stress were assessed as indices of hydraulic conductivity for five commercially available BPC-GCLs permeated with seven different solutions ranging in pH, ionic strength, relative abundance of monovalent and polyvalent cation, and anion ratio. A moisture-affinity test was developed to estimate the moisture content of the polymer gel and bentonite fractions of a BPC, the former being used to define the flow stress of the polymer gel in the pore space. The following conclusions are drawn:

- Hydraulic conductivity of the BPC GCLs did not correspond with either BPC swell index or polymer flow stress, each of which represent only one of the two primary mechanisms controlling hydraulic conductivity in BPC-GCLs.
- The flow-swell index, which is the product of the NaB swell index and the polymer flow stress, accounts for both of the mechanisms controlling hydraulic conductivity in BPC-GCLs – swelling of NaB granules and clogging of pores by polymer gels.
- BPC-GCLs with a flow-swell index less than 11 kPa·mL/2g had high hydraulic conductivity ($>1 \times 10^{-9}$ m/s), and BPC-GCLs with a flow-swell index greater than 20 kPa·mL/2g had low hydraulic conductivity ($<1 \times 10^{-11}$ m/s).
- Increases in hydraulic conductivity were attributed to the opening of preferential pore paths as a result of polymer elution. The hydraulic conductivity of BPC-GCLs

may continue to change after meeting the termination criteria prescribed in ASTM D6766, especially for samples with a flow-swell index $<20 \text{ kPa}\cdot\text{mL}/2\text{g}$.

Future research is recommended to evaluate the applicability of the flow-swell index with a greater range of BPCs and permeating solutions, including BPCs containing differing types of NaB (e.g., powdered vs granular, natural vs activated).

4.7 ACKNOWLEDGEMENTS

This study was supported by CETCO and Minerals Technology Inc., the US Department of Energy's Consortium for Risk Evaluation with Stakeholder Participation (CRESP) III through Cooperative Agreement No. DE-FC01-06EW07053, the Environmental Research and Education Foundation through a fellowship to the first author, and the Jefferson Scholars Foundation at University of Virginia. Materials for the study were provided by CETCO.

Chapter 5: Hydraulic Conductivity of Bentonite-Polymer Composite Geosynthetic Clay Liners to Aggressive Solutions Under Elevated Temperature

5.1 INTRODUCTION

Bentonite polymer composite (BPC) geosynthetic clay liners (GCLs) are used to contain aggressive leachates that adversely impact the hydraulic performance of conventional sodium bentonite (NaB) GCLs. Aggressive leachates include those with very high (>12) or low (<2) pH, high ionic strength, or a preponderance of multivalent ions, such as leachates from mining and energy production wastes (Ashmawy et al. 2002, Athanassopoulos et al. 2015, Tian et al. 2016, Donovan et al. 2017, Tian and Benson 2018, Chen et al. 2019). The hydraulic conductivity of conventional NaB-GCLs is primarily attributed to the swelling of NaB granules, which is limited by aggressive solutions, resulting in higher hydraulic conductivity (Jo et al. 2005; Benson et al. 2010; Shackelford et al. 2010; Bouazza and Gates 2014; Liu et al. 2015). In contrast, the hydraulic conductivity of BPC-GCLs is controlled in part by hydrated polymer gels that clog pores to create narrow, tortuous flow paths, even when NaB swell is limited (Scalia et al. 2014; Chen et al. 2019; Tian et al. 2019). However, polymer may elute from BPC-GCLs during permeation, which can result in larger, less tortuous pores and higher hydraulic conductivity (Tian et al. 2019; Gustitus and Benson 2020).

BPC-GCLs may be exposed to elevated temperatures if heat generated in the bulk of the waste propagates to the liner (Klein et al. 2001; Koerner and Koerner 2006). For example, Klein et al. (2001) report that for an MSW incinerator ash landfill with waste temperatures up to 70°C , the liner temperature reached up to 46°C . Mining waste temperatures have been reported as high as 65°C , and MSW incinerator ash temperatures as high as 87°C (Yeşiller et al. 2015). As wastes

degrade, elevated temperatures may be maintained for years after the initial filling of a landfill (Koerner and Koerner 2006). Prolonged exposure to elevated temperatures may detrimentally impact the hydraulic conductivity, contaminant transport, and longevity of a liner (Rowe 2005).

As temperature increases from 20 to 60 °C, the hydraulic conductivity of NaB-GCLs may increase by an order of magnitude or more (Ishimori and Katsumi 2012; Özhan 2018). Ishimori and Katsumi (2012) report that a NaB-GCL had higher hydraulic conductivity at 60 °C than at 20 °C, despite an increase in swelling. Similarly, Ozhan (2018) report that the hydraulic conductivity of BPC-GCLs with either anionic or cationic polymers increased with increasing temperature when permeated with MgCl₂ solutions, though the BPC-GCLs maintained lower hydraulic conductivity than NaB-GCLs under the same conditions. In contrast, Yu et al. (2020) report that a BPC containing polyacrylamide had reduced healing capacity and higher hydraulic conductivity than unamended NaB when exposed to temperatures from 40 to 78 °C and permeated with brine.

In this study, the hydraulic conductivity of two commercially available BPC-GCLs to acidic, alkaline, and high ionic strength solutions were evaluated at 20 °C and 60 °C. BPC-GCLs were exposed to the elevated temperature through either constant permeation at 60 °C, or batch aging at 60 °C followed by permeation at 20 °C. Viscoelastic properties of the hydrated polymer component and swelling of the NaB component were also evaluated at 20 °C and 60 °C, and compared to the hydraulic conductivities of the BPC-GCL samples.

5.2 MATERIALS

Two commercially available BPC-GCLs were used in this study. BPC-GCL-P1, containing polymer P1, is designed for alkaline (high pH) or high ionic strength solutions. BPC-GCL-P2,

containing polymer P2, is designed for acidic (low pH) solutions. P1 and P2 are cross-linked polymers. The BPCs were constrained between non-woven upper and lower geotextiles bonded by needlepunching.

High and low pH solutions with chemistries prescribed in EN 14030, and a 50 mM CaCl₂ solution were used as permeant liquids. The acidic solution was comprised of 25 mM H₂SO₄, 1 mM FeSO₄, and 1 mM Fe₂(SO₄)₃. The alkaline solution was a saturated solution of Ca(OH)₂ (2.5 g/L). EC and pH of the solutions are in Table 5.1. BPC-GCL-P1 was permeated with the alkaline solution and 50 mM CaCl₂, and BPC-GCL-P2 was permeated with the acidic solution.

Table 5.1. pH and electrical conductivity (EC) of permeating solutions.

Solution	pH	EC (S/m)
Alkaline	12.4	0.88
Acidic	1.8	1.4
50 mM CaCl ₂	5.8	1.0

5.3 METHODS

5.3.1 Continuous Permeation at Elevated Temperature

Hydraulic conductivity testing on each BPC-GCL was conducted in a flexible-wall permeameter using the falling headwater constant tailwater method in accordance with ASTM D6766. The average effective stress was 29 kPa and the average hydraulic gradient was 115. No backpressure was used to preclude geochemical changes that would not occur at natural porewater pressures. Unless otherwise specified, tests were carried out at room temperature (approximately 20 °C, and not exceeding 24 °C). Samples that were continuously permeated at 20 °C and

demonstrated an increase in hydraulic conductivity by one order of magnitude or more over time were duplicated.

Flexible-wall permeameters were modified for hydraulic conductivity testing at elevated temperatures up to 60° C (Fig. 5.1). Heat was applied using by a flexible heating cord appended to the bottom plate and encircling the sample. Cell temperature was monitored by a thermocouple directly above the sample and regulated by a temperature controller connected to the thermocouple. Insulation was used to reduce heat loss. Testing has indicated that the sample temperature is within 1 °C of the cell water temperature, and the cell water temperature is maintained within 1 °C of the set-point up to 60 °C. The uniform heating of the BPC-GCL in the permeameter is slightly different than would occur in the field, where heat is transferred vertically across the BPC-GCL. However, BPC-GCLs typically are 7-10 mm thick; therefore, the temperature differential across the GCL would be negligible in the field.

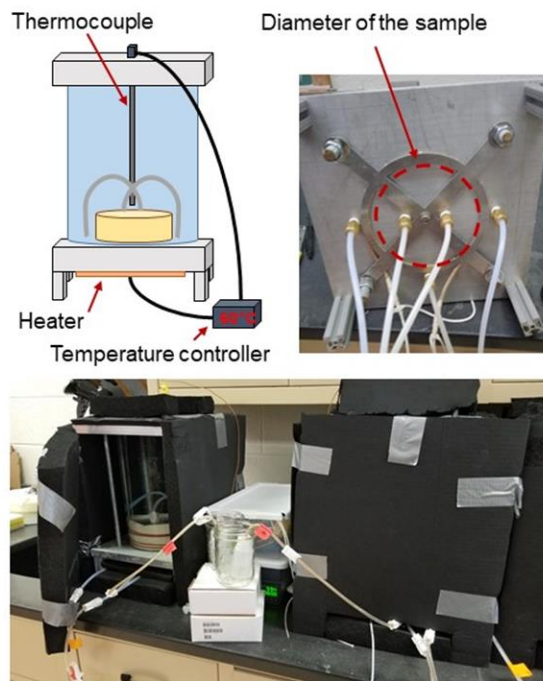


Figure 5.1. Elevated temperature permeameters used for measuring hydraulic conductivity at 60°C.

5.3.2 Batch Aging of BPC-GCLs

BPC-GCL samples were batch aged in the acidic and alkaline permeant solutions for periods of 15, 30, 60, 120, and 180 days. Batch aging was conducted in ultra-high molecular weight HDPE hydration cells (Fig. 5.2) submerged in glass-coated steel pots. The top and bottom plates of the hydration cells are perforated with 3-mm-diameter holes that allow solution to contact the sample. The permeant solution was refreshed every 15 days. Spacing between the plates was set to 12 mm to constrain swelling of the BPC-GCL. A 5- μm polypropylene filter and a non-woven geotextile were placed between the plates and the BPC-GCL to promote even hydration (geotextile) and minimize polymer elution (filter).

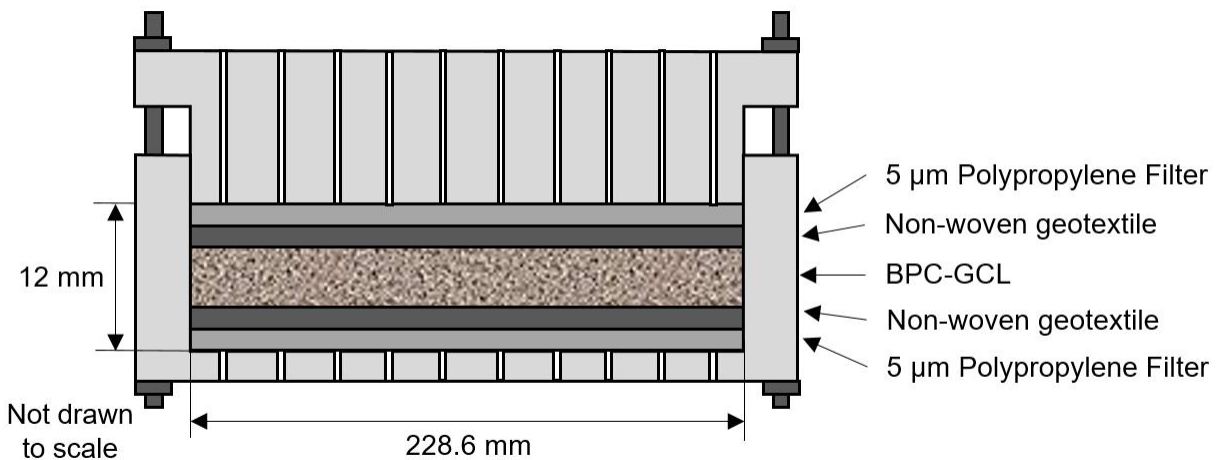


Figure 5.2. Schematic illustration of hydration cell used for batch aging.

BPC-GCL samples in the cell have a diameter of 230 mm. At the end of the batch aging period, a 152 mm diameter sample was cut out using a scalpel and transferred to an ambient temperature permeameter. The remaining sample was used to assess the polymer loading in the BPC-GCL following batch aging and preceding permeation.

5.3.3 Batch Aging of Polymer Gels

Polymers P1 and P2 hydrated with the permeant solutions were batch aged in air-tight glass containers with minimal headspace for periods of 15, 30, 60, 90, 120 and 180 days at 60 °C. A unique sample was used for each condition so that the containers remained sealed until the termination of the batch aging period. The gels were hydrated at a moisture content of 500% which is similar to the in-situ gel moisture content in the unaged BPC-GCLs, as determined by the bentonite-polymer moisture affinity test described in Chapter 4.

5.3.4 Flow Stress

Flow stress is the shear stress at which a viscoelastic gel begins to behave more like a liquid (viscous) than a solid (elastic), and has been suggested as an indicator of polymer elution (Gustitus and Benson 2020). Flow stress of the polymer gels was determined by conducting shear-strain-amplitude sweeps with controlled-shear deformation using a parallel plate rheometer (Anton Paar MCR 302, Austria) following the method in Gustitus and Benson (2020). Amplitude sweeps were completed over a range of 0.01-10,000% shear strain using a 25-mm-diameter sand-blasted parallel plate. Storage modulus and loss modulus were measured, and flow stress was computed as the stress at which the storage modulus and loss modulus were equivalent. Tests were carried out at 20 °C for all batch aged gels, and at 20, 40, and 60°C for unaged gels. Duplicate measurements were averaged to determine flow stress.

5.3.5 Swell Index

Swell index was measured in general accordance with ASTM D5890, except the BPC was ground to 100% passing the US No. 40 mesh sieve and 65% passing the US No. 60 mesh sieve. A

coarser grind was used to reduce the effect of grinding on the polymer structure, and to reduce the risk of polymer segregation that has been seen when the finer grind prescribed in ASTM D5890 is used (Christian et al. 2020). Scalia et al. (2019) demonstrate that swell indices of bentonite ground to pass a No. 40 sieve are similar to those for bentonite ground to pass a No. 200 sieve.

5.4 RESULTS

5.4.1 Hydraulic Conductivity

A summary of the current hydraulic conductivities is in Table 5.2. Tests of batch aged samples, and the second continuously permeated replicate of BPC-GCL-P2 in acidic solution at 20 °C are still being conducted. For the tests that are still being conducted, all of the hydraulic conductivities reported herein were measured at the time this paper was prepared.

The hydraulic conductivities for BPC-GCLs permeated at ambient temperature and 60 °C with no external aging are compared in Figure 5.3. The hydraulic conductivity of BPC-GCL-P1 permeated with the alkaline solution was similar at 20 °C (6.2×10^{-12} m/s) and 60 °C (4.3×10^{-12} m/s), but was more consistent over time when permeated at ambient temperature. Clogs of $\text{Ca}(\text{OH})_2$ precipitate and polymer were regularly removed from the tubing on the 60 °C sample, which contributed to the irregularity of the hydraulic conductivity. The hydraulic conductivity of BPC-GCL-P1 permeated with 50 mM CaCl_2 increased to above 5×10^{-9} m/s in both the 20 and 60 °C samples between 1 to 2 pore volumes of flow (PVF), and the initial hydraulic conductivity was higher for the 60 °C sample. The hydraulic conductivity of BPC-GCL-P2 permeated with the acidic solution at 60 °C (7.5×10^{-12} m/s) is lower than one replicate at 20 °C (1.1×10^{-10} m/s), and similar to the other replicate at 20 °C (6.2×10^{-12} m/s).

Table 5.2. Hydraulic conductivities of each test at the time that this paper was prepared. “Active permeation” refers to the time that flow was being conducted through the permeameter, which was not necessarily constant when samples had hydraulic conductivity above 10^{-8} m/s.

BPC-GCL	Solution	Condition		Hydraulic Conductivity (m/s)	Duration of Active Permeation (days)
BPC-GCL-P1	Alkaline	Unaged, 20°C permeation temperature		6.2×10^{-12}	579
		Unaged, 60°C permeation temperature		4.3×10^{-12}	180
		Batch aged at 60°C, 20° C permeation temperature	15 days	3.5×10^{-12}	501
			30 days	1.0×10^{-11}	414
			60 days	1.6×10^{-11}	341
			120 days	1.2×10^{-11}	310
	180 days	2.0×10^{-11}	101		
	50 mM CaCl ₂	Unaged, 20°C permeation temperature		4.2×10^{-8}	62
				1.3×10^{-7}	133
Unaged, 60°C permeation temperature		4.9×10^{-9}	16		
BPC-GCL-P2	Acidic	Unaged, 20°C permeation temperature		1.1×10^{-10}	299
				6.2×10^{-12}	225
		Unaged, 60°C permeation temperature		7.5×10^{-12}	432
		Batch aged at 60°C, 20° C permeation temperature	15 days	1.6×10^{-11}	624
			30 days	4.4×10^{-11}	395
			60 days	2.9×10^{-11}	342
	120 days		7.5×10^{-12}	298	
	180 days	2.9×10^{-7}	< 1		

Hydraulic conductivity of batch aged samples of BPC-GCLs are compared to the hydraulic conductivity of samples with no external aging in Figure 5.4. Hydraulic conductivities of all batch aged samples are similar, with the exception of BPC-GCL-P2 aged in acidic solution for 180 days which had much higher hydraulic conductivity (2.9×10^{-7} m/s). The hydraulic conductivities of the other batch aged samples ranged from 3.5×10^{-12} m/s (BPC-GCL-P1, alkaline, aged for 15 days) to 4.4×10^{-11} m/s (BPC-GCL-P2, acidic, aged for 30 days).

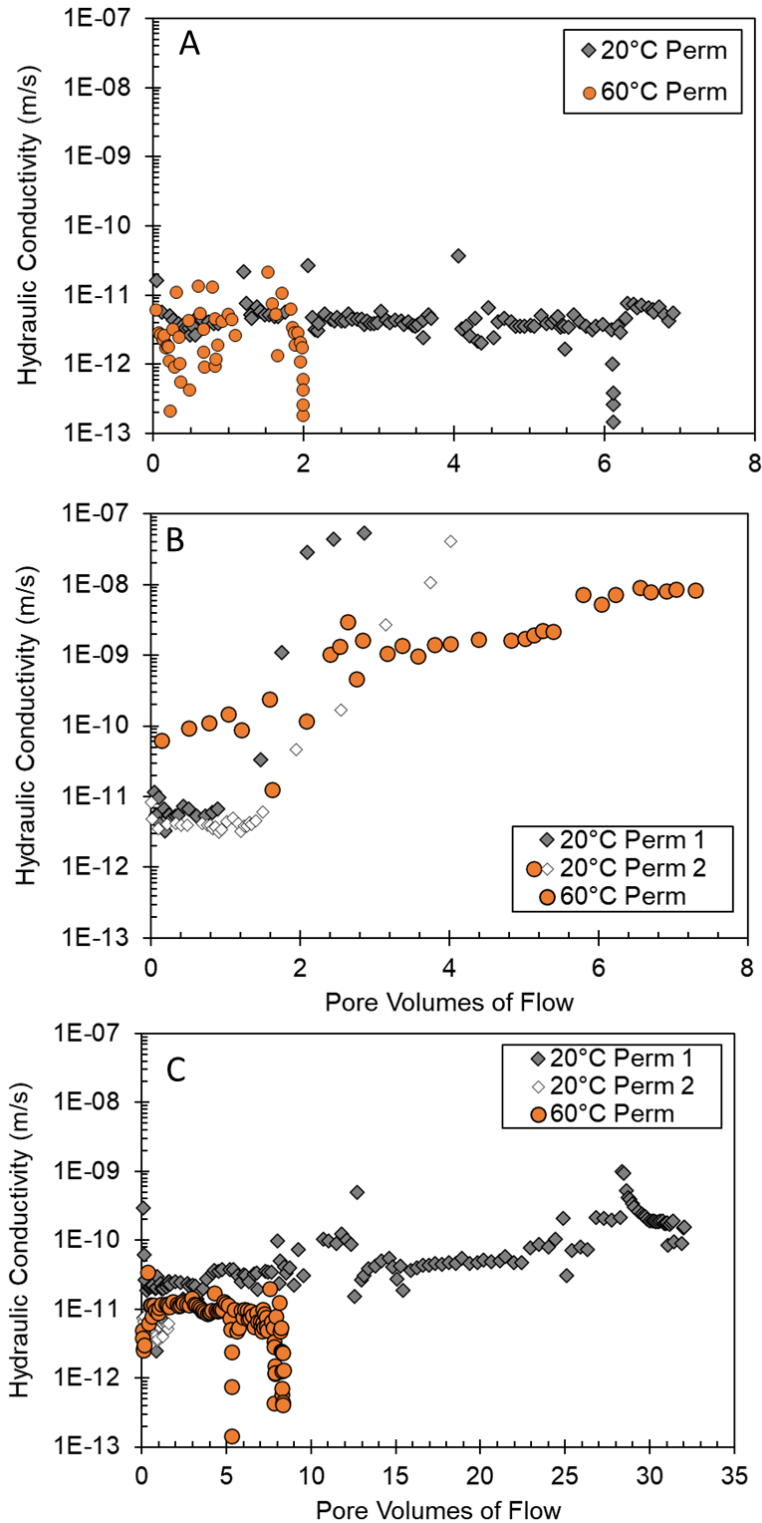


Figure 5.3. Hydraulic conductivity of (A) BPC-GCL-P1 with an alkaline solution, (B) BPC-GCL-P1 with 50 mM CaCl₂ and (C) BPC-GCL-P2 with an acidic solution continuously permeated at 20 and 60 °C. BPC-GCLs had no external aging.

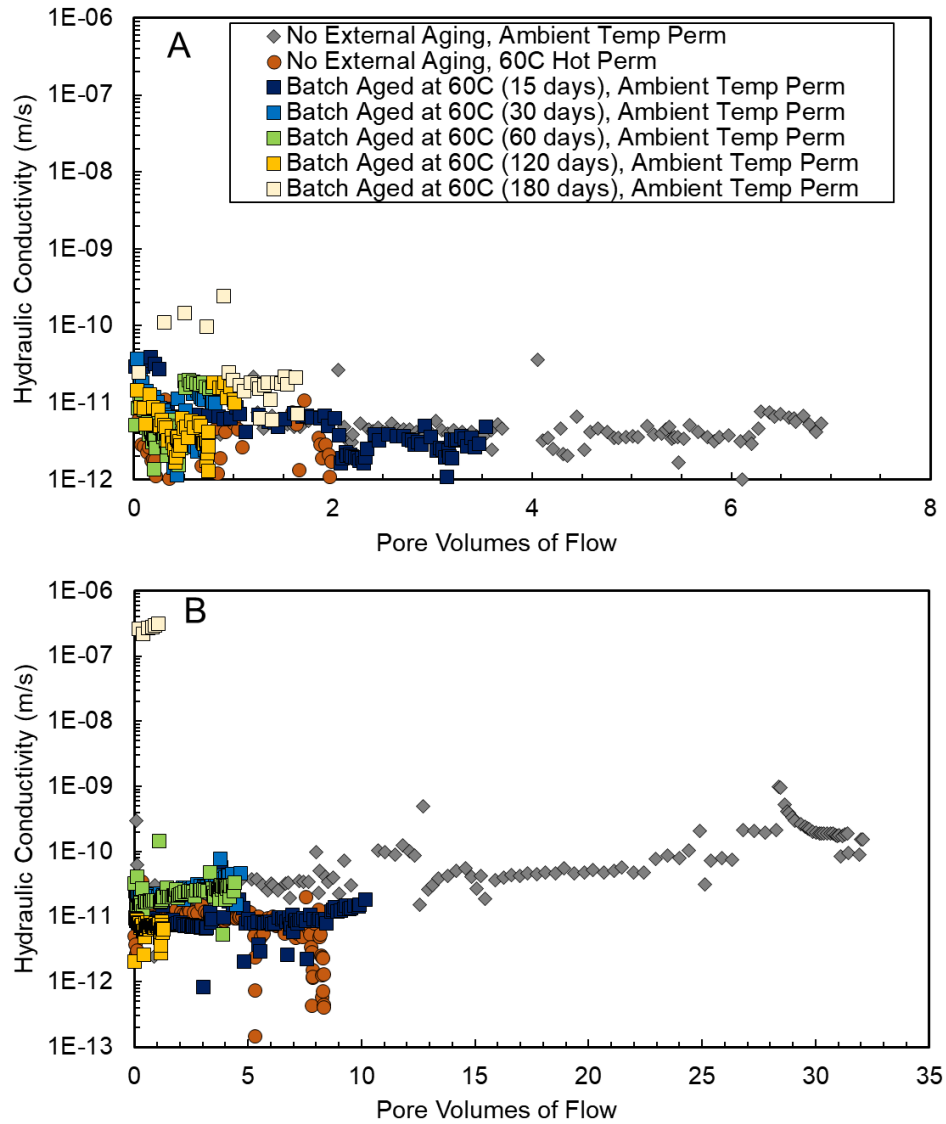


Figure 5.4. Hydraulic conductivity of A) BPC-GCL-P1 with an alkaline solution, and B) BPC-GCL-P2 with an acidic solution.

5.4.2 Flow Stress of Polymer Gels

Flow stress of the unaged polymer gels at 20, 40, and 60 °C is shown in Figure 5.5. Flow stress of the P1-alkaline gel decreases from 1.4 kPa at 20°C to 1.1 kPa at 40 °C, then increases to 1.3 kPa at 60°C. In contrast, flow stress of the P1-CaCl₂ gel consistently increases from 0.9 kPa at

20 °C to 1.4 kPa at 60 °C. Flow stress of the P2-acidic solution gel decreases from 1.3 kPa at 20°C to 0.8 kPa at 40 °C and 60 °C.

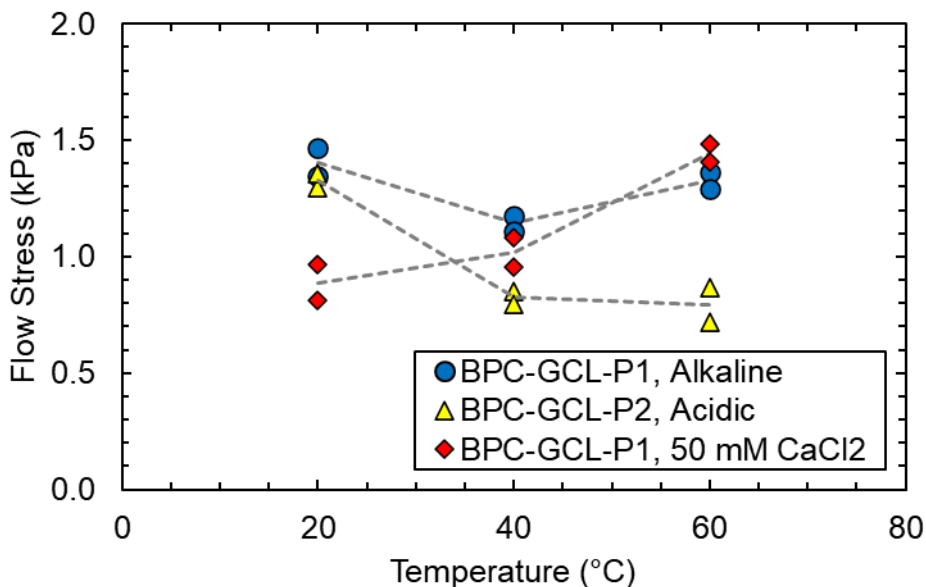


Figure 5.5. Flow stress of unaged polymer gels as a function of temperature. Polymer gels were hydrated to a moisture content of 500%.

Flow stress of batch aged P1 and P2 gels as a function of aging time is shown in Figure 5.6. Flow stress of all three gels aged at 80 °C decreased to 0 (completely liquid behavior) within 60 days. Flow stress of the P1-alkaline gel peaked at 90 days when aged at 60 °C, and at 180 days when aged at 40°C. Following the peak, the flow stress of gel aged at 60 °C systematically decreased until it approached a liquid state (flow stress = 0) by 180 days. Over the course of 180 days of aging at 60 °C, gel changed from hydrated granules on the order of 1 mm wide to a uniform viscoelastic gel with a consistency of raw honey (Fig. 5.7, first row). Flow stress of both the P1-CaCl₂ gel and the P2-acidic gel remained relatively constant over 180 days when aged at 40 and 60 °C. The P1-CaCl₂ gel maintained the form of individual hydrated granules through 120 days, and transitioned to a mixture of hydrated granules and stringy, stretchy gel at 180 days (Fig.5.7, second row). The P2-acidic gel maintained a form of individual hydrated granules throughout 180

days of aging, and the color of the gel changed slightly from clean to a light brown tint (Fig. 5.7, third row).

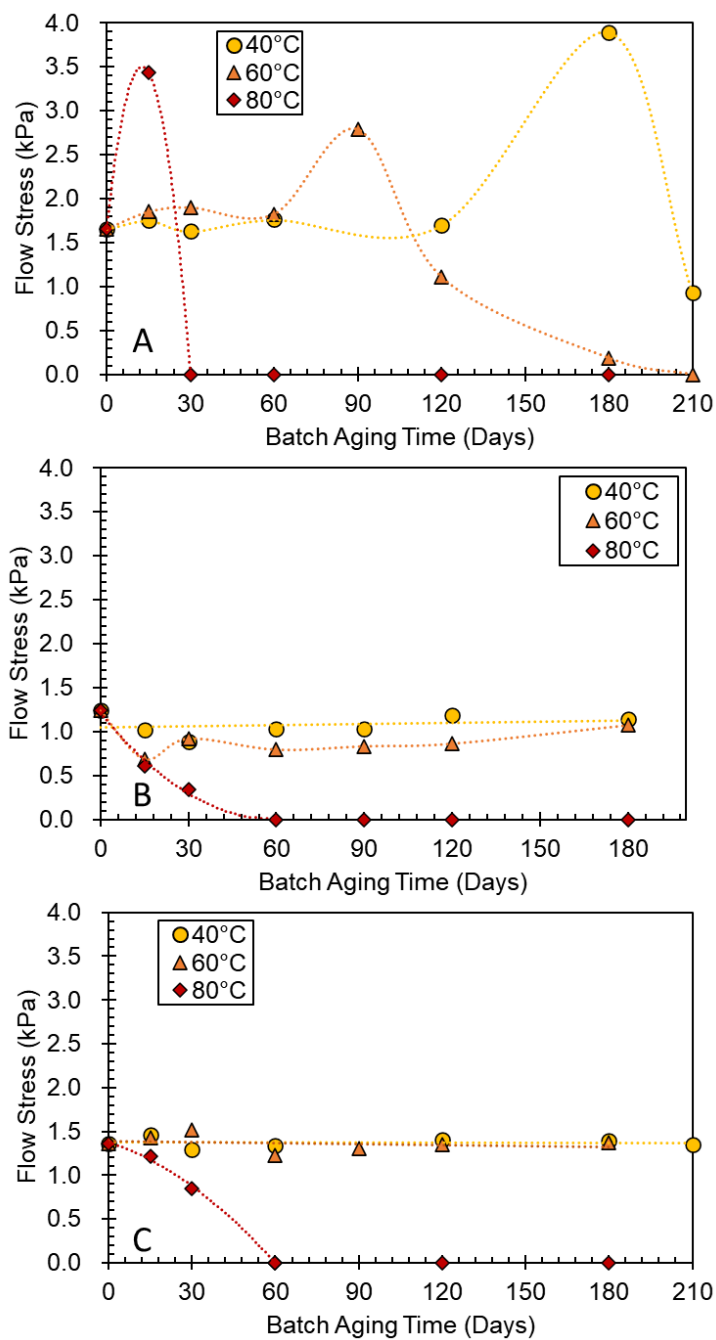


Figure 5.6. Flow stress of polymer gels aged at various temperatures for P1 with alkaline solution (A), P1 with 50 mM CaCl₂ (B) and P2 with acidic solution (C).

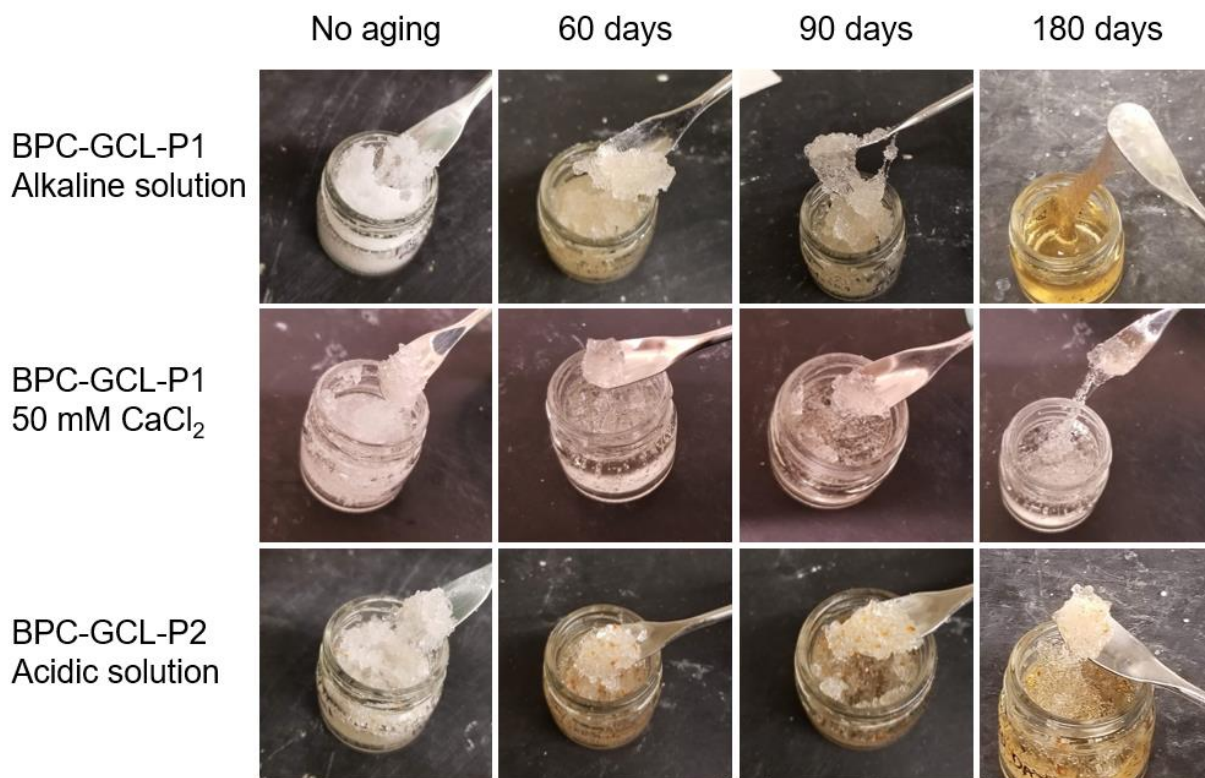


Figure 5.7. Hydrated polymer gels batch aged at 60 °C.

5.4.3 Swell Index

Swell indices of the base bentonite and each BPC in their respective permeating solutions are shown in Fig. 5.8. Swell index of the base bentonite in the acidic and alkaline solutions, and BPC-P1 in the alkaline solution increases slightly with increasing temperature. The swell index of the base bentonite has greater sensitivity to temperature in the alkaline solution than the acidic solution, which may be attributed to the decreasing solubility of $\text{Ca}(\text{OH})_2$ with increasing temperature. The swell index of the base bentonite and BPC-P1 in 50 mM CaCl_2 , and BPC-P2 in acidic solution were unaffected by temperature. The swell index of BPC-P1 in alkaline solution and BPC-P2 in acidic solution were higher than the swell index of the base bentonite in the respective solutions, while the swell index of BPC-P1 and the base bentonite were the same in 50 mM CaCl_2 .

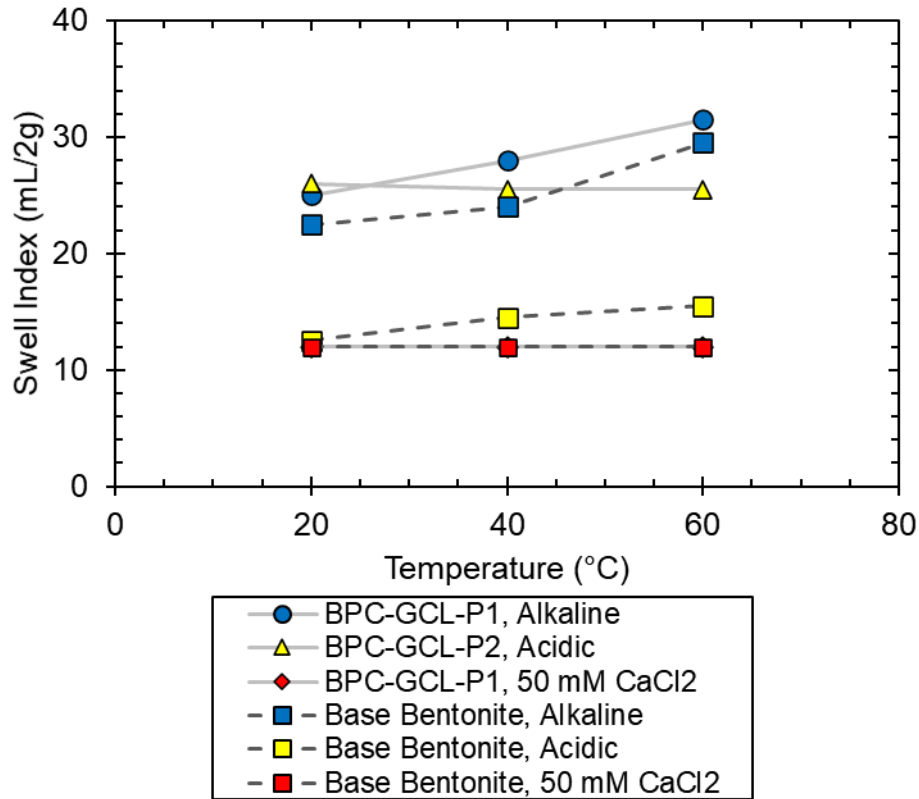


Figure 5.8. Swell index of base bentonite, BPC-P1, and BPC-P2 as a function of temperature.

5.4.4 Polymer Loading

Polymer loading of each sample is shown in Figure 5.9. Two sections (25 mm x 25 mm) of each BPC-GCL were sampled to assess polymer loading. Samples were removed post-permeation for continuously permeated samples, and post-batch aging for batch aged samples, which are still being permeated. Polymer loading decreased over the course of 180 days for both batch aged BPC-GCLs as a result of elution into the batch aging solution. Decreased polymer loading can lead to increased gel moisture content, as shown in Figure 5.10 for unaged gels based on the bentonite-polymer moisture affinity test. Higher moisture content is associated with lower

flow stress, which may be indicative of increased propensity for elution (Gustitus and Benson 2020).

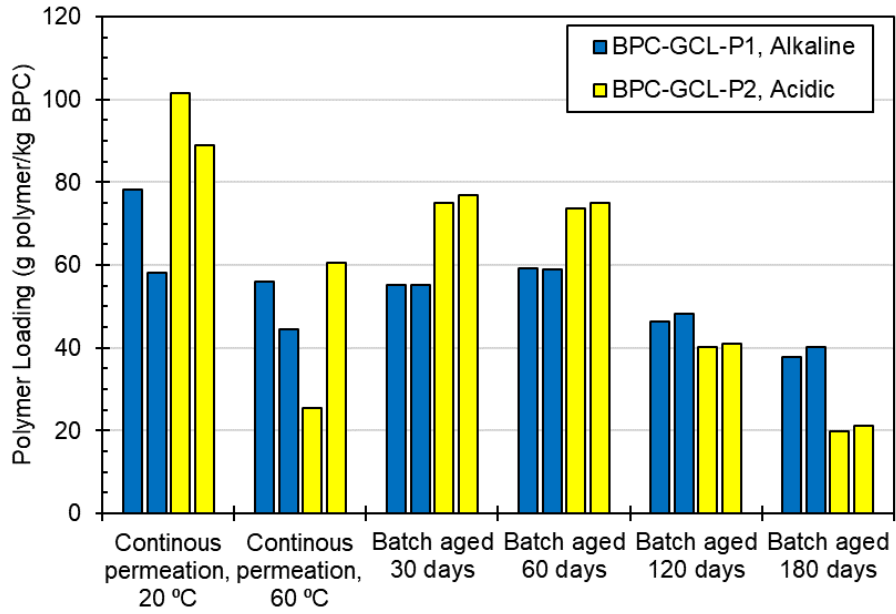


Figure 5.9. Polymer loading remaining in continuously permeated and batch aged BPC-GCLs.

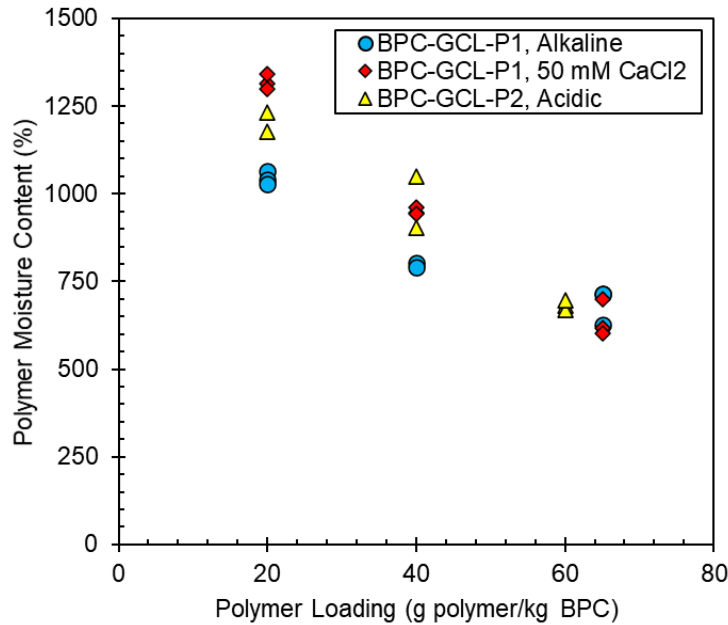


Figure 5.10. The moisture content of in-situ polymer gels decreases as polymer loading increases.

5.5 DISCUSSION

Continuous permeation at elevated temperature had no measurable impact on BPC-GCL-P1 permeated with the alkaline solution, which had comparable hydraulic conductivity at 20 °C and 60 °C over the test duration. This is consistent with the negligible change in flow stress, which was only 6% lower at 60 °C relative to 20 °C. That is, the polymer in BPC-GCL-P1 was no more likely to elute at 60 °C than at 20 °C. The swell index of the BPC is also 29% higher at 60 °C than at 20 °C, which should promote lower hydraulic conductivity.

BPC-GCL-P1 permeated with 50 mM CaCl₂ initially demonstrated higher hydraulic conductivity when permeated at 60 °C, but at termination of the tests the samples permeated at 20 and 60 °C had similar hydraulic conductivity on the order of 10⁻⁸ m/s. The increase in hydraulic conductivity was more gradual for the sample permeated at 60 °C (5.4 PVF to exceed 5 x 10⁻⁹ m/s) than those permeated at 20 °C (1.8 and 3.2 PVF to exceed 5 x 10⁻⁹ m/s), which is consistent with a higher flow stress, and therefore greater resistance to elution at 60 °C. The continuously permeated sample at 60 °C is still being run. The swell index of both the NaB and the BPC was unaffected by changes in temperature, and therefore should not have contributed to any differences in hydraulic conductivity.

The hydraulic conductivity of one replicate of BPC-GCL-P2 permeated with acidic solution at 20 °C (no external aging) is higher than the sample permeated at 60 °C, and has been slowly increasing. This same effect has not yet been observed for the sample permeated at 60 °C, or for the second replicate at 20 °C, which is still being permeated. The flow stress of the hydrated P2-gel decreases by 40% from 20 to 60°C, and there is a concurrent modest increase in the swell index of the BPC by 4%. A decrease in flow stress would be expected to result in an increase in polymer elution, and therefore an increase in hydraulic conductivity; however, the opposite

occurred for BPC-GCL-P2, which has retained higher polymer loading in the sample permeated at 20 °C. The modest increase in swell index is unlikely to account for the lower hydraulic conductivity at 60 °C; therefore, additional change(s) to the bentonite or polymer may be occurring that are not accounted for in these experiments.

Hydraulic conductivity of batch aged BPC-GCLs is plotted versus batch aging time (Fig. 5.11), flow stress (Fig. 5.12), and polymer content (Fig. 5.13). There are no distinct relationships between hydraulic conductivity and any of these parameters. The lack of correspondence is attributed to the minimal differences in hydraulic conductivity, with the exception of BPC-GCL-P2 aged in acidic solution for 180 days. This sample had the highest hydraulic conductivity by approximately four orders of magnitude (2.9×10^{-7} m/s), and the lowest polymer loading (2.0 g polymer/kg BPC) of any of the samples tested. Permeation with rhodamine dye revealed that flow was directed through one spot that was approximately 20 mm wide, suggesting that significant polymer elution resulted in preferential flow. The BPC-GCLs appear to be resistant to thermal effects, provided the enough polymer is retained to sufficiently clog pores.

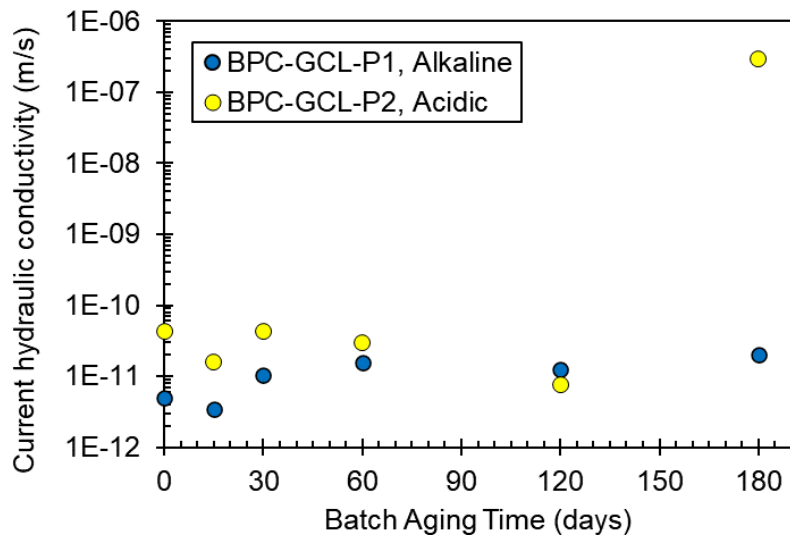


Figure 5.11. Hydraulic conductivity of batch aged BPC-GCLs versus batch aging time.

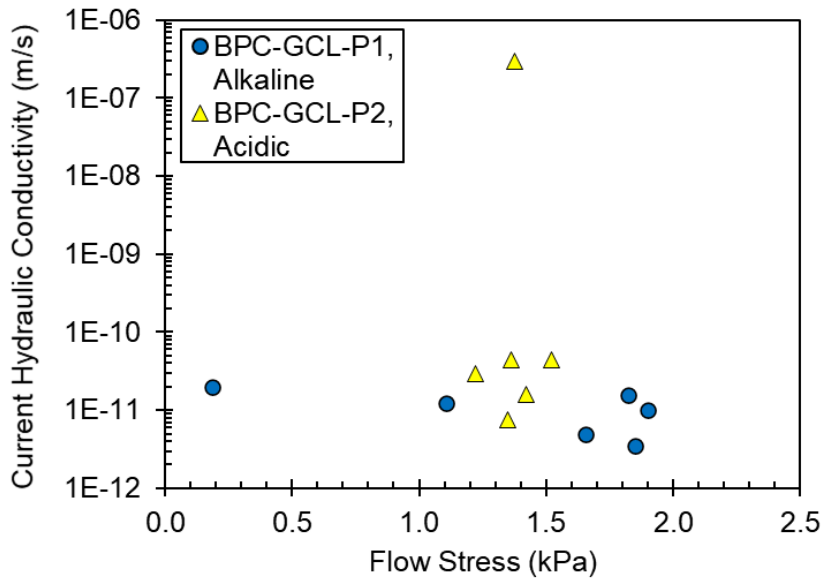


Figure 5.12. Hydraulic conductivity of batch aged BPC-GCLs versus flow stress of the corresponding polymer gel.

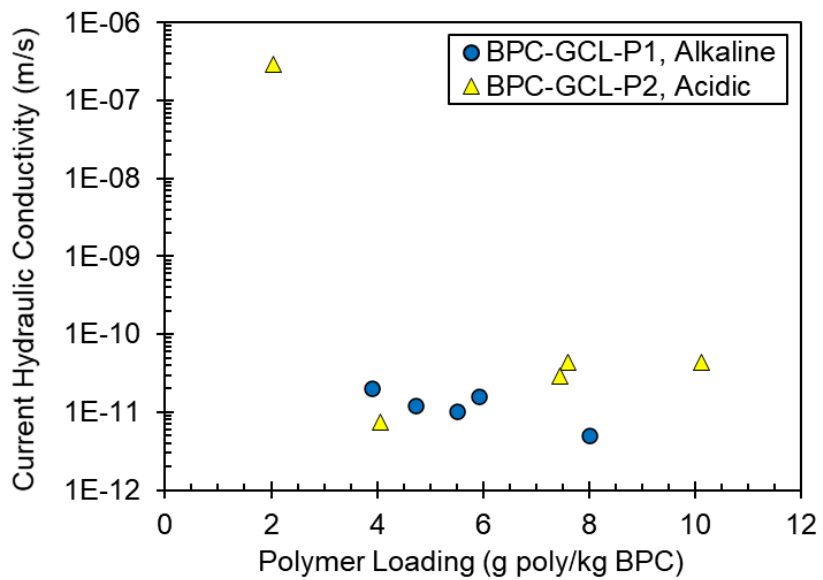


Figure 5.13. Hydraulic conductivity of batch aged BPC-GCLs versus polymer loading of the BPC-GCL after batch aging.

The BPC-GCLs that were batch aged for 180 days retained less polymer than any of the other batch aged samples and the BPC-GCLs that were continuously permeated at either 20 or 60 °C. Despite the inclusion of the 5- μ m polypropylene filter, a significant amount of polymer

dissolved in solution and eluted out of the BPC-GCL over the batch aging period. The top and bottom plates in the batch aging container each contain 49 holes (3 mm diameter) spaced across the surface of the plate (Fig. 5.14A), so the maximum distance that polymer at the surface of the BPC-GCL would have to travel to elute through a hole in the container was 30 mm. Comparatively, the plates constraining the BPC-GCLs in permeameters contain a single effluent line with a relatively small diameter (6.4 mm diameter) compared to overall sample diameter (152 mm; Fig. 5.14B). The permeameter plates also contain a “Z” shaped channel and additional tubing that was only opened to clear clogs in the effluent line. The maximum distance that polymer would have to travel to the “Z” shaped channel was 50 mm, and the total length of the channel was approximately 300 mm. Despite the constant flow in the permeameter, polymer elution may have been inhibited by the design of the constraining plates. Therefore, the batch aged samples may be more representative of field conditions, where polymer may elute from any point throughout the BPC-GCL. Further investigation into the effect of constraining plates on polymer elution is warranted, and may help improve the design of tests that accurately represent the behavior of BPC-GCLs under field conditions.

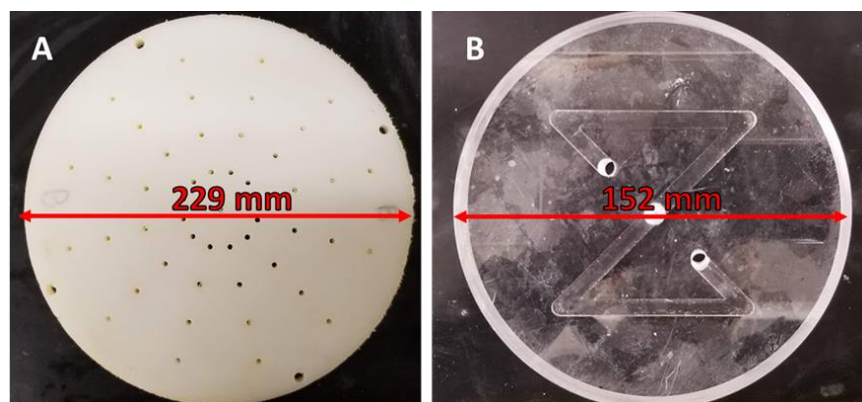


Figure 5.14. Plates constraining samples in (A) batch aging containers and (B) permeameters. The batch aging container contains 49 holes (3 mm diameter) in both the top and bottom plates, all of which are continuously open. The permeameter plate contains two holes (6.4 mm diameter) – one for effluent to flow through, and the other is only opened to facilitate clearing of clogs when necessary.

Similar to prior studies, hydraulic conductivity is not necessarily inversely related to swell index when comparing the hydraulic conductivity of GCLs permeated at different temperatures. Neither is hydraulic conductivity related to polymer flow stress for permeation at different temperatures. Therefore, other mechanisms may contribute to controlling hydraulic conductivity of BPC-GCLs at elevated temperatures. These mechanisms may include differences in precipitation of dissolved species in the permeating solution (e.g., for the saturated solution of $\text{Ca}(\text{OH})_2$ used here), or changes to polymer structure that are not captured by measuring only the flow stress of the polymer. Additionally, the presence of bentonite can affect the thermal degradation of polymers in BPCs (Ramos Filho et al. 2005; Gustitus et al. 2020), therefore analyzing changes to flow stress for polymers aged independent of the BPC may be insufficient – hence, the prolonged low hydraulic conductivity of BPC-GCL-P1 with alkaline solution past 180 days, when the batch aged polymer transitioned to a viscoelastic liquid. Whereas this study demonstrates decreased or similar hydraulic conductivity of BPC-GCLs at 20 and 60 °C, previous studies have found increased hydraulic conductivity with increased temperatures (Özhan 2018; Yu et al. 2020). The effects of temperature on hydraulic conductivity appear to be dependent on polymer and solution chemistry, which may account for the differing outcomes between this study and previous studies which employed BPC-GCLs containing different polymers and permeated with different solutions.

5.6 SUMMARY AND CONCLUSIONS

The effects of elevated temperature on two BPC-GCLs permeated with aggressive solutions was investigated. The hydraulic conductivity of the BPC-GCLs was compared for continuous permeation at 20 and 60 °C, and for permeation at 20 °C following various periods of

batch aging at 60 °C. Properties of the polymer and bentonite components of the BPC-GCLs at 20 and 60 °C were also compared.

The BPC-GCLs exposed to elevated temperatures either during permeation or during batch aging maintained hydraulic conductivity below 1×10^{-10} m/s, provided sufficient polymer was retained to fill pores. The hydraulic conductivity of the BPC-GCLs permeated at 60 °C was comparable to or lower than the hydraulic conductivity of those permeated at 20 °C for all three GCL-solution pairs tested. BPC-GCLs batch aged for periods of up to 120 days all had comparable hydraulic conductivity, regardless of changes in polymer loading or flow stress of the polymer gels. Only BPC-GCL-P2 aged for 180 days in acidic solution had a significantly higher hydraulic conductivity, which is attributed to greater polymer elution during batch aging compared to the other batch aged samples.

The findings of this study differ from the findings of previous studies that have found increased hydraulic conductivity of BPC-GCLs at elevated temperatures. The effects of elevated temperatures may be dependent on the polymer and solution chemistry, and therefore testing of site-specific leachates with site-specific BPC-GCLs should be performed to understand the potential impacts of elevated temperatures. Additionally, batch aged BPC-GCL samples eluted more polymer than continuously permeated BPC-GCLs, which is attributed to more even distribution of possible elution pathways in batch aging containers. The distributed elution pathways may be more representative of field conditions. Therefore, additional research is recommended to assess whether traditional permeameter design (i.e., a single effluent line with small diameter relative to total sample surface area) affects elution.

5.7 ACKNOWLEDGMENTS

This study was supported by CETCO, the US Department of Energy's Consortium for Risk Evaluation with Stakeholder Participation (CRESP) III through Cooperative Agreement No. DE-FC01-06EW07053, the Environmental Research and Education Foundation through a fellowship to the first author, and the Jefferson Scholars Foundation at University of Virginia. Materials for the study were provided by CETCO.

Chapter 6: Pore Scale Modeling of Polymer Elution in Bentonite-Polymer Composite Geosynthetic Clay Liners

6.1 INTRODUCTION

Bentonite-polymer composite geosynthetic clay liners (BPC-GCLs) are used to line containment systems with leachates that are too aggressive for conventional sodium bentonite GCLs to maintain low hydraulic conductivity. BPC-GCLs maintain low hydraulic conductivity through narrow, tortuous pore paths that are created when bentonite granules swell and/or hydrated polymer gels clog intergranular spaces (Scalia et al. 2011, 2014; Tian et al. 2016b; Özhan 2018; Chen et al. 2019). Hydraulic conductivity of BPC-GCLs can increase over time as polymer is eluted, especially when the swelling of bentonite granules is limited (Tian et al. 2019; Gustitus and Benson 2020). When a critical amount of polymer is eluted to increase the hydraulic conductivity above design criteria, the service life of the BPC-GCL is ended.

Traditional permeation tests of BPC-GCLs can take years to complete, and hydraulic conductivity of samples may increase even after the equilibrium criteria prescribed in ASTM D6766 has been reached. Reliance on empirical testing alone may be insufficient for predicting service lives on the order of tens to hundreds of years. Therefore, expedited methods of predicting long-term hydraulic conductivity are needed. In this study, simplified hydraulic models are developed and employed to simulate the movement of polymer in the pore space of a BPC-GCL. The results of the models are compared to experimental observations to validate mechanisms purported based on empirical studies. These models provide a basis for developing more complex and realistic models for predicting hydraulic conductivity and service life of BPC-GCLs.

6.2 MATERIALS AND METHODS

6.2.1 Materials

The viscosity of two proprietary polymers, P1 and P3, were empirically determined and used as model inputs. Polymers P1 and P3 are used in commercially available BPC-GCLs that also contain granular sodium bentonite. P1 is a cross-linked polymer for use with alkaline or high ionic strength leachates, and P3 is a linear polymer for use with high ionic strength leachates. Both polymers were hydrated with 50 mM CaCl₂ solution (pH = 5.8, EC = 1.0 S/m) to moisture contents of 200%, 500%, 1000% and 2000% by mass, which represent a range of moisture contents possible in the pores of BPC-GCLs.

6.2.2 Methods

The viscosity of the polymer gels was measured using a shear rate sweep on an Anton Paar MCR 302 rheometer (Anton Paar, Austria). Shear rate sweeps were completed over a range of 0.0001 to 10 s⁻¹ performed using a 25 mm diameter sandblasted parallel plate.

Models were generated using COMSOL Multiphysics software. The geometry of the model consisted of two NaB granules (400 μm diameter) separated by 160 μm, with a polymer gel (150 μm diameter) positioned just below the center of the pore (Fig. 6.1). NaB granules were positioned 20 μm away from the edge of the study area. The models were based on laminar flow with two-phase flow, level set multiphysics. The mesh was composed of “extremely fine” elements, arranged in a free triangular pattern. A pressure differential of 3 kPa was applied from the inlet to outlet. Backflow was suppressed.

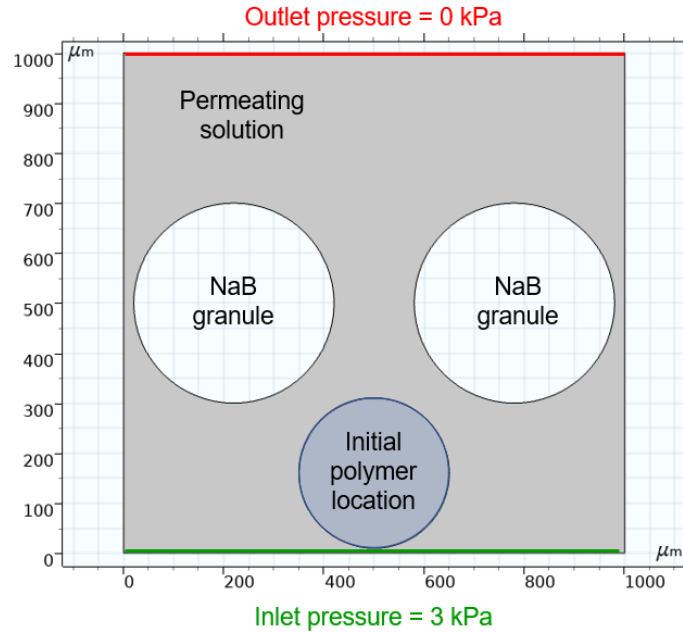


Figure 6.1. Geometry employed in each of the models, consisting of two NaB granules and a single polymer gel positioned just below the pore space between the NaB granules.

Actual flow through a BPC-GCL is more likely to be considered creeping flow ($Re \ll 1$) than laminar flow ($Re < 2300$). However, the laminar flow physics within COMSOL offers greater flexibility for modeling two-phase flow, as well as reduced computation time. To ensure that laminar flow multiphysics was appropriate, separate COMSOL models using laminar and creeping flow physics were developed employing geometry from Keller et al. (1997). This geometry is derived from a 2-D section through Berea sandstone, but is expected to have similar complexity to the expected geometry of NaB pores with limited swelling. Hydraulic conductivity of the laminar flow model (2.46×10^{-4} m/s) was less than 2% lower than the hydraulic conductivity of the creeping flow model (2.52×10^{-4} m/s). Additionally, the pore velocities were similar throughout the geometry (Fig. 6.2). Therefore, the laminar flow physics was deemed appropriate for this study.

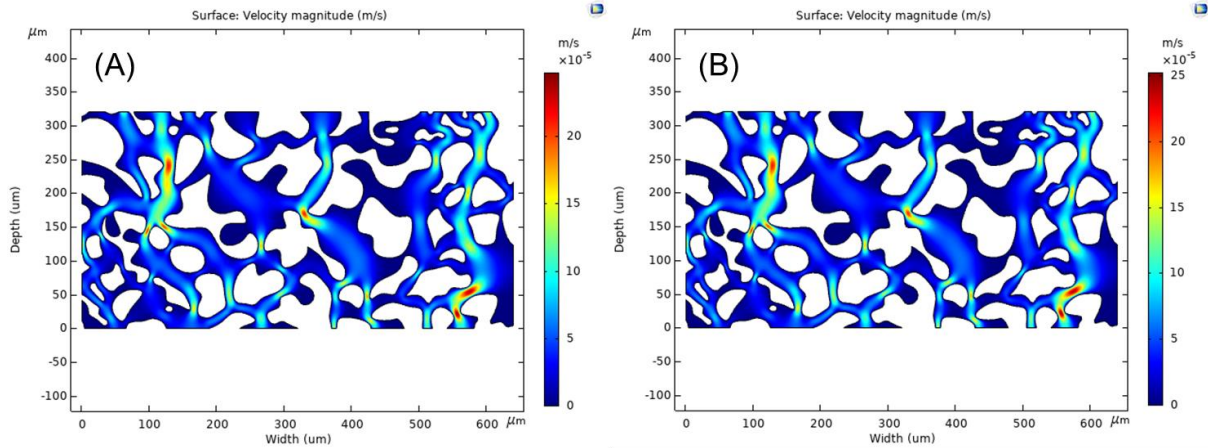


Figure 6.2. Velocity profiles of preliminary testing model using (A) laminar and (B) creeping flow physics.

6.3 RESULTS AND DISCUSSION

6.3.1 Experimental results

The viscosity of polymers P1 and P3 versus shear rate is shown in Figure 6.3. Both polymers demonstrate shear-thinning behavior, with viscosities decreasing by several orders of magnitude for shear rates from 0.001 to 10 s⁻¹. At low shear rate (~ 0.0001 s⁻¹), the peak viscosity of polymer P1 ranges from 4.6×10^5 Pa·s for the 2000% moisture content gel, to 2.0×10^6 Pa·s for the 500% moisture content gel. The viscosity of polymer P3 is more sensitive to changes in moisture content than the viscosity of polymer P1. The peak viscosity of polymer P3 ranges from 2.8×10^3 Pa·s for the 2000% moisture content gel to 2.7×10^5 Pa·s for the 500% moisture content gel.

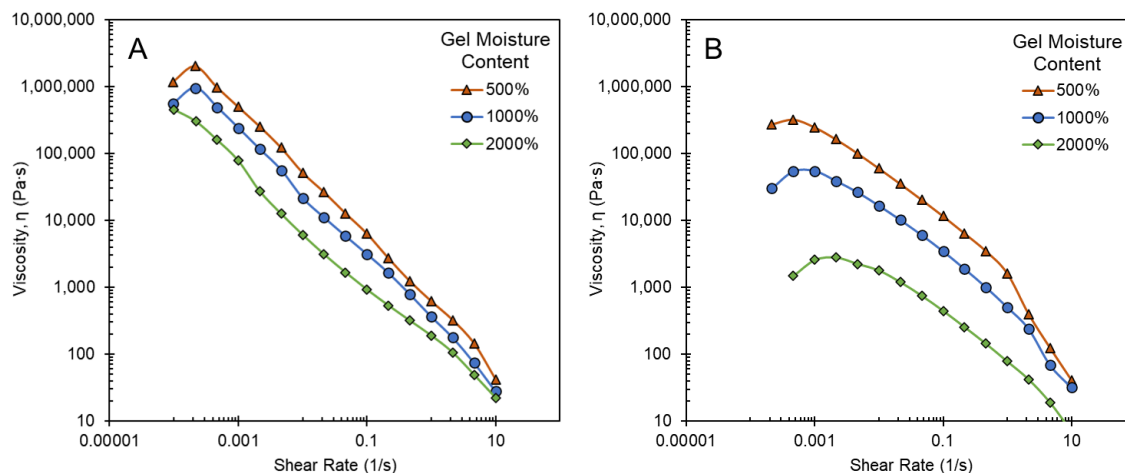


Figure 6.3. Viscosity (η) of polymer P1 (A) and P3 (B) gels at moisture contents of 500%, 1000%, and 2000%.

6.3.2 Model results

6.3.2.1 Polymer movement

Simplified models employing constant viscosity were used to understand the effect of viscosity on polymer elution. Three viscosities (η) were chosen: $\eta = 1 \times 10^6$ Pa·s, the approximate peak viscosity of the 500% moisture content P1 gel; $\eta = 3 \times 10^3$ Pa·s, the approximate peak viscosity of the 2000% moisture content P3 gel; and $\eta = 1 \times 10^2$ Pa·s, the approximate viscosity of gels approaching $\dot{\gamma} = 10 \text{ s}^{-1}$, and capturing a possible situation where polymer structure is degraded to an extent that the viscosity decreases precipitously. The models were run for simulation times of five seconds. This time span is extremely short, and therefore only represents the expected initial behavior of the gels in question. Simulation time was limited by long computation times (up to several days) on the available computing hardware.

The distribution of polymer for of each model at $t = 5 \text{ s}$ is shown in Figure 6.4. Blue corresponds to polymer, and red corresponds to the permeating solution. When $\eta = 1 \times 10^6$ Pa·s,

the gel moved towards the pore space, protruding into the pore space by $t = 1$ s, then remained in that location with only mild fluctuations in shape through $t = 5$ s. When $\eta = 3 \times 10^3$ Pa·s, the polymer began protruding into the pore space by $t = 0.1$ s, and had elongated and stretched past the top of the pore space by $t = 5$ s. When $\eta = 1 \times 10^2$ Pa·s, the polymer enters the pore space by $t = 0.1$ s and completely exits the pore space by $t = 1.2$ s.

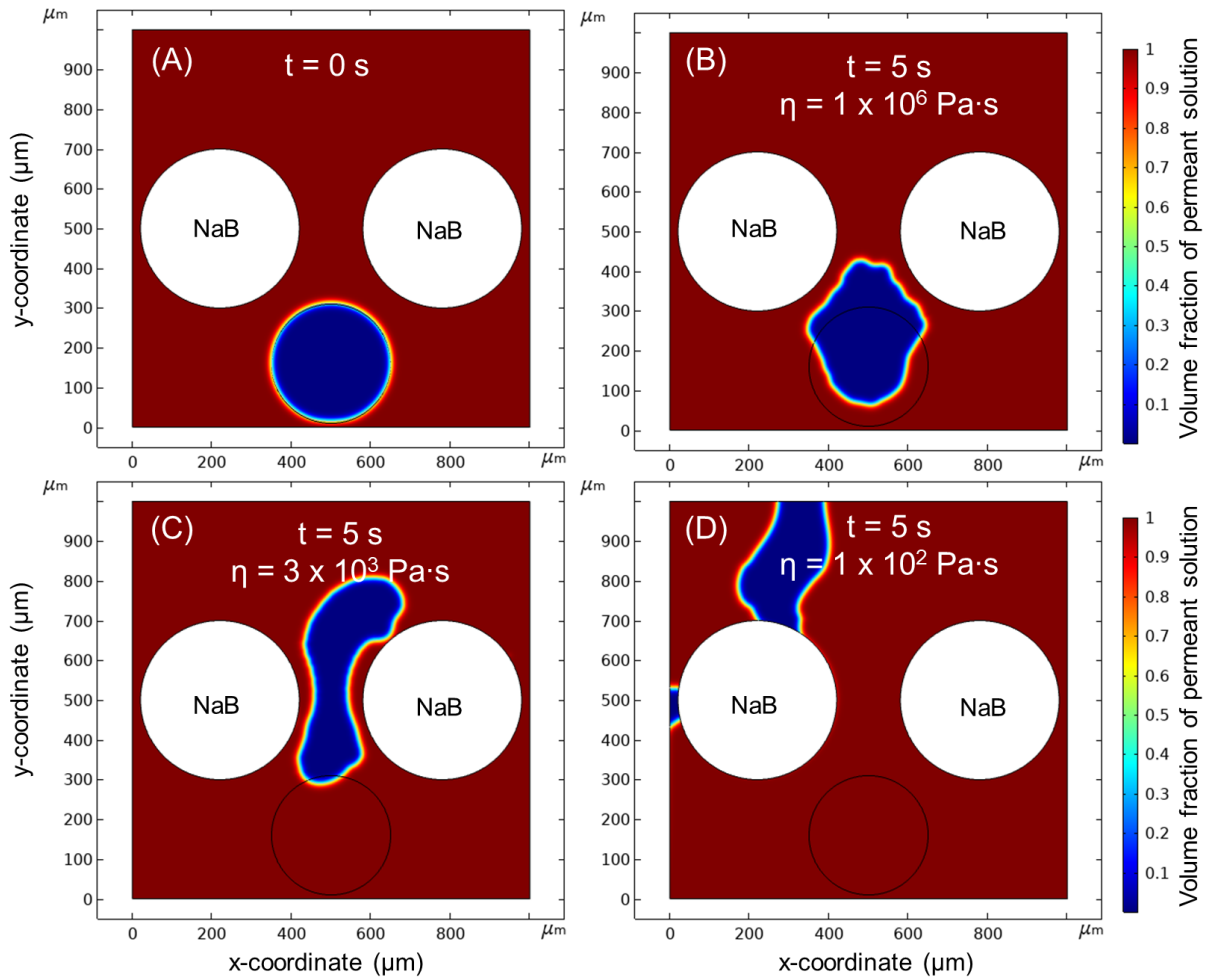


Figure 6.4. Distribution of the polymer at $t = 0$ (A), and $t = 5$ for $\eta = 1 \times 10^6$ Pa·s (B), $\eta = 3 \times 10^3$ Pa·s (C), and $\eta = 1 \times 10^2$ Pa·s (D). The polymer is indicated in blue, the permeant solution is indicated in red, and the NaB granules are indicated in white.

6.3.2.2 Changes in flow patterns

When polymer fills the pore space (e.g., $t = 5$ for $\eta = 1 \times 10^6 \text{ Pa}\cdot\text{s}$), flow is primarily directed through the narrow channels to the sides of the NaB granules, with maximum velocities on the order of 10^{-5} m/s and an average velocity across the outlet of $6.2 \times 10^{-5} \text{ m/s}$ (Fig. 6.5B). In contrast, when polymer has completely eluted from the pore space (e.g., $t = 5 \text{ s}$ for $\eta = 1 \times 10^2 \text{ Pa}\cdot\text{s}$), flow is directed through the center of the pore path with maximum velocities on the order of 1 m/s , and an average velocity across the outlet of $3.1 \times 10^{-1} \text{ m/s}$ (Fig. 6.5A).

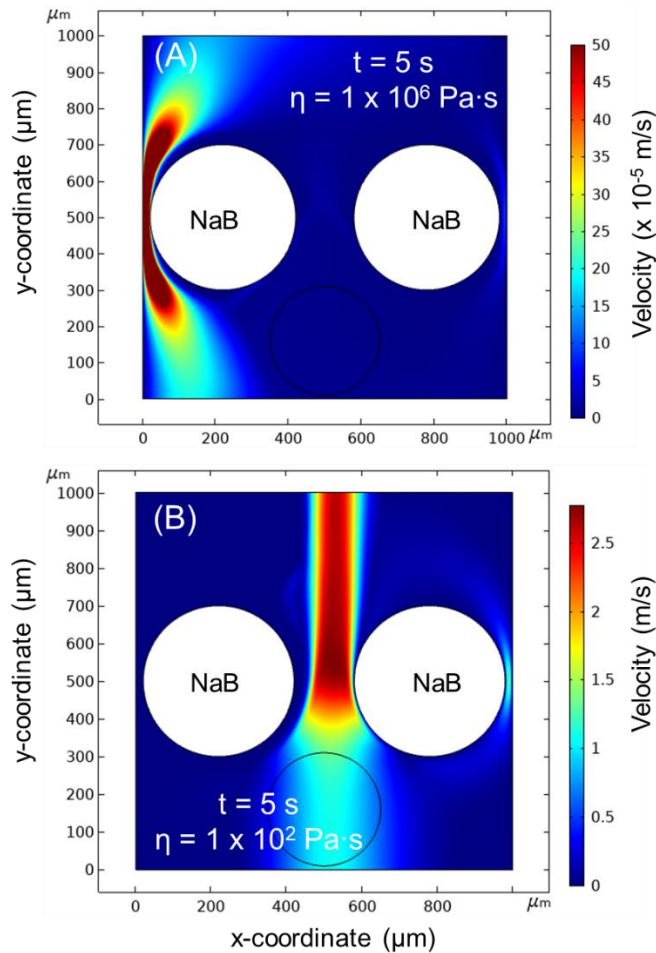


Figure 6.5. Velocity profiles when polymer is in the pore space (A; corresponding to Fig. 6.4B), and after polymer elutes from the pore space (B; corresponding to Fig. 6.4D).

6.3.2.3 Shear rate and shear stress

Due to the shear-thinning behavior of the polymer gels, the shear rate within the pore space will have a significant effect on the viscous behavior of the gel. Shear rate was assessed at four points throughout the model with $\eta = 1 \times 10^6 \text{ Pa}\cdot\text{s}$, for which the polymer stayed in the pore space (Fig. 6.6). The lowest shear rate was $3.4 \times 10^{-4} \text{ s}^{-1}$ at point 1 ($t = 5 \text{ s}$), and the highest shear rate was 1.2 at point 4 ($t = 0.6 \text{ s}$). The shear rate at point 4 decreased with time to 0.0074 s^{-1} at $t = 5$, at which time the shear rate was highest at point 2 (0.35 s^{-1}). This corresponds with expectations that shear rate should be highest near the wall of a pore (Gerhart et al. 2017).

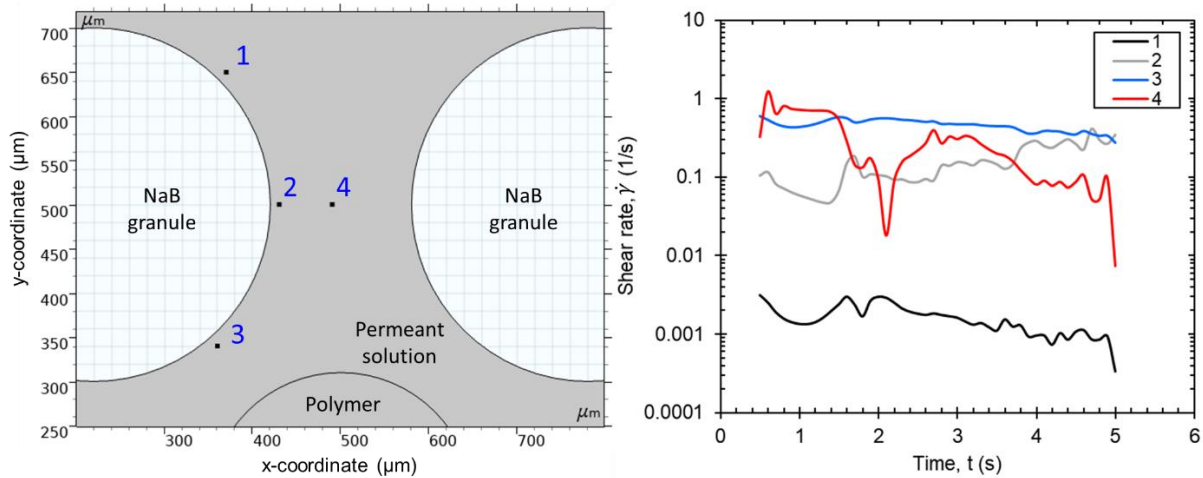


Figure 6.6. Shear rate, $\dot{\gamma}$, measured at various points for $\eta = 1 \times 10^6 \text{ Pa}\cdot\text{s}$.

The model with $\eta = 1 \times 10^6 \text{ Pa}\cdot\text{s}$ was based on the peak viscosity of the 500% moisture content P1 gel. However, the viscosity of this gel varies with shear rate. The shear rate, resulting viscosity (based on Fig. 6.3), and shear stress (the product of shear rate and viscosity) for conditions near the wall and at the center of the pore are summarized in Table 6.1. for the 500% moisture content P1 gel.

Table 6.1. Shear rate, approximate viscosity (based on Fig. 6.3), and approximate shear stress near the NaB granule, and in the center of the pore for the model with $\eta = 1 \times 10^6$ Pa·s. Approximate viscosity is based on the 500% moisture content P1 gel.

Condition	Corresponding point in model	Shear rate (1/s)	Approximate viscosity (Pa·s)	Approximate shear stress (kPa)
Near the wall	2	0.0074	62,000	0.46
Center of the pore	4	0.35	1,700	0.60

6.4 DISCUSSION

The mechanisms demonstrated in the models are consistent with empirical evidence of polymer elution in Chapters 3, 4 and 5. When polymer is retained in the pore space, flow is primarily directed through a narrow pore path at a low velocity. In contrast, when polymer elutes from the pore path, flow is concentrated through the larger pore at a much higher velocity.

BPC-GCLs containing polymers P1 and P3 (assessed in Ch. 4) had high hydraulic conductivities on the order of 10^{-8} m/s to 50 mM CaCl₂ (Fig. 6.7A). BPC-GCL-P1 initially maintained a low hydraulic conductivity on the order of 10^{-12} m/s before hydraulic conductivity dramatically increased after 1 pore volume of flow. In contrast, BPC-GCL-P3 maintained high hydraulic conductivity throughout the duration of permeation. Average velocities across the surfaces of these samples (i.e., Darcy velocities) were on the order of 10^{-10} m/s at low hydraulic conductivities, and on the order of 10^{-6} m/s at high hydraulic conductivities. The empirical velocities are orders of magnitude lower than the velocities in the model when the polymer was retained in the pore space (6.2×10^{-5} m/s) and when the polymer was eluted from the pore space (3.1×10^{-1} m/s). The differences in Darcy velocity can likely be attributed to the simplified geometry of the model compared to the complex geometry of pores in a BPC-GCL. Nevertheless,

the significant post-elution increases in pore and Darcy velocities are consistent with observations of increased flow rates in BPC-GCLs that experience significant polymer elution.

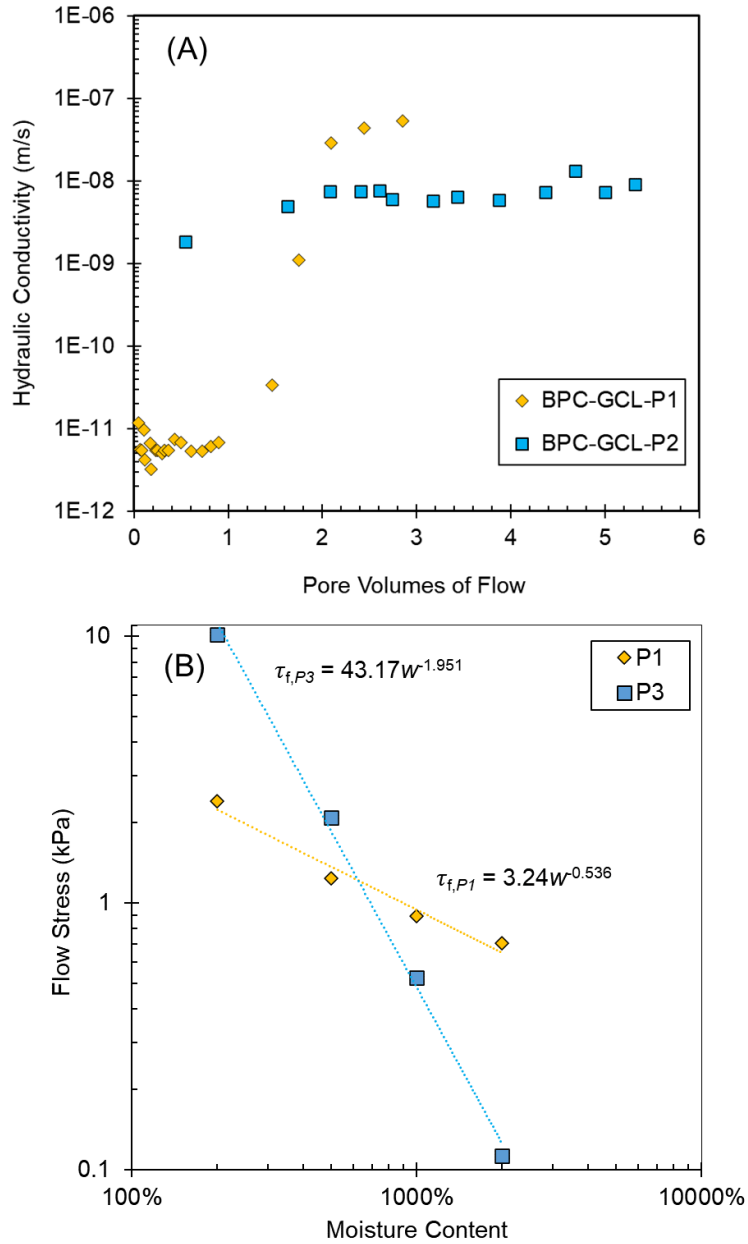


Figure 6.7. Hydraulic conductivity (A) of BPC-GCL-P1 and P3 to 50 mM CaCl₂, and and flow stress (B) of the corresponding polymer gels.

Flow stress is the shear stress at which polymers begin to behave more like liquids (viscous) than solids (elastic). Therefore when a polymer gel's flow stress is lower than the shear stress in the pore, the gel is more likely to elute. The shear stresses exhibited in the model (Table 6.1), are similar to flow stresses of P1 and P3 gels hydrated with 50 mM CaCl₂ to moisture contents above 500% (Fig. 6.7B). The moisture contents of these polymer gels based on the bentonite-polymer moisture affinity test are 613% for P1 and 667% for P3 (Ch. 4). Therefore, limited polymer elution may result in increased moisture content of the remaining gel to the point where shear stress is greater than flow stress, and a preferential flow path can open. This is consistent with BPC-GCL-P1 and -P3 both having high hydraulic conductivity to 50 mM CaCl₂, as well as preferential flow paths (Ch. 4).

6.5 RECOMMENDATIONS

The models developed in this study employ simplified geometries and constant property values to develop a basic model of polymer movement in a BPC-GCL pore space. To develop more realistic models, the complexity of geometry should be increased and time-dependent mathematic descriptions of property values should be developed.

The current model depicts a single pore path between two circular NaB granules. Realistically, NaB granules are irregular, and there are many pores that span the length of a hydrated BPC-GCL. Furthermore, depending on the swelling of the NaB component, the width of pores may change significantly. A model is recommended that employs irregular geometry with various linked pores and polymer placed throughout the pore spaces. Such a model could provide insight into the development of preferential flow paths that are seen in experimental studies of BPC-GCLs.

Viscosity was varied between simulations for this study, but the value of viscosity in a given simulation remained constant. Furthermore, no additional properties of the polymer gel (e.g., density, surface tension) were varied. Realistically, each of these properties may vary temporally as a result of aging (Chmelir et al. 1980), temperature (Ghannam and Esmail 1998), or dissolution (Miller-Chou and Koenig 2003). Additionally, polymer viscosity changes as a function of shear rate (Fig. 6.3), and shear rate can vary spatially and temporally by an order of magnitude or more (Fig. 6.6). To provide realistic service life predictions, mathematical descriptions of these properties should be developed based on empirical studies and input into the model. Additional variation in the size, shape, and number of polymer units in the model may help account for differences between cross-linked and linear polymers. For example, a cross-linked polymer may be modeled as several small units clustered together, as opposed to one larger unit as in this study.

6.6 SUMMARY AND CONCLUSIONS

A simplified model of polymer movement between NaB granules is developed here. This model further validates the mechanisms purported in previous chapters, whereby polymer elution results in preferential flow paths and high hydraulic conductivity in BPC-GCLs. The following conclusions are drawn:

- Polymer gels in the BPC-GCLs displayed decreases in viscosity with increasing moisture content and increasing shear rate.
- Decreased viscosity of polymer gels corresponds to decreased time to elution.
- When polymer fills the largest pore space available, flow is directed at lower velocities through more narrow pores, resulting in an overall decrease in velocity across the surface.

- Shear rate varies across a polymer-filled pore space, and is highest near the NaB granule (i.e., the wall of the pore).
- Shear stresses determined based on the model in this study are comparable to flow stresses of corresponding polymer gels with moisture contents >500%, and may therefore be sufficiently high to cause the polymer elution and high hydraulic conductivity observed during permeation of the corresponding BPC-GCLs.

The model developed in this study is too simplified and simulates too short a time span to adequately predict hydraulic conductivity or service life of BPC-GCLs. Nevertheless, this model serves as a basis for developing far more complex models that can adequately synthesize empirical data on NaB and polymer gel properties to produce service life predictions faster than currently possible through reliance on permeation tests.

6.7 ACKNOWLEDGMENTS

This study was completed in collaboration with Juan Hou of Shanghai University. This study was supported by CETCO, the US Department of Energy's Consortium for Risk Evaluation with Stakeholder Participation (CRESP) III through Cooperative Agreement No. DE-FC01-06EW07053, the Environmental Research and Education Foundation through a fellowship to the first author, and the Jefferson Scholars Foundation at University of Virginia. Materials for the study were provided by CETCO.

Chapter 7: Conclusions, Limitations, and Recommendations

7.1 SUMMARY AND CONCLUSIONS

BPC-GCLs containing proprietary polymers were permeated with aggressive solutions to assess the mechanisms controlling hydraulic conductivity and potential indices of compatibility. Hydraulic conductivity tests were also completed at 60 °C for selected samples. The viscoelastic properties of polymer gels were assessed and used to further understand the movement of polymers within BPC-GCLs. Models were developed using COMSOL to predict polymer elution in BPC-GCLs, which correspond well with empirical observations. These models are currently limited in their complexity and duration of modeling period; nevertheless, these models show promise for predicting the long-term compatibility between BPC-GCLs and aggressive solutions. Based on the studies presented here, the following conclusions are drawn:

- Excessive polymer elution results in preferential flow paths and high hydraulic conductivity in BPC-GCLs.
- Low flow-swell index, which is the product of the swell index of the NaB component and the flow stress of the polymer component, corresponds to high hydraulic conductivity in BPC-GCLs.
- The BPC-GCLs examined here maintained comparable hydraulic conductivity when permeated at 20 and 60 °C.
- BPC-GCLs that were batch aged at 60 °C maintained comparable hydraulic conductivity to continuously permeated samples, provided sufficient polymer was retained during the batch aging process.

- Viscosity of polymer gels decreases with increasing moisture content or shear rate, and decreases in viscosity correspond to faster rate of elution.

7.2 DEVELOPED OR IMPROVED METHODOLOGIES

Throughout the course of this research, several methods were either developed or improved for testing various properties of BPC-GCLs. These methods include:

- Bentonite-polymer moisture affinity test to approximate in-situ moisture content of the polymer and bentonite components of BPC-GCLs.
- Elevated temperature permeameters capable of maintaining consistent temperatures up to 60 °C.
- Batch aging in hydration containers with distributed elution points.
- Component total carbon analysis to determine polymer loading prior to and following hydration with salt solutions (Appendix A).

Methods traditionally utilized for testing NaB-GCLs are often applied to BPC-GCLs, but these methods may not accurately reflect the properties of BPC-GCLs. For example, Christian et al. (2020) recently demonstrated that swell index as measured by ASTM D5890 does not accurately capture the swell of BPCs due to polymer segregation during sample preparation. The test methods developed or improved through this research have been developed specifically for BPC-GCLs, and are therefore useful for accurately assessing BPC-GCL characteristics that are pertinent to service life predictions.

7.3 LIMITATIONS

Due to the proprietary nature of the polymers used in this study, detailed analysis of chemical degradation of polymers could not be completed. If the chemical formulations of the polymers were known or could be investigated, further understanding of reactions between dissolved species in leachates and functional groups on the polymers could be assessed. Nevertheless, proprietary polymers currently dominate the BPC-GCL market, therefore development of tests that don't require knowledge of the polymer chemistry are necessary for practical applications.

BPC-GCLs from a single manufacturer, containing a single type of granular NaB were used for all experiments in this research. The applicability of the flow-swell index and the effect of temperature on hydraulic conductivity should be further assessed using a greater variety of BPC-GCLs and leachates in the future.

Due to computing limitations, the COMSOL models developed in Chapter 6 utilized simplified geometry and short simulation times. Access to supercomputers could allow significantly more complex models to run for longer simulation times, which would improve the usefulness of these models for predicting the service lives of BPC-GCLs.

7.4 RECOMMENDATIONS

This research primarily focused on changes to the NaB and polymer components as processes that occur independent of each other, but simultaneously contribute to the size and tortuosity of pore paths, and consequently to hydraulic conductivity of BPC-GCLs. Future research should examine the bond between hydrated polymers and the NaB particle surface, for example through adsorption experiments (Heller and Keren 2003). A more robust understanding of the

bonding between polymers and NaB could improve the accuracy of the COMSOL models, improve the flow-swell index by incorporating a third crucial mechanism, and provide insight into the lack of correspondence between hydraulic conductivities at elevated temperatures and flow stress and swell indices.

Development of more realistic COMSOL models that can run for longer computation times is recommended. Longer computation times are desirable because polymer continued to elute throughout permeation experiments, (albeit with low polymer flux for low hydraulic conductivities). Thus, continuous elution could eventually lead to high hydraulic conductivities that are not captured in experimental studies in a timely fashion, especially for BPC-GCLs that are expected to maintain low hydraulic conductivity for up to hundreds of years. By developing more realistic COMSOL models, service lives may be predicted using a combination of results from short (< 1 month to complete) laboratory experiments and flow models in a much shorter time frame.

References

- Abdelaal, F. B., and Rowe, R. K. (2014). Effect of high temperatures on antioxidant depletion from different HDPE geomembranes. *Geotextiles and Geomembranes*, 42(4), 284–301.
- Abuel-Naga, H. M., and Bouazza, A. (2013). Thermomechanical Behavior of Saturated Geosynthetic Clay Liners. *Journal of Geotechnical and Geoenvironmental Engineering*, 139(4), 539–547.
- Abuel-Naga, H. M., Bouazza, A., and Gates, W. (2013). Impact of bentonite form on the thermal evolution of the hydraulic conductivity of geosynthetic clay liners. *Géotechnique Letters*, 3(2), 26–30.
- Ahmed, E. M. (2015). Hydrogel: Preparation , characterization , and applications: A review. *Journal of Advanced Research*, 6(2), 105–121.
- Akin, I. D., Chen, J., Likos, W. J., and Benson, C. H. (2017). Water Vapor Sorption of Bentonite-Polymer Mixtures Contacted with Aggressive Leachates. *Geotechnical Frontiers 2017*, 209–218.
- Ashe, L. E., Rowe, R. K., Brachman, R. W. I., and Take, W. A. (2015). Laboratory study of downslope erosion for 10 different GCLs. *Journal of Geotechnical and Geoenvironmental Engineering*, 141(1), 04014079-1-04014079–8.
- Ashmawy, A. K., El-Hajji, D., Sotelo, N., and Muhammad, N. (2002). Hydraulic performance of untreated and polymer-treated bentonite in inorganic landfill leachates. *Clays and Clay Minerals*, 50(5), 546–552.
- Athanassopoulos, C., Benson, C., Donovan, M., and Chen, J. (2015). Hydraulic Conductivity of a Polymer - Modified GCL Permeated with High - pH Solutions. *Geosynthetics 2015*, Industrial Fabrics Association International, St. Paul, MN, 181–186.

- Azad, F. M., El-Zein, A., Rowe, R. K., and Airey, D. W. (2012). Modelling of thermally induced desiccation of geosynthetic clay liners in double composite liner systems. *Geotextiles and Geomembranes*, Elsevier Ltd, 34, 28–38.
- Azad, F. M., Rowe, R. K., El-Zein, A., and Airey, D. W. (2011). Laboratory investigation of thermally induced desiccation of GCLs in double composite liner systems. *Geotextiles and Geomembranes*, Elsevier Ltd, 29(6), 534–543.
- Bag, R., and Rabbani, A. (2017). Effect of temperature on swelling pressure and compressibility characteristics of soil. *Applied Clay Science*, Elsevier B.V., 136, 1–7.
- Benson, C. H., Ören, A. H., and Gates, W. P. (2010). Hydraulic conductivity of two geosynthetic clay liners permeated with a hyperalkaline solution. *Geotextiles and Geomembranes*, Elsevier Ltd, 28(2), 206–218.
- Bouazza, A., Abuel-Naga, H. M., Gates, W. P., and Laloui, L. (2008). Temperature Effects on Volume Change and Hydraulic Properties of Geosynthetic Clay Liners. *The First Pan American Geosynthetics Conference & Exhibition*, 102–109.
- Bouazza, A., and Gates, W. P. (2014). Overview of performance compatibility issues of GCLs with respect to leachates of extreme chemistry. *Geosynthetics International*, 21(2), 151–167.
- Bouazza, A., Singh, R. M., Rowe, R. K., and Gassner, F. (2014). Heat and moisture migration in a geomembrane-GCL composite liner subjected to high temperatures and low vertical stresses. *Geotextiles and Geomembranes*, Elsevier Ltd, 42(5), 555–563.
- De Camillis, M., Di Emidio, G., Bezuijen, A., and Verástegui-Flores, R. D. (2016). Hydraulic conductivity and swelling ability of a polymer modified bentonite subjected to wet–dry cycles in seawater. *Geotextiles and Geomembranes*, 44(5), 739–747.
- De Camillis, M., Di Emidio, G., Bezuijen, A., Verastegui Flores, D., Van Stappen, J., and Cnudde,

- V. (2017). Effect of wet-dry cycles on polymer treated bentonite in seawater: swelling ability, hydraulic conductivity and crack analysis. *Applied Clay Science*, Elsevier B.V., 142, 52–59.
- Chai, J. C., and Prongmanee, N. (2020). Barrier properties of a geosynthetic clay liner using polymerized sodium bentonite. *Geotextiles and Geomembranes*, Elsevier, 48, 392–399.
- Chen, J., Benson, C. H., Likos, W. J., and Edil, T. B. (2017). Interface Shear Strength of a Bentonite-Polymer Geosynthetic Clay Liner and a Textured Geomembrane. *Geotechnical Frontiers 2017*, (November), 219–226.
- Chen, J., Salihoglu, H., Benson, C. H., and Likos, W. J. (2019). Hydraulic Conductivity of Bentonite-Polymer Geosynthetic Clay Liners to Coal Combustion Product Leachates. *Journal of Geotechnical and Geoenvironmental Engineering*, 145(9), 04019038.
- Chmelir, M., Kunschner, A., and Barthell, E. (1980). Water soluble acrylamide polymers, aging and viscous flow of aqueous solutions of polyacrylamide and hydrolyzed polyacrylamide. *Die Angewandte Makromolekular Chemie*, 89(1376), 145–165.
- Cho, W. J., Lee, J. O., and Chun, K. S. (1999). The temperature effects on hydraulic conductivity of compacted bentonite. *Applied Clay Science*, 14, 47–58.
- Christian, W., Zainab, B., Tian, K., and Abichou, T. (2020). Effect of specimen preparation on the swell index of bentonite-polymer GCLs. *Geotextiles and Geomembranes*, Elsevier Ltd, In Press.
- Conzelmann, J. T., Scalia IV, J., and Shackelford, C. D. (2017). Effect of backpressure saturation on the hydraulic conductivity of GCLs. *Geotechnical Frontiers*, 227–235.
- Donovan, M. S., Valorio, R., and Gebka, B. (2017). Polymer Enhanced Geosynthetic Clay Liners for Bauxite Storage. *Proceedings of 35th International ICSOBA Conference, Hamburg, Germany, 2-5 October, 2017*, 469–478.

- Di Emidio, G., Van Impe, W. F., and Verástegui-Flores, R. D. (2011). Advances in Geosynthetic Clay Liners: Polymer Enhanced Clays. *Geo-Frontiers 2011*, 1931–1940.
- Di Emidio, G., Mazzieri, F., Verastegui-Flores, R.-D., Van Impe, W., and Bezuijen, A. (2015). Polymer-treated bentonite clay for chemical-resistant geosynthetic clay liners. *Geosynthetics International*, 22(1), 125–137.
- Ewais, A. M. R., and Rowe, R. K. (2014). Effect of aging on the stress crack resistance of an HDPE geomembrane. *Polymer Degradation and Stability*, Elsevier Ltd, 109, 194–208.
- Geng, W., Likos, W. J., and Benson, C. H. (2016). Viscosity of Polymer-Modified Bentonite as a Hydraulic Performance Index. *Geo-Chicago 2016*, 498–507.
- Gerhart, P. M., Gerhart, A. L., and Hochstein, J. I. (2017). *Munson's Fluid Mechanics*. John Wiley & Sons Inc.
- Ghannam, M. T., and Esmail, M. N. (1998). Rheological properties of aqueous polyacrylamide solutions. *Journal of Applied Polymer Science*, 69(8), 1587–1597.
- Ghazizadeh, S., Bareither, C. A., Scalia, J., and Shackelford, C. D. (2018). Synthetic mining solutions for laboratory testing of geosynthetic clay liners. *Journal of Geotechnical and Geoenvironmental Engineering*, 144(10), 1–9.
- Gleason, M. H., Daniel, D. E., and Eykholt, G. R. (1997). Calcium and sodium bentonite for hydraulic containment applications. *Journal of Geotechnical Engineering*, 123(5), 438–445.
- Gustitus, S. A., and Benson, C. H. (2020). Assessing polymer elution and hydraulic conductivity of bentonite-polymer composite geosynthetic clay liners permeated with aggressive solutions. *4th Pan American Conference on Geosynthetics*.
- Gustitus, S. A., Nguyen, D., Chen, J., and Benson, C. H. (2020). Quantifying Polymer Loading in Bentonite-Polymer Composites Using Loss on Ignition and Total Carbon Analyses.

Geotechnical Testing Journal, In Press.

Heller, H., and Keren, R. (2003). Anionic polyacrylamide polymer adsorption by pyrophyllite and montmorillonite. *Clay and Clay Minerals*, 51(3), 334–339.

Hornsey, W. P., Scheirs, J., Gates, W. P., and Bouazza, A. (2010). The impact of mining solutions/liquors on geosynthetics. *Geotextiles and Geomembranes*, Elsevier Ltd, 28(2), 191–198.

Ishimori, H., and Katsumi, T. (2012). Temperature effects on the swelling capacity and barrier performance of geosynthetic clay liners permeated with sodium chloride solutions. *Geotextiles and Geomembranes*, 33, 25–33.

Jo, H. Y., Benson, C. H., Shackelford, C. D., Lee, J., and Edil, T. B. (2005). Long-Term Hydraulic Conductivity of a Geosynthetic Clay Liner Permeated with Inorganic Salt Solutions. *Journal of Geotechnical and Geoenvironmental Engineering*, 131(4), 405–417.

Jo, H. Y., Katsumi, T., Benson, C. H., and Edil, T. B. (2001). Hydraulic Conductivity and Swelling of Nonprehydrated GCLs Permeated with Single-Species Salt Solutions. *Journal of Geotechnical and Geoenvironmental Engineering*, 127(7), 557–567.

Keller, A. A., Blunt, M. J., and Roberts, P. V. (1997). Micromodel Observation of the Role of Oil Layers in Three-Phase Flow. *Transport in Porous Media*, 26(3), 277–297.

Klein, R., Baumann, T., Kahapka, E., and Niessner, R. (2001). Temperature development in a modern municipal solid waste incineration (MSWI) bottom ash landfill with regard to sustainable waste management. *Journal of Hazardous Materials*, 83(3), 265–280.

Koerner, G. R., and Koerner, R. M. (2006). Long-term temperature monitoring of geomembranes at dry and wet landfills. *Geotextiles and Geomembranes*, 24(1), 72–77.

Kolstad, D. C., Benson, C. H., and Edil, T. B. (2004). Hydraulic Conductivity and Swell of

- Nonprehydrated Geosynthetic Clay Liners Permeated with Multispecies Inorganic Solutions. *Journal of Geotechnical and Geoenvironmental Engineering*, 130(12), 1236–1249.
- Krushelnitzky, R. P., and Brachman, R. W. I. (2013). Buried high-density polyethylene pipe deflections at elevated temperatures. *Geotextiles and Geomembranes*, Elsevier Ltd, 40, 69–77.
- Liu, Y., Bouazza, A., Gates, W. P., and Rowe, R. K. (2015). Hydraulic performance of geosynthetic clay liners to sulfuric acid solutions. *Geotextiles and Geomembranes*, Elsevier Ltd, 43(1), 14–23.
- McRory, J. A., and Ashmawy, A. K. (2005). Polymer Treatment of Bentonite Clay for Contaminant Resistant Barriers. *Geo-Frontiers Congress 2005*, Austin, TX.
- Mezger, T. G. (2015). *Applied Rheology*. Anton Paar GmbH, Austria.
- Miller-Chou, B. A., and Koenig, J. L. (2003). A review of polymer dissolution. *Progress in Polymer Science*, 28(8), 1223–1270.
- Mitchell, J. K., and Soga, K. (2005). *Fundamentals of Soil Behavior*. John Wiley & Sons.
- Moore, D. M., and Reynolds, R. C. (1989). *X-Ray Diffraction and the Identification and Analysis of Clay Minerals*. Oxford University Press, Oxford.
- Norris, A., Scalia, J., and Shackelford, C. (2019). Fluid indicator test (FIT) for screening the hydraulic conductivity of enhanced bentonites to inorganic aqueous solutions. *Proceedings of the 8th International Congress on Environmental Geotechnics*, 2, 446–453.
- Norrish, K., and Quirk, J. P. (1954). Crystalline swelling of montmorillonite: use of electrolytes to control swelling. *Nature*, 173, 255–256.
- Ören, A. H., Öztürk, M., Özdamar Kul, T., and Nart, Z. (2019). Barrier performance of geosynthetic clay liners to copper (II) chloride solutions. *Environmental Geotechnics*, 1–10.

- Özhan, H. O. (2017). Problems and solutions for GCLs used in waste containment facilities: temperature concerns and polymer treatment related to GCLs used in waste containment areas. *Innovative Infrastructure Solutions*, 2(1), 43.
- Özhan, H. O. (2018). Hydraulic capability of polymer-treated GCLs in saline solutions at elevated temperatures. *Applied Clay Science*, 161, 364–373.
- Petrov, R. J., Rowe, R. K., and Quigley, R. M. (1997). Selected factors influencing GCL hydraulic conductivity. *Journal of Geotechnical Engineering*, 123(8), 683–695.
- Prongmanee, N., and Chai, J. C. (2019). Performance of Geosynthetic Clay Liner with Polymerized Bentonite in Highly Acidic or Alkaline Solutions. *International Journal of Geosynthetics and Ground Engineering*, Springer International Publishing, 5, 1–11.
- Prongmanee, N., Chai, J. C., and Shen, S. (2018a). Hydraulic properties of polymerized bentonites. *Journal of Materials in Civil Engineering*, 30(10), 04018247.
- Prongmanee, N., Chai, J. C., and Shrestha, S. (2018b). Effect of cations on consolidation and permeability of polymerized bentonite. *Lowland Technology International 2018*, 20(3), 297–304.
- Ramos Filho, F. G., Melo, T. J. A., Rabello, M. S., and Silva, S. M. L. (2005). Thermal stability of nanocomposites based on polypropylene and bentonite. *Polymer Degradation and Stability*, 89(3), 383–392.
- Razakamanantsoa, A. R., Barast, G., and Djeran-maigre, I. (2012). Hydraulic performance of activated calcium bentonite treated by polyionic charged polymer. *Applied Clay Science*, Elsevier B.V., 59–60, 103–114.
- Razakamanantsoa, A. R., and Djeran-Maigre, I. (2016). Long term chemo-hydro-mechanical behavior of compacted soil bentonite polymer complex submitted to synthetic leachate. *Waste*

- Management*, Elsevier Ltd, 53, 92–104.
- Rowe, R. K. (2005). Long-term performance of contaminant barrier systems. *Geotechnique*, 55(9), 631–678.
- Rowe, R. K., Brachman, R. W. I., Take, W. A., Rentz, A., and Ashe, L. E. (2016a). Field and laboratory observations of down-slope bentonite migration in exposed composite liners. *Geotextiles and Geomembranes*, Elsevier Ltd, 44(5), 686–706.
- Rowe, R. K., and Islam, M. Z. (2009). Impact of landfill liner time-temperature history on the service life of HDPE geomembranes. *Waste Management*, Elsevier Ltd, 29(10), 2689–2699.
- Rowe, R. K., Mukunoki, T., and Sangam, H. P. (2005). BTEX diffusion and sorption for a geosynthetic clay liner at two temperatures. *Journal of Geotechnical and Geoenvironmental Engineering*, 131(10), 1211–1221.
- Rowe, R. K., Rentz, A. K., Brachman, R. W. I., and Take, W. A. (2016b). Effect of GCL type on downslope erosion in an exposed composite liner. *Journal of Geotechnical and Geoenvironmental Engineering*, 142(12), 1–10.
- Rowe, R. K., Rimal, S., and Sangam, H. (2009). Ageing of HDPE geomembrane exposed to air, water and leachate at different temperatures. *Geotextiles and Geomembranes*, 27(2), 137–151.
- Salemi, N., Abtahi, S. M., Rowshanzamir, M. A., and Hejazi, S. M. (2019). Improving hydraulic performance and durability of sandwich clay liner using super-absorbent polymer. *Journal of Sandwich Structures and Materials*, 21(3), 1055–1071.
- Scalia, J., Benson, C. H., Bohnhoff, G. L., Edil, T. B., and Shackelford, C. D. (2014). Long-Term Hydraulic Conductivity of a Bentonite-Polymer Composite Permeated with Aggressive Inorganic Solutions. *Journal of Geotechnical and Geoenvironmental Engineering*, 140(3),

04013025.

- Scalia, J., Benson, C. H., Edil, T. B., Bonhoff, G. L., and Shackelford, C. D. (2011). Geosynthetic Clay Liners Containing Bentonite Polymer Nanocomposite. *Geo-Frontiers 2011*, 2001–2009.
- Scalia, J., Benson, C. H., and Finnegan, M. (2019). Alternate Procedures for Swell Index Testing of Granular Bentonite from GCLs. *Geotechnical Testing Journal*, 42(5), 1169–1184.
- Scalia, J., Bohnhoff, G. L., Shackelford, C. D., Benson, C. H., Sample-Lord, K. M., Malusis, M. A., and Likos, W. J. (2018). Enhanced bentonites for containment of inorganic waste leachates by GCLs. *Geosynthetics International*, 25(4), 392–411.
- Shackelford, C. D., Benson, C. H., Katsumi, T., Edil, T. B., and Lin, L. (2000). Evaluating the hydraulic conductivity of GCLs permeated with non-standard liquids. *Geotextiles and Geomembranes*, 18(2–4), 133–161.
- Shackelford, C. D., Sevick, G. W., and Eykholt, G. R. (2010). Hydraulic conductivity of geosynthetic clay liners to tailings impoundment solutions. *Geotextiles and Geomembranes*, Elsevier Ltd, 28(2), 149–162.
- Southen, J. M., and Rowe, R. K. (2005). Modelling of thermally induced desiccation of geosynthetic clay liners. *Geotextiles and Geomembranes*, 23(5), 425–442.
- Stutzmann, T., and Siffert, B. (1977). Contribution to the Adsorption Mechanism of Acetamide and Polyacrylamide on to Clays. *Clays and Clay Minerals*, 25(6), 392–406.
- Tian, K., and Benson, C. H. (2018). Containing Bauxite Liquor Using Bentonite-Polymer Composite Geosynthetic Clay Liners. *Proc. 8th Intl. Conference on Environmental Geotechnics*, L. Zhan, ed., Springer Nature, Singapore, 672–678.
- Tian, K., Benson, C. H., and Likos, W. J. (2016a). Hydraulic Conductivity of Geosynthetic Clay Liners to Low-Level Radioactive Waste Leachate. *Journal of Geotechnical and*

- Geoenvironmental Engineering*, 142(8), 04013037.
- Tian, K., Benson, C. H., and Likos, W. J. (2017a). Effect of an anion ratio on the hydraulic conductivity of a bentonite-polymer geosynthetic clay liner. *Geotechnical Frontiers 2017*, 180–189.
- Tian, K., Benson, C. H., Tinjum, J. M., and Edil, T. B. (2017b). Antioxidant Depletion and Service Life Prediction for HDPE Geomembranes Exposed to Low-Level Radioactive Waste Leachate. *Journal of Geotechnical and Geoenvironmental Engineering*, 143(6), 04017011-1-04017011–11.
- Tian, K., Likos, W., and Benson, C. (2019). Polymer Elution and Hydraulic Conductivity of Bentonite – Polymer Composite Geosynthetic Clay Liners. *Journal of Geotechnical and Geoenvironmental Engineering*, 145(10), 04019071.
- Tian, K., Likos, W. J., and Benson, C. H. (2016b). Pore-Scale Imaging of Polymer-Modified Bentonite in Saline Solutions. *Proc. Geo-Chicago 2016*, American Society of Civil Engineers, ed., Reston, VA, 468–477.
- Villar, M. V., and Lloret, A. (2004). Influence of temperature on the hydro-mechanical behaviour of a compacted bentonite. *Applied Clay Science*, 26(1-4 SPEC. ISS.), 337–350.
- Wang, B., Dong, X., Chen, B., and Dou, T. (2019). Hydraulic Conductivity of Geosynthetic Clay Liners Permeated with Acid Mine Drainage. *Mine Water and the Environment*, Springer Berlin Heidelberg, 38, 658–666.
- Yeşiller, N., Hanson, J. L., and Yee, E. H. (2015). Waste heat generation: A comprehensive review. *Waste Management*, 42, 166–179.
- Young, R. J., and Lovell, P. A. (2011). *Introduction to Polymers*. CRC Press.
- Yu, B., El-Zein, A., and Rowe, R. K. (2020). Effect of added polymer on the desiccation and

healing of a geosynthetic clay liner subject to thermal gradients. *Geotextiles and Geomembranes*, Elsevier Ltd, In Press.

Appendix A



Geotechnical Testing Journal

Sarah A. Gustitus,¹ Dorian Nguyen,¹ Jiannan Chen,¹ and Craig H. Benson²

DOI: 10.1520/GTJ20200007

Quantifying Polymer Loading in
Bentonite-Polymer Composites
Using Loss on Ignition and Total
Carbon Analyses

Sarah A. Gustitus,¹ Dorian Nguyen,¹ Jiannan Chen,¹ and Craig H. Benson²

Quantifying Polymer Loading in Bentonite-Polymer Composites Using Loss on Ignition and Total Carbon Analyses

Reference

S. A. Gustitus, D. Nguyen, J. Chen, and C. H. Benson, "Quantifying Polymer Loading in Bentonite-Polymer Composites Using Loss on Ignition and Total Carbon Analyses," *Geotechnical Testing Journal* <https://doi.org/10.1520/GTJ20200007>

ABSTRACT

Three methods were evaluated to measure polymer loading in bentonite-polymer composites (BPCs): component loss on ignition (LOI), composite LOI, and composite total carbon (TC). Component methods are based on a series of measurements (e.g., LOI) conducted independently on bentonite and polymer components. Composite methods are based on a series of measurements (e.g., LOI or TC) conducted on BPCs with known polymer loadings. All three methods were evaluated using three different BPCs, with polymer loading ranging from 20 to 100 g polymer/kg BPC. Polymer loading measured with the component LOI method was biased because of the effects of the bentonite on thermal degradation reactions occurring in the polymer component. Polymer loading of unhydrated BPCs measured with the composite LOI or TC methods showed no polymer-dependent bias. Measured polymer loading deviated from actual polymer loading by an average of -3.3 to 0.1 g polymer/kg BPC for the composite LOI method, and by an average of 2.5 to 3.8 g polymer/kg BPC for the composite TC method. Hydration of the BPCs influenced the accuracy of the composite LOI method, which produced consistently lower polymer loading measurements for BPCs hydrated with DI water than 50 mM CaCl_2 . In contrast, polymer loading measured with the composite TC method was not measurably different for hydrated and unhydrated samples. The composite LOI method is recommended for quality control testing on BPCs prior to hydration, whereas the composite TC method is recommended for testing BPCs prior to and/or following hydration.

Keywords

bentonite-polymer composite, geosynthetic clay liner, polymer loading, loss on ignition, total carbon

Manuscript received January 7, 2020; accepted for publication July 31, 2020; published online xxxx xx, xxxx.

¹ Department of Engineering Systems and Environment, University of Virginia, 151 Engineers Way, 114 Olsson Hall, Charlottesville, VA 22903, USA, <https://orcid.org/0000-0001-7225-2395> (S.G.), <https://orcid.org/0000-0002-1775-340X> (D.N.)

² School of Engineering, University of Virginia, 351 McCormick Rd., Thornton Hall A124, Charlottesville, VA 22904, USA (Corresponding author), e-mail: chbenson@virginia.edu, <https://orcid.org/0000-0001-8871-382X>

Introduction

Bentonite-polymer composite (BPC) geosynthetic clay liners (GCLs) are used for lining containment facilities with leachates that are too aggressive for conventional GCLs containing sodium bentonite. BPCs maintain low hydraulic conductivity when permeated with aggressive leachates provided the polymer component fills larger pore spaces between bentonite clusters, creating narrower and more tortuous pores that constrain flow even if swelling of the bentonite is limited (Scalia et al. 2014; Athanassopoulos et al. 2015; Tian, Benson, and Likos 2016; Tian, Likos, and Benson 2016; Chen, Tian, and Benson 2018; Tian and Benson 2018). To maintain low hydraulic conductivity, BPC-GCLs must have sufficient polymer loading (mass polymer/mass BPC on a dry mass basis) and must retain the polymer during permeation (Tian, Likos, and Benson 2016, 2019; Chen et al. 2019).

Measuring polymer loading of a BPC-GCL is necessary for manufacturing quality control, construction quality control, and forensic assessment of BPCs (Scalia et al. 2014; Tian, Benson, and Likos 2016; Chen et al. 2019). No standard method currently exists to measure the polymer loading of BPCs. One approach to measure polymer loading is to assume that the polymer loading equals the loss on ignition (LOI) measured using an LOI thermal degradation procedure, such as those described in ASTM D7348-13, *Standard Test Methods for Loss on Ignition (LOI) of Solid Combustion Residues*. LOI is a measurement of the mass lost during a high-temperature heating ramp relative to the original mass of the sample, and it is traditionally used as a measure of the organic matter content of a mixture. Directly relating LOI to polymer loading implicitly assumes that the only mass lost during an LOI test is associated with the polymer (i.e., the organic component) and that the polymer is fully degraded during the LOI test. This direct approach can misrepresent polymer loading if polymer degradation during the LOI test is incomplete or if the bentonite component (i.e., the inorganic component) loses mass during an LOI test (e.g., from tightly held water released at high temperature) (Grim 1968; Scalia et al. 2014; Williams 2018). For example, Scalia et al. (2014) report that only 74.7 % of the mass of polyacrylate polymer (decomposition temperature $\sim 200^{\circ}\text{C}$) in a BPC was degraded during an LOI test at 550°C and that the bentonite lost 1.6 % of its mass during the LOI test.

Scalia et al. (2014) developed the component method to address discrepancies between LOI measurements and polymer loading. In the component method, LOI tests are conducted independently on the separate components—the polymer and the bentonite—to account for incomplete degradation of the polymer and loss of mass from the bentonite component during LOI testing. The mass loss during heating for each component is used to develop a relationship between polymer loading and LOI of the BPC. The component method assumes explicitly that the mass loss of the polymer and the bentonite during heating is the same regardless of whether the components are exposed to high temperatures independently or in a BPC. These assumptions may or may not be realized for a given BPC.

Composite methods avoid the assumptions about polymer degradation and mass loss in the bentonite that are inherent in the component method. In the composite method, “BPC standards” are prepared with known polymer loading over a range that represents polymer loadings encountered in practice. An LOI test is conducted on each BPC standard, and a relationship is developed between the known polymer loading and the measured LOI. This relationship is then used to determine the polymer loading of a BPC with unknown polymer loading based on the measured LOI of that BPC. Composite methods can also employ alternative parameters for measuring the organic component, such as total carbon (TC).

In this study, the efficacy of the component and composite methods for measuring polymer loading in BPCs via LOI testing were compared and evaluated. An additional composite method was evaluated that relies on TC measurements in lieu of LOI measurements. A summary of the component and composite methods that were evaluated is provided in [Table 1](#). Tests were conducted on BPCs containing three different commercially available proprietary polymers with polymer loading ranging from 20 to 100 g polymer/kg BPC.

TABLE 1

Methods evaluated to measure polymer loading in this study

Method	Component LOI Method	Composite LOI Method	Composite TC Method
Synopsis	Relates fraction of bentonite, polymer, and BPC remaining after LOI test to polymer loading.	Relates LOI directly to known polymer loading of BPC standards.	Relates NDIR signal directly to known polymer loading of BPC standards.
Applicable equations	$L = \frac{r_b - r_p}{r_b - r_p}$ L = polymer loading; r_o , r_p , and r_b = fractions of BPC, polymer, bentonite mass remaining after LOI test	$LOI = \frac{(m_i - m_f - \Delta m_e)}{m_i - m_e} m_e$ m_e = initial mass of empty crucible; m_i = initial mass of specimen and crucible; m_f = final mass of specimen and crucible; Δm_e = change in mass of the empty crucible	None applicable
Instruments	Drying oven, scale, muffle furnace	Drying oven, scale, muffle furnace	Drying oven, scale, total carbon analyzer
Sample mass	4–5 g	4–5 g	0.08–0.4 g
Sample particle size	<US No. 60 sieve (0.25 mm)	<US No. 60 sieve (0.25 mm)	<US No. 60 sieve (0.25 mm)
Crucible preparation	Heat at 110°C for ≥ 24 h until no mass change.	Heat at 110°C for ≥ 24 h until no mass change.	None applicable
Drying sample prior to test	Heat at 110°C for ≥ 24 h until no mass change. After transferring to crucible, heat at 110°C for additional 1 h.	Heat at 110°C for ≥ 24 h until no mass change. After transferring to crucible, heat at 110°C for additional 1 h.	Heat at 110°C for ≥ 24 h until no mass change.
Test temperature ramp	Increase to 500°C over 1 h, increase again to 750°C over 1 h, maintain at 750°C for 2 h.	Increase to 500°C over 1 h, increase again to 750°C over 1 h, maintain at 750°C for 2 h.	Preheat TC furnace to 900°C, hold at 900°C for duration of testing.
Weighing procedure	Cool in a desiccator ~ 5 min, rapidly weigh.	Cool in a desiccator ~ 5 min, rapidly weigh.	None applicable

Note: NDIR = nondispersive infrared detector.

Methods Evaluated to Measure Polymer Loading

COMPONENT METHOD

The component method is based on a mass balance of the BPC and its bentonite and polymer fractions before and after LOI testing:

$$r_c m_c = r_p m_p + r_b m_b \quad (1)$$

In equation (1), m_i corresponds to initial masses of BPC, polymer, or bentonite ($i = c, p, \text{ or } b$) prior to the LOI test, and r_i is the fraction of BPC, polymer, or bentonite mass remaining after the LOI test. Polymer loading, L , of the BPC is obtained by rearranging equation (1):

$$L = \frac{m_p}{m_c} = \frac{r_b - r_c}{r_b - r_p} \quad (2)$$

In the component LOI method, r_b and r_p are defined a priori based on LOI tests conducted on standards of the base bentonite alone and the polymer alone. LOI tests are conducted on BPC test specimens with unknown polymer loading to determine r_c for each specimen. The polymer loading for a given BPC test specimen is then computed with equation (2) using r_c from the LOI test on the BPC sample, and r_b and r_p are determined a priori from the LOI tests on the bentonite alone and polymer alone.

The component method assumes that thermal degradation of the polymer is not affected by the presence of bentonite. The component method also implicitly assumes that the loss of tightly held water molecules associated with the bentonite is independent of chemical interactions with the bentonite that may occur prior to the LOI test (e.g., if the BPC is contacted by leachate). These conditions may not always be realized. For example, Ramos Filho et al. (2005) report that polypropylene degrades differently when heated alone compared to when heated in a composite with bentonite. They attribute the difference to bentonite being a catalyst for polymer oxidation. Similarly, the fraction of tightly held water molecules liberated during LOI testing of bentonite depends on the composition of the exchange complex of the bentonite, which is altered when a salt solution contacts a BPC. For example, Yeşilbaş, Holmboe, and Boily (2018) compared the mass loss of sodium-montmorillonite (MMT) and calcium-MMT using thermogravimetric analysis (TGA) and report that the mass loss from calcium-MMT is higher than that of sodium-MMT at 750°C, all other factors being equal.

The component LOI method evaluated in this study is a modified version of the component method developed by Scalia et al. (2014). The LOI procedure in this study employs the temperature ramp and particle size prescribed in Method A of ASTM D7348, as summarized in Table 1. The heating ramp stipulated in ASTM D7348 has a maximum temperature of 750°C, whereas a maximum temperature of 550°C was used by Scalia et al. (2014). ASTM D7348 also requires that the test material be ground to pass a US No. 60 sieve, whereas Scalia et al. (2014) ground test material must pass a US No. 20 sieve. The impact of the differences between the experimental procedure in Scalia et al. (2014) and the one used here were not investigated and are outside of the scope of this study.

COMPOSITE METHODS

The composite LOI method relies on a relationship between polymer loading and LOI of BPC standards with known polymer loading, as opposed to LOI of individual components. BPC standards are prepared with different polymer loadings that bracket the range of polymer loading encountered in practice, and a direct relationship is developed between LOI and polymer loading of the BPC standards (Table 1). An LOI test is then performed on a BPC with unknown polymer loading, and the aforementioned relationship is used to determine polymer loading of the unknown BPC based on the LOI measurement. The composite method is a more direct method than the component method, but it provides no information about the thermal degradation of the independent components.

Other methods to quantify the polymer fraction of a BPC can be used in lieu of LOI in the composite method or the component method. In this study, a variant of the composite method was evaluated using TC as a surrogate

measure of polymer in the BPC test specimen. TC analysis can be used to measure polymer content because carbon is a major fraction of the polymer in BPCs, whereas bentonite normally contains only trace amounts of carbon. This procedure is referred to as the composite TC method in [Table 1](#).

Experimental Materials and Procedures

POLYMERS

Three polymers (P1, P2, and P3) used for commercially available BPC-GCLs were used to create BPCs with known polymer loading. The polymers are synthetic and water-soluble or water-swelling. P1 is a cross-linked polymer for use with alkaline solutions, P2 is a cross-linked polymer for acidic solutions, and P3 is a linear polymer for use with neutral or alkaline solutions. These polymers were selected because they are being used in BPC-GCL products distributed globally and for which test methods to determine polymer loading are needed. The polymers are proprietary to the manufacturers; therefore, their chemical formulations are not available.

BENTONITE

Sodium bentonite was used as the base clay for all BPCs. Cation exchange capacity (CEC) and mole fractions of the primary bound cations (Na^+ , K^+ , Ca^{2+} , and Mg^{2+}) were determined by ASTM [D7503-18](#), *Standard Test Method for Measuring the Exchange Complex and Cation Exchange Capacity of Inorganic Fine-Grained Soils*. CEC of the bentonite is 83.4 ± 6.9 cmol⁺/kg (5 tests), and Na^+ is the predominant bound cation (mole fraction = 0.68), with K^+ (0.01), Ca^{2+} (0.14), and Mg^{2+} (0.12) in lesser quantities. Quantitative X-ray diffraction conducted using the methods in Moore and Reynolds ([1989](#)) and Scalia et al. ([2014](#)) indicate that the montmorillonite content of the bentonite is 96.5 % along with measurable quantities of quartz (1 %), halite (1 %), pyrite (1 %), and chlorite (0.5 %).

BPC PREPARATION

BPCs were created by thoroughly mixing known masses of air-dry polymer and bentonite with a spatula using great care to ensure that the mixture was as uniform as possible. Water contents of the polymer and bentonite at the time of mixing were measured following ASTM [D2216-19](#), *Standard Test Methods for Laboratory Determination of Water (Moisture) Content of Soil and Rock by Mass*, and were used to compute the polymer loading on a dry mass basis. After mixing, the BPCs were ground using a mechanical mortar grinder (Retsch RM 200, Haan, Germany) until 100 % passed a US No. 60 sieve (0.25-mm opening) to meet the requirements of Method A of ASTM [D7348](#) used for LOI testing. Ground samples were hand mixed again with the spatula to ensure that the ground BPC was as uniform as possible.

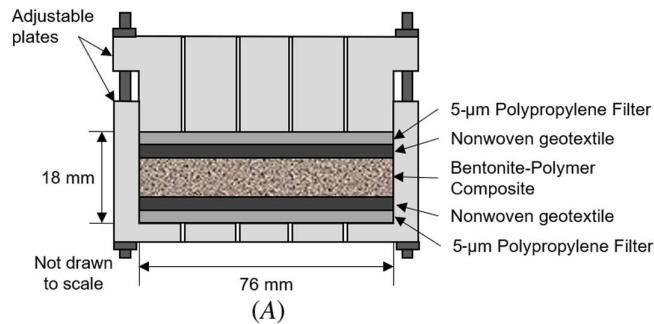
Some BPC mixtures evaluated by the composite method were hydrated prior to testing to evaluate how hydration and cation exchange may affect measurements of polymer loading. Hydration was conducted in a hydration cell ([fig. 1](#)) submerged in a 1.6-L container filled with test solution of either deionized (DI) water or 50 mM CaCl_2 . The hydration cell contains a 76 by 76-mm BPC specimen that can have a thickness up to 18 mm (8-mm-thick specimens were used in this study). The top and bottom plates are perforated with 3-mm-diameter holes that allow solution to contact the BPC. A 5- μm polypropylene filter is placed between the plates and geotextiles on either side of the BPC to minimize polymer elution. The geotextiles facilitate an even distribution of solution across the sample. Based on visual inspection, 7 days was sufficient for uniform hydration of the sample. After 7 days of hydration, the entire BPC sample was removed from the container, dried at 110 °C, then ground following the same grinding procedure used for unhydrated samples. Ground samples were manually mixed for homogenization.

LOI

The LOI of BPC specimens and components was measured following the procedure in Method A of ASTM [D7348](#). Because of the relatively low changes in mass that were measured (as low as 0.25 g for the bentonite

FIG. 1

Hydration cell for hydrating BPCs: (A) schematic and (B) photograph.



component) and the propensity of the polymer to absorb moisture, great care was taken during preparation of samples to minimize the effects of moisture absorption from the atmosphere prior to testing.

Approximately 5 g of oven-dry BPC was used for each LOI test. To ensure that moisture would not affect the LOI measurement, all crucibles, BPCs, and components were oven-dried at 110°C for at least 24 h and until constant mass was reached to remove any water prior to testing. The dried samples were transferred to an oven-dried crucible and dried again for an additional 1 h at 110°C to remove any moisture absorbed during transfer. After this second drying period, the test specimen was cooled in a desiccator for approximately 5 min, rapidly weighed (minimizing uptake of atmospheric moisture) to determine the initial mass, then transferred immediately to the muffle furnace.

Dried test specimens were heated in a muffle furnace (Lindberg Blue M; Thermo Scientific, Waltham, MA) using the temperature ramp in Method A of ASTM D7348. The temperature was increased to 500°C over 1 h, increased again to 750°C over 1 h, and then maintained at 750°C for 2 h. The furnace was then cooled to 110°C. After the furnace temperature was lowered to 110°C, test specimens were rapidly transferred from the furnace to a desiccator, allowed to cool in the desiccator for 5 min, then rapidly weighed using a microbalance with an accuracy of 0.1 mg. One control blank (crucible with no test specimen) was included with each set of test specimens to account for any crucible mass loss during the test.

LOI was calculated as

$$LOI = \frac{(m_i - m_f - \Delta m_e)}{m_i - m_e} \quad (3)$$

where m_e is the initial mass of the oven-dry empty crucible, m_i is initial mass of the test specimen and crucible after drying, m_f is final mass of the test specimen and crucible after the LOI test, and Δm_e is the change in mass of the empty crucible during the LOI test. The change in mass for BPC samples during the LOI test was on the order

of 0.3–0.7 g. Changes in the crucible mass were typically less than 1 % of the total change in mass measured for the BPC and crucible, but they periodically accounted for up to 10 % of the total change in mass. Hence, accounting for changes in the crucible mass can be important.

TC ANALYSIS

TC analyses were conducted on the BPCs in general accordance with ASTM D6316-17, *Standard Test Method for Determination of Total, Combustible and Carbonate Carbon in Solid Residues from Coal and Coke*, using a Shimadzu total organic carbon (TOC)-L analyzer (Kyoto, Japan) paired with a solid sample module. The TOC-L analyzer employs a nondispersive infrared detector (NDIR) sensitive to carbon loading. Each BPC specimen (0.08–0.4 g) was combusted in the analyzer at 900°C until no signal was measured. The area under the NDIR signal curve was integrated as a measure of TC in the specimen. Preliminary analysis showed that inorganic carbon content of the polymer and bentonite was below the detection limit of the analyzer, meaning that TC was effectively measuring TOC in this study.

TGA AND DIFFERENTIAL SCANNING CALORIMETRY

TGA and differential scanning calorimetry (DSC) were conducted on BPCs as interpretive measurements to identify mechanisms occurring during LOI testing. TGA describes the mass lost from the BPC as components within the specimen are degraded or transformed in response to an increase in temperature. DSC describes the energy released or consumed by reactions occurring within the specimen during heating.

TGA and DSC were conducted using a STA 449 F1 Jupiter simultaneous thermogravimeter–differential scanning calorimeter (NETZSCH, Burlington, MA) in general accordance with ASTM C1872-18e2, *Standard Test Method for Thermogravimetric Analysis of Hydraulic Cement*. Analyses were performed under argon with platinum/rhodium (80/20) sample pans. The temperature was increased to 750°C at 10°C/min, held at 750°C for 2 h, then decreased at 10°C/min until reaching 110°C. Temperature, mass remaining, and heat flux were recorded in 1-min increments throughout each test. The maximum temperature of the TGA heat ramp (750°C) is the same temperature used during LOI analyses.

Because TGA was conducted under argon (nonoxidizing environment), the TGA is not directly analogous to conditions during LOI in a muffle furnace (oxidizing environment). Nevertheless, the TGA does provide insight into differences in the extent of degradation and mass loss that occur during heating.

Evaluation of Methods for Unhydrated BPCs

Tests were conducted using base bentonite, the three proprietary polymers for commercially available BPC-GCLs, and BPCs with known polymer loading prepared with each of the polymers. Tests were conducted on BPCs in their unhydrated initial state. The polymer loading was varied from 20 to 100 g polymer/kg BPC.

COMPONENT LOI METHOD

LOI tests for the component method were conducted on triplicate specimens of each component (bentonite, each polymer alone) and 10 distinct specimens of individually mixed BPCs prepared with different polymer loadings ranging from 20 to 100 g polymer/kg BPC. This range of polymer loading encompasses the common range of polymer loadings used in commercial BPC-GCLs. The individually mixed BPCs were prepared directly in the crucibles so that polymer loading was known precisely. Replicates were not performed for each of these BPC specimens. Polymer loading was calculated from the LOI data using equation (2) with r_c from the LOI tests on the BPCs, r_p from the LOI test on the polymer alone, and r_b from the LOI test on the bentonite alone.

Polymer loading determined by the component LOI method is shown versus actual polymer loading in [figure 2](#) for BPCs prepared with polymers P1, P2, and P3. Loading was computed with equation (2) using $r_p = 0.399$ for P1, 0.227 for P2, and 0.061 for P3; and $r_b = 0.937$ for the bentonite. The average deviation (measured–actual polymer loading) for each BPC is summarized in [Table 2](#). Polymer loading determined by the

component LOI method is in good agreement with the actual polymer loading for P3-BPC, deviating by only 0.3 g polymer/kg BPC on average. In contrast, the polymer loading is overestimated by 13.5 g polymer/kg BPC, on average, for P1-BPC and underestimated by 6.3 g polymer/kg BPC, on average, for P2-BPC. For P1-BPC, the deviation between measured and actual polymer loading increases with polymer loading, whereas the deviation is essentially constant for P2-BPC.

Source of Bias in Component LOI Method

TGA was conducted on the BPCs as well as the polymers and base bentonite comprising each BPC to identify mechanisms contributing to the bias in the component LOI method evident in [figure 2](#). TGA was conducted to determine if thermal degradation of the polymers was altered by the presence of bentonite, thereby contributing to an error in polymer loading based on r_p defined by LOI testing on the polymer alone. BPCs used in TGA were individually mixed immediately prior to analysis so that the quantity of polymer and bentonite in the mixture was known precisely.

TGA tests on the BPC as well as the polymer and the bentonite alone were used to estimate the fraction of polymer in the BPC as a function of time during heating. Because the fraction of polymer remaining within the

FIG. 2

Polymer loading measured using the component LOI method versus actual polymer loading for unhydrated P1-, P2-, and P3-BPCs.

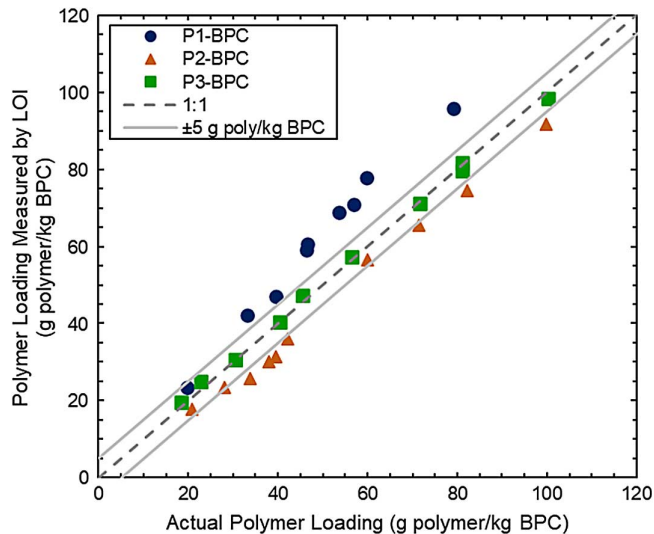


TABLE 2

Summary of average deviation in polymer loading measured by component LOI method, composite LOI method, and composite TC method; positive deviation corresponds to measured polymer loading exceeding prepared polymer loading

Method	Polymer	Measured-Actual Polymer Loading (g polymer/kg BPC)		
		Unhydrated	Hydrated in DI Water	Hydrated in 50 mM CaCl ₂
Component LOI method	P1	13.5	Not tested	Not tested
	P2	-6.3	Not tested	Not tested
	P3	0.3	Not tested	Not tested
Composite LOI method	P1	-0.2	-12.1	0.5
	P2	0.1	-4.4	2.5
	P3	-3.3	-13.9	-3.4
Composite TC method	P1	3.8	1.5	1.9
	P2	3.7	5.2	1.9
	P3	2.5	-5.1	-2.1

BPC at any given time ($r_{p,t}$ at time, t) during the TGA test could not be directly measured, $r_{p,t}$ for the polymer in the BPC was calculated using the fraction of bentonite remaining ($r_{b,t}$) and the fraction of BPC remaining ($r_{c,t}$) at any given time based on measurements made on the base bentonite and the BPC:

$$r_{p,t} = \frac{r_{c,t}m_c - r_{b,t}m_b}{m_p} \quad (4)$$

where m_c is the initial mass of BPC, m_b is the initial mass of bentonite in the BPC, and m_p is the initial mass of polymer in the BPC. The effect of the polymer on the bentonite was assumed to be negligible compared with the effect of the bentonite on the polymer, given that bentonite comprises 90–99 % of the dry mass in a BPC and is much more thermally stable than polymer.

Comparison of the TGA curves in **figure 3** indicates that the mass remaining of polymer heated alone (**fig. 3**, dark blue line) and the mass remaining of polymer heated within the BPC (**fig. 3**, light blue line) differs measurably for each polymer. When P1 is heated in the BPC, less mass remains (18.0 %) than when the polymer is heated alone (36.8 % remaining). In contrast, when P2 is heated within the BPC, more mass remains (33.3 %) than when heated alone (22.8 % remaining). P3 loses less mass initially when heated in the BPC than when heated alone, but slightly less mass of P3 ultimately remains when the polymer is heated in the BPC (12.5 % remaining) than when heated alone (17.0 % remaining).

The differences in the mass remaining between polymers heated alone or in a BPC have implications regarding the efficacy of using the component LOI method to determine polymer loading. If a smaller fraction of the polymer remains in the BPC than remains of the polymer heated alone during LOI testing, polymer loading will be overestimated using the component LOI method (e.g., P1, **figs. 2** and **3A**). Conversely, if a larger fraction of the polymer remains in the BPC than remains of the polymer heated alone during LOI testing, polymer loading will be underestimated using the component LOI method (e.g., P2, **figs. 2** and **3B**). A reliable estimate of polymer loading will be obtained only if the fraction of polymer remaining in the BPC is comparable to the fraction of polymer remaining when heated alone (e.g., P3, **figs. 2** and **3C**).

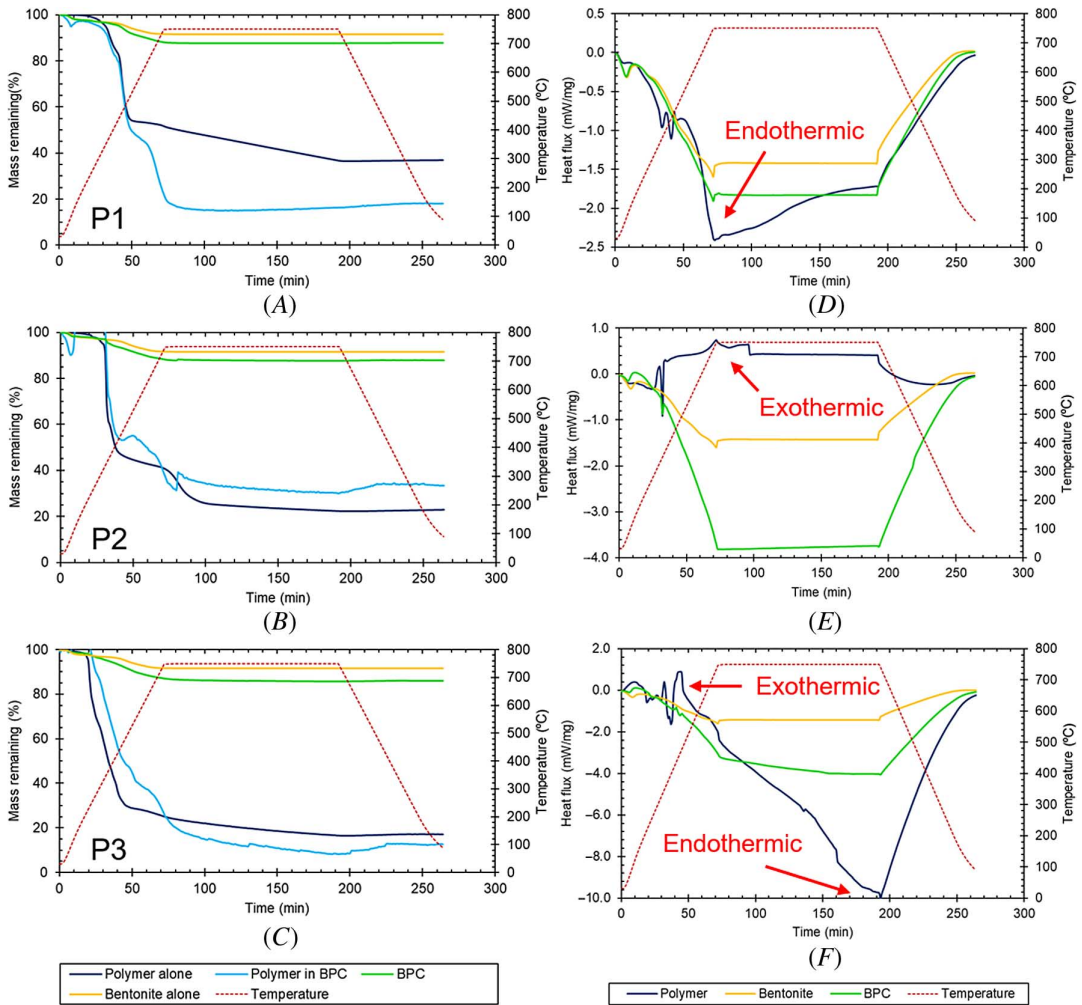
Degradation Reactions in Polymer Component

DSC was used to determine whether the degradation reactions occurring during heating were exothermic or endothermic, which could explain any effects of the bentonite on the thermal degradation of the polymer. The differences between the TGA curves for polymer heated alone and polymer heated within the BPC indicate that bentonite affects thermal degradation of the polymer and that the effect of the bentonite differs for each polymer. To verify this hypothesis, energy consumed or released during thermal degradation was measured with the DSC. As illustrated by the DSC curves in **figure 3**, the type of degradation varied between polymers even though they were exposed to the same thermal regime in the TGA. P1 predominantly undergoes endothermic degradation during heating, indicated by the downward trend in the DSC curve. P2 undergoes predominantly exothermic degradation, indicated by the upward trend in the DSC curve. P3 undergoes exothermic degradation followed by endothermic degradation. Endothermic reactions corresponded with less polymer mass remaining in the BPC (e.g., P1), whereas exothermic reactions corresponded to more polymer mass remaining in the BPC (e.g., P2). For P3, more polymer mass remains in the BPC initially while an exothermic event occurs, but eventually less polymer mass remains in the BPC in response to the subsequent endothermic event. These reactions are affected by the bentonite, causing polymers that degrade via endothermic reactions to experience greater degradation (less mass remaining) when heated within a BPC, whereas polymers that degrade via exothermic reactions experience less degradation (more mass remaining) when heated within a BPC.

COMPOSITE LOI METHOD

The composite LOI method defines a relationship between polymer loading and LOI by conducting LOI tests on BPC standards with known polymer loading prepared over the range of polymer loadings commonly encountered in

FIG. 3 Mass remaining during thermogravimetric analysis (A–C) and heat flux determined by differential scanning calorimetry (D–F) for polymers P1 (A, D), P2 (B, E), and P3 (C, F). Polymer in BPC was calculated based on the mass remaining at a given time for the bentonite alone and the BPC. All other data were measured directly.



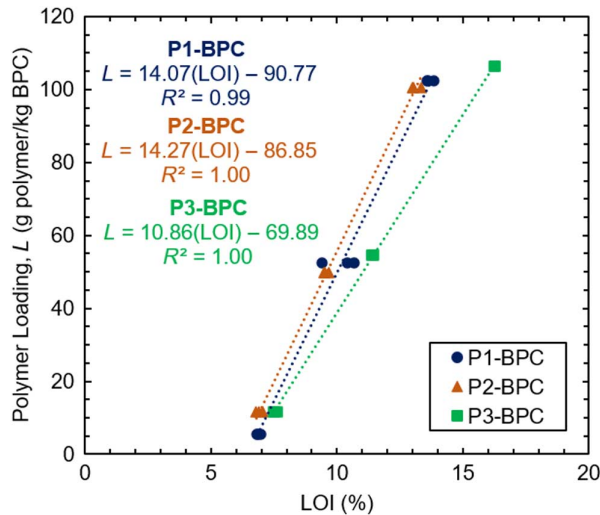
practice (Table 1). The method employs the same LOI testing procedure as the component LOI method, but the tests to develop the relationship are conducted on the composite material (BPC) rather than on individual components.

Batches of BPC standards were prepared with polymer loadings of 10, 50, and 100 g polymer/kg BPC. LOI was measured using ASTM D7348 following the procedures described previously, with LOI computed using equation (3). The relationships between polymer loading and LOI for each BPC are shown in figure 4. The procedure was then checked by testing triplicate samples of BPCs with polymer loadings of approximately 20, 60, and 100 g polymer/kg BPC, conducting LOI tests on the specimens following D7348 and computing the polymer loading based on the relationships between polymer loading and LOI in figure 4.

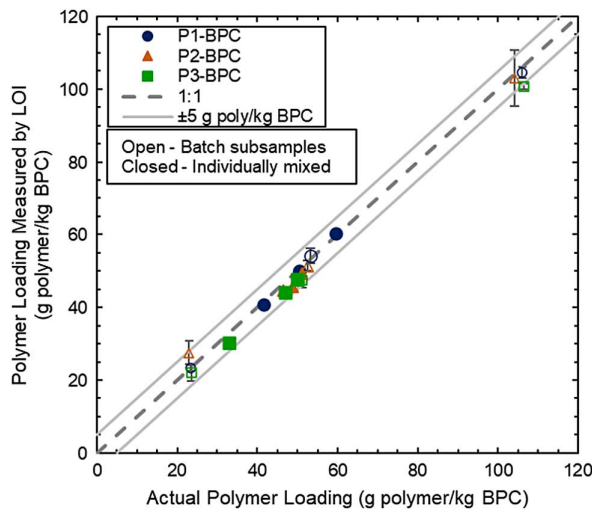
Polymer loading measured using the composite LOI method versus actual polymer loading for the three BPCs is shown with open symbols in figure 5. Very good agreement was obtained, with minimal bias. The average deviation between time measured and actual loading is summarized in Table 2. Polymer loading measured by the composite LOI method deviated from the actual polymer loading by an average of -0.2 g polymer/kg BPC for P1-BPC, 0.1 g polymer/kg BPC for P2-BPC, and -3.3 g polymer/kg BPC for P3-BPC. The deviation is largest

FIG. 4

Relationships between polymer loading (L) and LOI obtained for composite LOI method using standard BPCs with known polymer loading for P1-BPC, P2-BPC, and P3-BPC.

**FIG. 5**

Polymer loading measured using composite LOI method versus actual polymer loading for unhydrated BPCs with polymers P1, P2, and P3. Batch subsamples (open symbols) were tested in triplicate. Some samples had very low error and the error bars are obscured by the symbol.



for P3-BPC because the polymer loading was underestimated for all but one replicate for P3-BPC. There is no relationship between the error and the known polymer loading for any of the BPCs using the composite LOI method. By relying on composite standards in lieu of component standards, the composite LOI method avoids the bias of the component LOI method provided the polymer thermally degrades at or below 750°C. This temperature is sufficient to thermally degrade a wide range of organic polymers (Stuart 2002).

There was minimal bias and good agreement between measured and actual polymer loading for samples taken from ground batches of BPC (open symbols, fig. 5). However, bias may result from the sample preparation process if there is preferential mass loss of either polymer or bentonite during the grinding process, or if the ground BPC is not sufficiently homogenized before samples are taken for LOI testing. For example, in some cases, up to 8 % of the sample mass was lost by dispersion in the headspace above the grinder or by adhering to the mortar and pestle, but the exact composition (i.e., the fraction of bentonite or polymer) of the lost mass could not be tracked. Bias introduced by the preparation procedure is unlikely because of the good agreement of

results in [figure 5](#); nevertheless, to check for bias introduced by sample preparation, “individually mixed” BPCs were prepared and tested without being ground in batches. These individually mixed BPCs were prepared by mixing ground, oven-dried bentonite with unground, oven-dried polymer directly in the crucibles so that the polymer loading in each sample was known precisely. The bentonite was ground using the same grinding method as BPCs (i.e., mechanically ground to pass a US No. 60 sieve). The polymer was not ground because its propensity to absorb moisture from the air when not surrounded by bentonite limited size reduction. Polymer loading of individually mixed BPCs determined by the composite LOI method is shown in [figure 5](#) with closed symbols. No difference is apparent between the polymer loading determined using either method, suggesting that the grinding and homogenization process does not introduce measurable bias.

COMPOSITE TC METHOD

The composite TC method defines a relationship between polymer loading and TC by conducting tests on BPC standards with known polymer loading prepared over the range of polymer loadings commonly encountered in practice ([Table 1](#)). TC analyses were conducted on BPC standards prepared with polymer loadings of approximately 15, 60, and 120 g polymer/kg BPC. Relationships between polymer loading and the integrated NDIR signal from the TC analysis are shown in [figure 6](#). Similar relationships between polymer loading and the NDIR signal were obtained for P1-BPC and P2-BPC, whereas a different relationship was obtained for P3-BPC, which is likely a result of differences in polymer structures, as the TC analyzer can be sensitive to the form of carbon used for calibration. Thus, a unique relationship is needed between polymer loading and NDIR signal for each BPC.

The composite TC method was initially evaluated by preparing BPC test specimens with known polymer loading (20, 60, 100 g polymer/kg BPC), conducting TC analysis on triplicate samples of each BPC, and computing the polymer loading from the relationships shown in [figure 6](#). As with the composite LOI method, tests were conducted on BPCs prepared in batches, as well as individually mixed samples prepared directly in the test crucible. In each case, extreme care was used to ensure the BPCs were well mixed and as uniform as practical. Polymer loading determined using the composite TC method is shown in [figure 7](#) versus actual polymer loading for the three BPCs. The average deviation for each BPC is summarized in [Table 2](#).

Good agreement between measured and actual polymer loading was obtained with the TC method ([fig. 7](#)). Polymer loading was overestimated modestly for each BPC, deviating by an average of 3.8 g polymer/kg BPC for the P1-BPC, 3.7 g polymer/kg BPC for the P2-BPC, and 2.5 g polymer/kg BPC for the P3-BPC. For all replicates

FIG. 6

Relationships between polymer loading (L) and integrated NDIR signal (A) obtained for composite TC method using standard BPCs with known polymer loading for P1-BPC, P2-BPC, and P3-BPC.

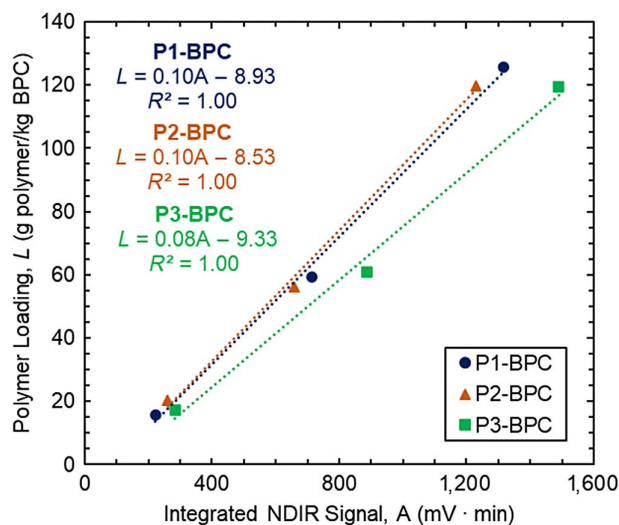
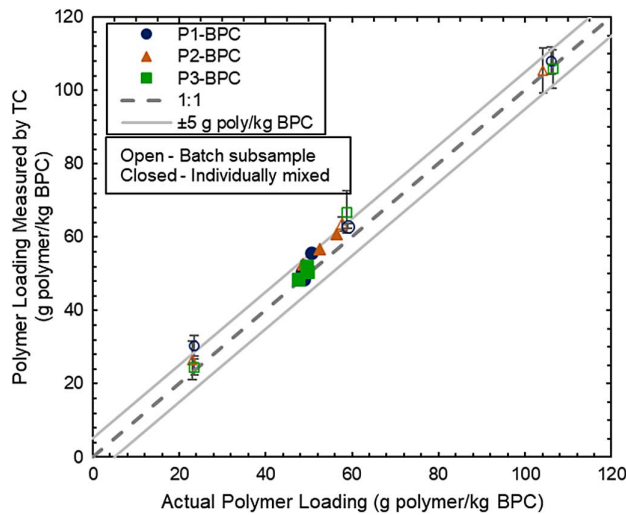


FIG. 7

Polymer loading measured using composite TC method versus actual polymer loading for unhydrated BPCs with polymers P1, P2, and P3. Batch subsamples (open symbols) were tested in triplicate. Some samples had very low error and the error bars are obscured by the symbol.



tested for all BPCs (36 total, including BPCs prepared in batches, as well as individually mixed samples prepared directly in the crucible), 78 % resulted in overestimated polymer loading. The source of this error is unclear. The deviation was independent of polymer type (P1 versus P2 versus P3). These deviations are slightly higher for the composite LOI method for P1- and P2-BPCs and lower for the P3-BPC compared with measurements using the modified composite LOI calibration method.

Smaller specimens were used for the composite TC method (0.08–0.4 g) compared with the composite LOI method (4–5 g) because of limitations on carbon loading for the instrument. This limited specimen size could have contributed to the modestly higher deviations for the composite TC method. For this reason, additional replicates should be tested when using the composite TC method.

Evaluation of Methods for Hydrated BPCs

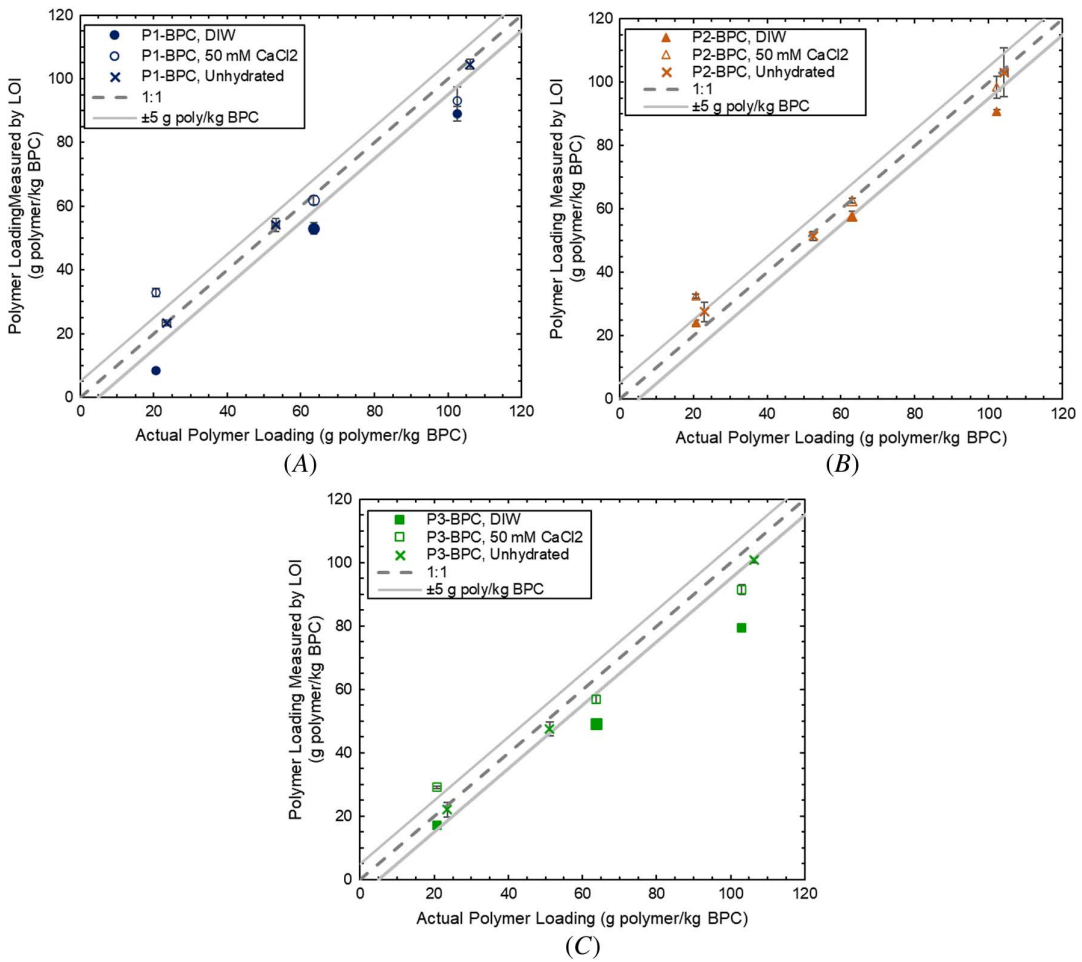
Forensic assessment of polymer elution from BPC-GCLs requires measurements of the polymer loading for BPCs that have been hydrated (e.g., during permeation, [Scalia et al. 2014](#)). Dissolved species in the hydrating solution may alter properties of the bentonite or the polymer, or both, that affect thermal degradation during LOI or TC analysis. For this reason, the relationship between polymer loading versus LOI or TC created using standard BPCs that have never been hydrated may not be representative of the polymer loading versus LOI or TC relationship for BPCs that have been hydrated.

To evaluate whether hydration of samples introduced bias, the composite LOI and composite TC methods were used to measure polymer loading in BPCs hydrated in the hydration cell using DI water or 50 mM CaCl₂ solution for 7 days. LOI and TC analyses were conducted on the BPCs using the aforementioned methods, and polymer loading was computed using polymer loading versus LOI relationships for dry batches of BPC shown in [figure 4](#), or the polymer loading versus NDIR signal relationship shown in [figure 6](#).

COMPOSITE LOI METHOD

Polymer loading measured using the composite LOI method is shown in [figure 8](#) versus actual polymer loading for BPCs hydrated in DI water or 50 mM CaCl₂ solution. The average deviation for each BPC in either hydration liquid is summarized in [Table 2](#). Analysis of soluble cations in the mixture by ASTM [D7503](#) indicated that salts made up no more than 0.8 % of the mass of bentonite after hydration with 50 mM CaCl₂, which introduces an

FIG. 8 Polymer loading measured using composite LOI method versus actual polymer loading for BPCs hydrated in DI water and 50 mM CaCl₂: (A) P1-BPC, (B) P2-BPC, and (C) P3-BPC. Samples were tested in triplicate. Some samples had very low error and the error bars are obscured by the symbol.



error in polymer loading no more than ± 0.2 g polymer/kg BPC; therefore, the retention of salt was not accounted for when computing the polymer loading from the polymer loading versus LOI relationship.

In most cases, the measured polymer loading is comparable to or less than the actual polymer loading (fig. 8). For P3-BPC, the difference between measured and actual polymer loading increases with polymer loading. The differences between measured and actual polymer loading are generally larger for BPCs hydrated in DI water than 50 mM CaCl₂, suggesting that the chemical interactions between the BPC and the solution affect thermal degradation of BPCs during LOI testing. For example, Yeşilbaş, Holmboe, and Boily (2018) demonstrate that the water loss of tightly bound water on the bentonite surface during heating is altered by Ca²⁺ replacing Na⁺ in the exchange complex.

To illustrate the effect of cation exchange, the base bentonite was hydrated in DI water, and 20, 50, and 100 mM CaCl₂ solutions for 7 d. After hydration, the mole fraction of Ca²⁺ in the exchange complex was measured following methods in ASTM D7503, and the LOI of the bentonite was determined by ASTM D7348 (Method A). As shown in figure 9, LOI of the bentonite and the mole fraction of Ca²⁺ in the exchange complex increase with increasing concentration of CaCl₂ in the hydrating solution. LOI of the bentonite

increases with increasing mole fraction of Ca^{2+} because of dehydration of an increasing number of water molecules in the interlayer (Greene-Kelly 1952; Yeşilbaş, Holmboe, and Boily 2018). Therefore, BPCs hydrated with CaCl_2 solutions will appear to have higher polymer loading than BPCs hydrated with DI water when polymer loading is determined by LOI, all other factors being equal. This also suggests that hydration could have affected the polymer component. The mechanisms responsible for alterations in the polymer will likely depend on the chemistry of the polymer and the hydrating solution, which would not be known a priori. Additionally, elution of polymer from the BPC during hydration, as described in Tian, Likos, and Benson (2019) and Chen et al. (2019), may have occurred. These mechanisms were not investigated. However, clear bias is introduced as a result of cation exchange in the bentonite, regardless of the interplay of other possible sources of bias.

COMPOSITE TC METHOD

The composite TC method may avoid the bias of the composite LOI method associated with hydrating or permeating BPCs in salt solutions that alter the amount of tightly bound water or the polymer conformation. TC measures the total mass of carbon released during heating of a specimen, whereas LOI measured the total mass lost during heating (carbon, tightly bound water, etc.). Therefore, TC should be less affected by chemical interactions between the hydrating solution and the bentonite or the polymer.

The composite TC method was used to measure polymer loading of BPCs after hydration in DI water or 50 mM CaCl_2 using the methods described previously. Polymer loading of the hydrated BPCs measured using the composite TC method is shown in figure 10 versus actual polymer loading. The average deviations are summarized in Table 2. In contrast to the findings from the composite LOI method, the measured and actual polymer loadings generally are in good agreement regardless of the hydrating liquid. The average deviation ranges from -5.1 g polymer/kg BPC (P3-BPC) to 5.2 g polymer/kg BPC (P2-BPC) for DI water and from -2.1 g polymer/kg BPC (P1-BPC) to 1.9 g polymer/kg BPC (P1-BPC, P2-BPC) in 50 mM CaCl_2 . The deviations are smaller for BPCs hydrated in the CaCl_2 solution than DI water and are comparable to those obtained on BPC specimens that had never been hydrated. Deviations were unrelated to the magnitude of polymer loading for the P1- and P2-BPCs. For P3-BPC, the polymer loading was overestimated for unhydrated samples and underestimated for hydrated samples, and the deviation was largest for hydrated samples with the highest polymer loading. Similar to the

FIG. 9

LOI of bentonite as a function of mole fraction of calcium in the exchange complex. Calcium concentration of the hydrating solution is shown adjacent to each point. LOI and mole fraction of calcium in exchange complex both increase with increasing calcium concentration of the hydrating solution.

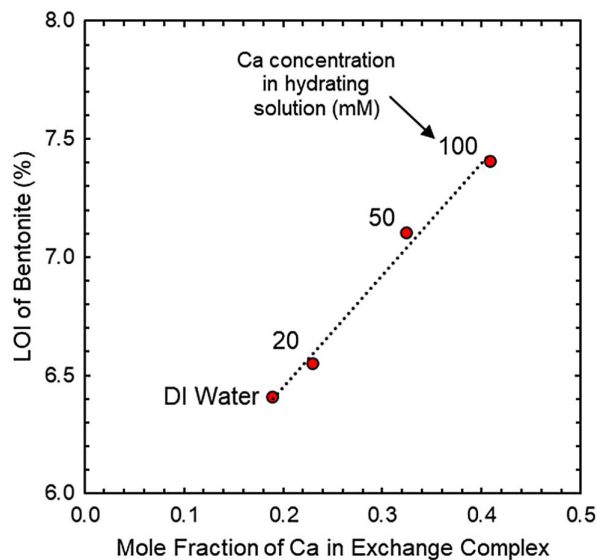
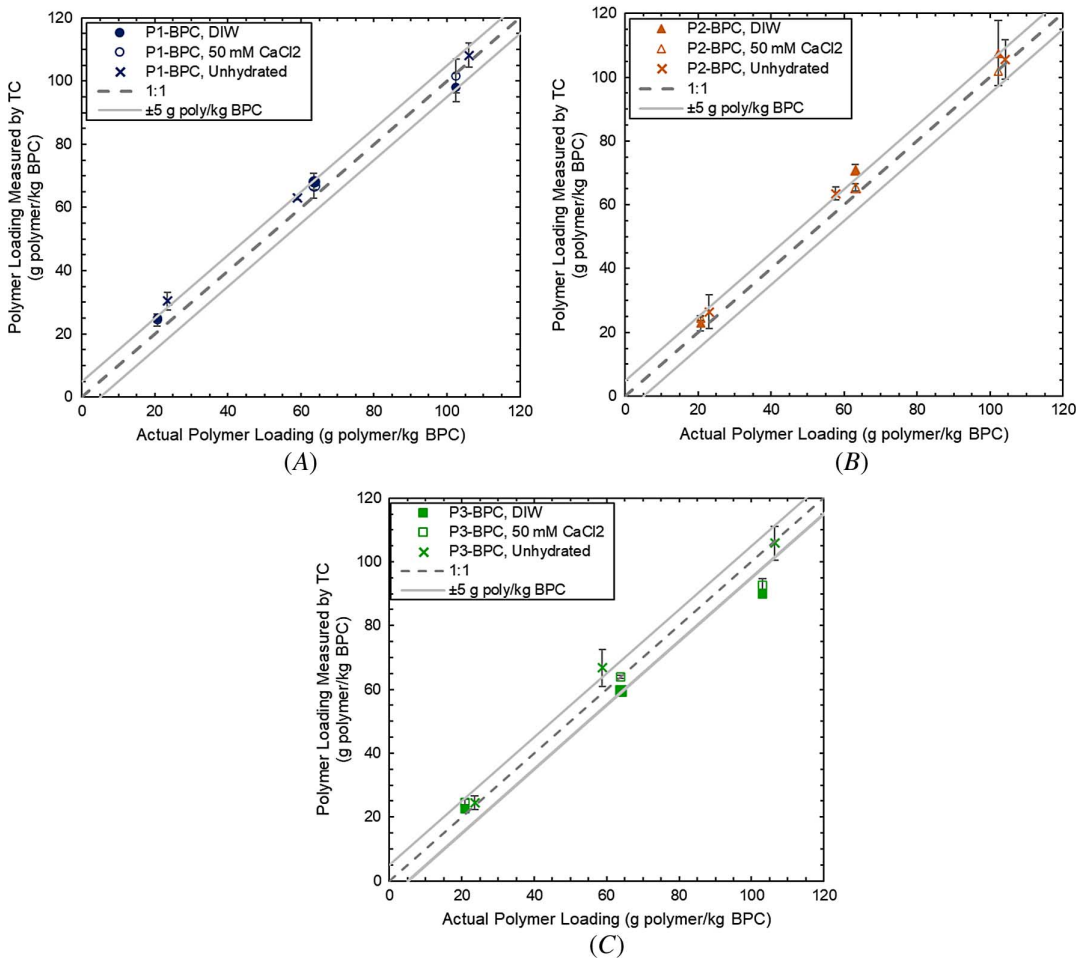


FIG. 10 Polymer loading measuring using composite TC method versus actual polymer loading for (A) P1-BPC, (B) P2-BPC, and (C) P3-BPC after hydration in DI water or 50 mM CaCl₂. Samples were tested in triplicate. Some samples had very low error, and the error bars are obscured by the symbol.



composite LOI method, deviations for hydrated samples could have been influenced by changes to polymer structure and polymer elution, which were not addressed.

Recommended Procedures

The composite LOI method is recommended for measuring polymer loading of unhydrated BPCs for applications such as manufacturing or construction quality control testing. For these applications, LOI is preferable because muffle furnaces are more commonly available and less expensive and require less training than TC analyzers. The composite LOI method also uses a larger specimen, reducing potential uncertainty associated with small specimens used in TC analysis. The following procedure is recommended:

1. Obtain samples of the polymer and bentonite contained in the BPC from the manufacturer.
2. Prepare BPC standards by mixing the polymer and bentonite over a range of polymer loadings encompassing the expected polymer loading of the BPC (e.g., 10, 50, and 110 g polymer/kg BPC in this study). Prepare at least three mixtures with different polymer loadings approximately equally spread over the

- range of polymer loadings that may exist. Batches of ~25 g are recommended and should be carefully mixed to promote uniformity.
3. Grind each BPC standard in accordance with the procedure in ASTM [D7348](#), and carefully mix the ground BPC standard again to promote uniformity. Oven dry all LOI crucibles and BPC standards at 110°C for at least 24 h and until constant mass is reached.
 4. Transfer ~5-g samples from each batch of BPC standards to test crucibles, taking care to minimize exposure of the sample to moisture in the air. Measure LOI of the BPC standards using the procedures in ASTM [D7348](#) (Method A). Measure the LOI of at least one empty crucible to control for crucible mass loss. Multiple replicates are recommended.
 5. Graph the relationship of polymer loading versus LOI using data from step 4 and fit the relationship with an equation using least-squares linear regression.
 6. Grind the BPC with unknown polymer loading in accordance with the procedure in ASTM [D7348](#), and carefully mix the ground BPC to promote uniformity. Oven dry the ground BPC and the test crucible at 110°C for at least 24 h and until constant mass is reached.
 7. Transfer ~5 g from each batch of ground BPC to a test crucible, taking care to minimize exposure of the specimen to moisture in the air. Conduct an LOI test on the test specimen using the procedures in ASTM [D7348](#) (Method A). Multiple replicates of the test are recommended.
 8. Use the polymer loading versus LOI equation from step 5 and the LOI measured in step 7 to determine the polymer loading of the BPC with unknown polymer loading.

The composite TC method is recommended for measuring polymer loading of BPCs that have been hydrated or permeated with inorganic salt solutions. The following procedure is recommended:

1. Obtain samples of the polymer and the bentonite contained in the BPC from the manufacturer.
2. Prepare BPC standards by mixing the polymer and bentonite over a range of polymer loadings encompassing the expected polymer loading of the BPC (e.g., 15, 60, and 120 g polymer/kg BPC in this study). Prepare at least three mixtures with different polymer loadings approximately equally spread over the range of polymer loadings that may exist. Batches of ~25 g are recommended and should be carefully mixed to promote uniformity.
3. Grind each BPC standard in accordance with the procedure in ASTM [D7348](#), and carefully mix the ground BPC standard again to promote uniformity.
4. Oven dry all BPC standards at 110°C for at least 24 h and until constant mass is reached.
5. Transfer ~0.08–0.4 g of each ground and dried BPC standard to test crucibles. Conduct TC analysis on the BPC standards using the solid state module of a TC analyzer in general accordance with ASTM [D6316](#). Record the integrated NDIR signal. Multiple replicates are recommended.
6. Graph the relationship between known polymer loading versus integrated NDIR signal using the data from step 5 and fit the relationship with an equation using least-squares linear regression.
7. Grind the BPC with unknown polymer loading in accordance with the procedure in ASTM [D7348](#), and carefully mix the ground BPC to promote uniformity. Oven dry the ground BPC at 110°C for at least 24 h and until constant mass is reached.
8. Transfer ~0.08–0.4 g of each ground and dried BPC with unknown polymer loading to a test crucible. Conduct a TC test on the test specimen using the procedures in ASTM [D6316](#), and record the integrated NDIR signal. Multiple replicates of each specimen are recommended.
9. Use the relationship in step 6 to compute the polymer loading of the BPC specimen from the integrated NDIR signal measured in step 8.

Summary and Conclusions

Measurements of polymer loading in BPC-GCLs are needed for manufacturing quality control, construction quality control, and forensic investigations. Polymer loading is most commonly measured using an LOI method. Two LOI-based methods were evaluated in this study: the component LOI method and the composite LOI

method. The component method is based on a functional relationship between polymer loading and individual measurements from LOI tests on the bentonite component, the polymer component, and the BPC sample with unknown polymer loading. The composite LOI method relies on a relationship between polymer loading and LOI developing using data from LOI tests on BPC standards with known polymer loading. A third method based on TC (composite TC method) was also evaluated. The composite TC method is similar to the composite LOI method, except TC is used to determine polymer loading in lieu of LOI. The methods were evaluated using BPCs that had never been hydrated, as well as BPCs that had been hydrated in DI water or a 50 mM CaCl₂ solution.

The following conclusions are drawn based on the findings from these experiments:

- Polymer loading measured by the component LOI method can be biased because the bentonite affects thermal degradation of the polymer during heating. The bias depends on the degradation reactions that the polymer undergoes, and is lowest when the polymer undergoes both exothermic and endothermic degradation with comparable energy.
- Polymer loading measured by the composite LOI method exhibits less bias than the component LOI method and is recommended for measuring polymer loading of unhydrated BPCs for manufacturing and construction quality control.
- Polymer loading of hydrated BPCs measured with the composite LOI method can be biased significantly, most likely because of the interactions that occur between the bentonite and the polymer with the hydrating solution. The bias appears to depend on the chemistry of the hydrating solution. The composite LOI method is not recommended for evaluating BPCs that have been hydrated or permeated.
- Polymer loading measured using the composite TC method was in good agreement with the actual polymer loading regardless of whether the BPC has been hydrated. The composite TC method is recommended for evaluating BPCs that have been hydrated or permeated. Extreme care must be used to ensure representative samples collected for TC analysis, as the test specimens are small relative to those used in LOI testing. The appropriateness of the composite TC method has not been evaluated for BPCs hydrated or permeated with solutions containing organic compounds or matter, which may affect the carbon content of the test specimen.

Sample collection methods, specimen size, and the number of tests required for statistical inferences were not evaluated in this study but can affect measurements of polymer loading by LOI or TC methods. Future studies are needed to assess the effects of sample preparation choices such as sample size, number of samples needed to draw statistical inferences, and sample collection procedures, including methods to exclude extraneous materials such as needle-punching fibers.

ACKNOWLEDGMENTS

This study was supported by CETCO and Minerals Technology Inc., the US Department of Energy's Consortium for Risk Evaluation with Stakeholder Participation (CRESP) III through Cooperative Agreement No. DE-FC01-06EW07053, the Environmental Research and Education Foundation through a fellowship to the first author, and the Jefferson Scholars Foundation at University of Virginia. Materials for the study were provided by CETCO. Beth Opila and Rebekah Webster provided training and insight into the TGA and DSC analyses.

References

- ASTM International. 2013. *Standard Test Methods for Loss on Ignition (LOI) of Solid Combustion Residues*. ASTM D7348–13. West Conshohocken, PA: ASTM International, approved September 1, 2013. <https://doi.org/10.1520/D7348-13>
- ASTM International. 2017. *Standard Test Method for Determination of Total, Combustible and Carbonate Carbon in Solid Residues from Coal and Coke*. ASTM D6316–17. West Conshohocken, PA: ASTM International, approved December 1, 2017. <https://doi.org/10.1520/D6316-17>
- ASTM International. 2018. *Standard Test Method for Measuring the Exchange Complex and Cation Exchange Capacity of Inorganic Fine-Grained Soils*. ASTM D7503–18. West Conshohocken, PA: ASTM International, approved March 1, 2018. <https://doi.org/10.1520/D7503-18>

- ASTM International. 2018. *Standard Test Method for Thermogravimetric Analysis of Hydraulic Cement*. ASTM C1872-18e2. West Conshohocken, PA: ASTM International, approved May 15, 2018. <https://doi.org/10.1520/C1872-18E02>
- ASTM International. 2019. *Standard Test Methods for Laboratory Determination of Water (Moisture) Content of Soil and Rock by Mass*. ASTM D2216-19. West Conshohocken, PA: ASTM International, approved March 1, 2019. <https://doi.org/10.1520/D2216-19>
- Athanassopoulos, C., C. H. Benson, M. Donovan, and J. N. Chen. 2015. "Hydraulic Conductivity of a Polymer-Modified GCL Permeated with High-pH Solutions." In *Geosynthetics 2015*, 181–186. Roseville, MN: Industrial Fabrics Association International.
- Chen, J., H. Salihoglu, C. H. Benson, W. J. Likos, and T. B. Edil. 2019. "Hydraulic Conductivity of Bentonite-Polymer Geosynthetic Clay Liners Permeated with Coal Combustion Product Leachates." *Journal of Geotechnical and Geoenvironmental Engineering* 145, no. 9: 04019038. [https://doi.org/10.1061/\(ASCE\)GT.1943-5606.0002105](https://doi.org/10.1061/(ASCE)GT.1943-5606.0002105)
- Chen, J., K. Tian, and C. H. Benson. 2018. "Hydraulic Conductivity of Bentonite-Polymer Geosynthetic Clay Liners to Coal Combustion Product Leachates." In *Eighth International Congress on Environmental Geotechnics*, 664–671. Singapore: Springer.
- Greene-Kelly, R. 1952. "Irreversible Dehydration in Montmorillonite." *Clay Minerals Bulletin* 1, no. 7 (June): 221–227. <https://doi.org/10.1180/claymin.1952.001.7.06>
- Grim, R. 1968. *Clay Mineralogy*. New York: McGraw-Hill.
- Moore, D. M. and R. C. Reynolds Jr. 1989. *X-Ray Diffraction and the Identification and Analysis of Clay Minerals*. Oxford, UK: Oxford University Press.
- Ramos Filho, F., T. Mélo, M. Rabello, and S. Silva. 2005. "Thermal Stability of Nanocomposites Based on Polypropylene and Bentonite." *Polymer Degradation and Stability* 89, no. 3 (September): 383–392. <https://doi.org/10.1016/j.polyimdegstab.2004.12.011>
- Scalia, J. IV, C. H. Benson, G. L. Bohnhoff, T. B. Edil, and C. D. Shackelford. 2014. "Long-Term Hydraulic Conductivity of a Bentonite-Polymer Composite Permeated with Aggressive Inorganic Solutions." *Journal of Geotechnical and Geoenvironmental Engineering* 140, no. 3 (March): 04013025. [https://doi.org/10.1061/\(ASCE\)GT.1943-5606.0001040](https://doi.org/10.1061/(ASCE)GT.1943-5606.0001040)
- Stuart, B. H. 2002. *Polymer Analysis*. Hoboken, NJ: John Wiley & Sons.
- Tian, K. and C. H. Benson. 2018. "Containing Bauxite Liquor Using Bentonite-Polymer Composite Geosynthetic Clay Liners." In *Eighth International Congress on Environmental Geotechnics*, 672–678. Singapore: Springer.
- Tian, K., C. H. Benson, and W. J. Likos. 2016. "Hydraulic Conductivity of Geosynthetic Clay Liners to Low-Level Radioactive Waste Leachate." *Journal of Geotechnical and Geoenvironmental Engineering* 142, no. 8 (August): 04016037. [https://doi.org/10.1061/\(ASCE\)GT.1943-5606.0001495](https://doi.org/10.1061/(ASCE)GT.1943-5606.0001495)
- Tian, K., W. J. Likos, and C. H. Benson. 2016. "Pore-Scale Imaging of Polymer-Modified Bentonite in Saline Solutions." In *Geo-Chicago 2016*, 468–477. Reston, VA: American Society of Civil Engineers.
- Tian, K., W. J. Likos, and C. H. Benson. 2019. "Polymer Elution and Hydraulic Conductivity of Bentonite-Polymer Composite Geosynthetic Clay Liners." *Journal of Geotechnical and Geoenvironmental Engineering* 145, no. 10 (October): 04019071. [https://doi.org/10.1061/\(ASCE\)GT.1943-5606.0002097](https://doi.org/10.1061/(ASCE)GT.1943-5606.0002097)
- Williams, T. R. "Hydraulic Properties of Geosynthetic Clay Liners." Master's thesis, University of Virginia, 2018.
- Yeşilbaş, M., M. Holmboe, and J. Boily. 2018. "Cohesive Vibrational and Structural Depiction of Intercalated Water in Montmorillonite." *ACS Earth and Space Chemistry* 2, no. 1: 38–47. <https://doi.org/10.1021/acsearthspacechem.7b00103>